



**FACILE SYNTHESIS OF N-VINYLCAPROLACTAM-
FUNCTIONALIZED NATURAL RUBBER WITH
TEMPERATURE RESPONSIVENESS**

BY

MISS SOPITCHA PHETRONG

**A THESIS SUBMITTED IN PARTIAL FULFILLMENT OF
THE REQUIREMENTS FOR THE DEGREE OF
MASTER OF SCIENCE (CHEMISTRY)
DEPARTMENT OF CHEMISTRY
FACULTY OF SCIENCE AND TECHNOLOGY
THAMMASAT UNIVERSITY
ACADEMIC YEAR 2016
COPYRIGHT OF THAMMASAT UNIVERSITY**

**FACILE SYNTHESIS OF N-VINYLCAPROLACTAM-
FUNCTIONALIZED NATURAL RUBBER WITH
TEMPERATURE RESPONSIVENESS**

BY

MISS SOPITCHA PHETRONG

**A THESIS SUBMITTED IN PARTIAL FULFILLMENT OF
THE REQUIREMENTS FOR THE DEGREE OF
MASTER OF SCIENCE (CHEMISTRY)
DEPARTMENT OF CHEMISTRY
FACULTY OF SCIENCE AND TECHNOLOGY
THAMMASAT UNIVERSITY
ACADEMIC YEAR 2016
COPYRIGHT OF THAMMASAT UNIVERSITY**

THAMMASAT UNIVERSITY
FACULTY OF SCIENCE AND TECHNOLOGY

THESIS

BY


MISS SOPITCHA PHETRONG

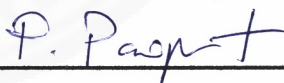
ENTITLED


FACILE SYNTHESIS OF N-VINYLCAPROLACTAM-FUNCTIONALIZED
NATURAL RUBBER WITH TEMPERATURE RESPONSIVENESS

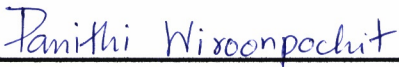
was approved as partial fulfillment of the requirements for
the degree of master of science (chemistry)

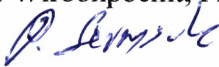
on July 7, 2017

Chairman 
(Nopparat Plucktaveesak, Ph.D.)

Member and Advisor 
(Assistant Professor Peerasak Paoprasert, Ph.D.)

Member 
(Associate Professor Sa-ad Riyajan, Ph.D.)

Member 
(Panithi Wiroonpochit, Ph.D.)

Dean 
(Associate Professor Pakorn Sermsuk, M.Sc.)

Thesis Title	FACILE SYNTHESIS OF N-VINYLCAPROLACTAM- FUNCTIONALIZED NATURAL RUBBER WITH TEMPERATURE RESPONSIVENESS
Author	Miss Sopitcha Phetrong
Degree	Master of Science (Chemistry)
Major Field/Faculty/University	Chemistry Science and Technology Thammasat University
Thesis Advisor	Assistant Professor Peerasak Paoprasert, Ph.D.
Academic Years	2016

ABSTRACT

Natural rubber (NR) has drawn much attention to be used in a broad range of applications, due to its superior properties such as high flexibility and tear resistance. However, NR industries in Thailand have confronted with a considerable drop in prices of NR. Hence, introducing new properties to the NR is a remarkable way for rectifying the problem, adding the value, and also widening its applications.

Herein, novel temperature-responsive materials had been successfully prepared by functionalizing NR with *N*-vinylcaprolactam (NVCL) and its polymer through two processes including crosslinking and graft copolymerization. The synthetic NVCL-functionalized NRs displayed a lower critical solution temperature (LCST) around 32-34 °C which close to the human physiological temperature. With this behavior, our materials were used to mimic controlled drug medical device *via* dye adsorption and desorption studies. This result showed that these materials were able to release dye at the temperature exceeded 32 °C. Therefore, the materials developed in this research work will be useful in a variety of biomedical applications that can extend the range of applications of NR.

Keywords: Temperature-responsive polymer, *N*-vinylcaprolactam, Natural rubber, Crosslinking, Graft copolymerization

ACKNOWLEDGEMENTS

First of all, special gratitude goes to my advisor, Assistant Professor Peerasak Paoprasert, Ph.D., for being ever so nice and enthusiastically interested in my research work. His help, guidance, and a load of supports during my study period since my bachelor degree has encouraged me to finish my research work and get through the tough tasks. I am not only having a wonderful experience but have also learned how to think and deal with every problem that really tested my capability. It was my pleasure to work with him.

Then, I would like to thank the Department of Chemistry, Faculty of Science and Technology, Thammasat University for all supports. Also, the staffs and other instructors of my department for their sincere helps and valuable suggestions during my research period.

Moreover, I gratefully acknowledge the financial support provided by Thammasat University under the TU Research Scholar (2017) as well as Scholarship for Talent Student to study graduate program in Faculty of Science and Technology, Thammasat University (2015-2016).

At last, I wish to express my deep appreciation to my parents who will be indispensable and my friends for their love, encouragement, and support, as well as for always being beside me in every situation. I think I cannot succeed and overcome the hardest time without them.

Miss Sopitcha Phetrong

TABLE OF CONTENTS

	Page
ABSTRACT	(1)
ACKNOWLEDGEMENTS	(2)
TABLE OF CONTENTS	(3)
LIST OF TABLES	(8)
LIST OF FIGURES	(10)
LIST OF ABBREVIATIONS	(15)
CHAPTER 1 INTRODUCTION	1
1.1 State of problems	1
1.2 Research objectives	4
1.3 Scope and limitations of the study	4
CHAPTER 2 REVIEW OF LITERATURE	6
2.1 Natural rubber (NR)	6
2.2 Chemical modification of NR	9
2.2.1 Crosslinking reaction of NR	10
2.2.2 Graft copolymerization of NR	12
2.3 Deproteinization of NR latex	15
2.4 Temperature-responsive polymer	19
2.4.1 Poly(<i>N</i> -vinylcaprolactam) (PNVCL)	20

CHAPTER 3 RESEARCH METHODOLOGY	27
3.1 Materials	27
3.1.1 Reagents	27
3.2 Methods and preparation	27
3.2.1 Synthesis of crosslinked material (PNVCL-NR)	28
3.2.1.1 Preparation of PNVCL	28
3.2.1.2 Preparation of dry rubber	28
3.2.1.3 Preparation of PNVCL-NR	28
3.2.1.4 Investigation of crosslink density	29
3.2.2 Synthesis of grafted material (NVCL-g-DPNR)	30
3.2.2.1 Preparation of DPNR latex	30
3.2.2.2 Preparation of NVCL-g-DPNR	31
3.2.3 Investigation of temperature-responsive behaviors	33
3.2.3.1 The water absorption measurement	33
3.2.3.2 The contact angle determination	34
3.2.3.3 Dye adsorption and desorption studies	34
3.2.4 Adsorption studies	35
3.2.4.1 Equilibrium adsorption isotherm models	35
(1) Langmuir adsorption isotherm	36
(2) Freundlich adsorption isotherm	37
(3) Temkin adsorption isotherm	38
(4) Dubinin-Radushkevich adsorption isotherm	39
3.3 Characterization	41
3.3.1 Fourier transform infrared spectroscopy (FT-IR)	41
3.3.2 ¹ H nuclear magnetic resonance spectroscopy (¹ H-NMR)	41
3.3.3 X-ray photoelectron spectroscopy (XPS)	42
3.3.4 Differential scanning calorimetry (DSC)	42
3.3.5 Thermogravimetric analysis (TGA)	42
3.3.6 Gel permeation chromatography (GPC)	43
3.3.7 Ultraviolet-visible spectroscopy (UV-vis)	43
3.3.8 The contact angle determination	43

3.3.9 Carbon nitrogen and hydrogen analysis (CHN)	43
3.3.10 Centrifugation	44
CHAPTER 4 RESULTS AND DISCUSSION	45
4.1 Synthesis and characterization of PNVCL-NR	45
4.1.1 Preparation of PNVCL	45
4.1.1.1 Morphological observation of PNVCL	45
4.1.1.2 Chemical structure and characteristics of PNVCL	45
(1) FT-IR analysis of PNVCL	45
(2) ¹ H-NMR analysis of PNVCL	47
4.1.1.3 Molecular weight determination of PNVCL	49
4.1.2 Preparation of PNVCL-NR	50
4.1.2.1 Morphological observation of PNVCL-NR	50
4.1.2.2 Chemical structure and characteristics of PNVCL-NR	52
(1) FT-IR analysis of PNVCL-NR	52
(2) XPS analysis of PNVCL-NR	54
4.1.2.3 Thermal properties of PNVCL-NR	55
(1) DSC analysis of PNVCL-NR	55
(2) TGA analysis of PNVCL-NR	56
4.1.2.4 Effect of reaction parameters on gel content of PNVCL-NR	58
(1) Effect of polymer concentration	58
(2) Effect of initiator concentration	59
(3) Effect of reaction temperature	60
(4) Effect of reaction time	60
4.1.2.5 Investigation of crosslink density of PNVCL-NR	61
4.1.2.6 Investigation of temperature-responsive behaviors of PNVCL-NR	62
(1) The water absorption measurement of PNVCL-NR	62
(2) The contact angle determination of PNVCL-NR	64

(3) Dye adsorption and desorption studies of PNVCL-NR	65
4.1.2.7 Adsorption studies of PNVCL-NR	67
4.2 Synthesis and characterization of NVCL- <i>g</i> -DPNR	71
4.2.1 Preparation of DPNR latex	71
4.2.2 Preparation of NVCL- <i>g</i> -DPNR	72
4.2.2.1 Morphological observation of NVCL- <i>g</i> -DPNR	72
4.2.2.2 Chemical structure and characteristics of NVCL- <i>g</i> -DPNR	74
(1) FT-IR analysis of NVCL- <i>g</i> -DPNR	74
(2) ¹ H-NMR analysis of NVCL- <i>g</i> -DPNR	76
(3) XPS analysis of NVCL- <i>g</i> -DPNR	78
4.2.2.3 Thermal properties of NVCL- <i>g</i> -DPNR	79
(1) DSC analysis of NVCL- <i>g</i> -DPNR	79
(2) TGA analysis of NVCL- <i>g</i> -DPNR	80
4.2.2.4 Effect of reaction parameters on grafting ratio of NVCL- <i>g</i> -DPNR	82
(1) Effect of monomer concentration	82
(2) Effect of initiator concentration	83
(3) Effect of reaction temperature	84
(4) Effect of reaction time	85
4.2.2.5 Investigation of temperature-responsive behaviors of NVCL- <i>g</i> -DPNR	85
(1) The water absorption measurement of NVCL- <i>g</i> -DPNR	85
(2) The contact angle determination of NVCL- <i>g</i> -DPNR	87
(3) Dye adsorption and desorption studies of NVCL- <i>g</i> -DPNR	88
4.2.2.6 Adsorption studies of NVCL- <i>g</i> -DPNR	91

	(7)
CHAPTER 5 CONCLUSIONS AND RECOMMENDATIONS	94
5.1 Conclusions	94
5.2 Recommendations for future work	96
REFERENCES	97
APPENDICES	112
APPENDIX A EFFECT OF REACTION PARAMETERS ON REACTION EFFICIENCY	113
APPENDIX B THE WATER ABSORPTION MEASUREMENT	115
APPENDIX C THE CONTACT ANGLE DETERMINATION	121
APPENDIX D ADSORPTION STUDIES	125
APPENDIX E DYE RELEASE STUDIES	127
APPENDIX F PUBLICATIONS	133
BIOGRAPHY	147

LIST OF TABLES

Tables	Page
2.1 Components of NR latex	6
2.2 Properties of NR	7
2.3 Research involved the graft copolymerization of NR	13
2.4 Distribution of centrifuged NR latex and its properties	16
2.5 Nitrogen content in several types of NR latex	18
2.6 Comparison between our proposed research and other related studies	26
3.1 Variable parameters used for preparation of PNVCL-NR	29
3.2 Variable parameters used for preparation of NVCL-g-DPNR	32
3.3 Type of adsorption process depending on the equilibrium parameter of the Langmuir adsorption isotherm	37
3.4 Type of adsorption process depending on the adsorption intensity of the Freundlich adsorption isotherm	38
3.5 Type of adsorption process depending on the B constant corresponded with heat of adsorption of the Temkin adsorption isotherm	39
3.6 Type of adsorption process depending on the mean sorption energy of the Dubinin-Radushkevich adsorption isotherm	40
3.7 Mathematical equations used for each adsorption isotherm	41
4.1 Assignment of corresponding FT-IR spectra for NVCL and PNVCL	46
4.2 Assignment of corresponding ¹ H-NMR spectra for NVCL and PNVCL	49
4.3 Average molecular weights and dispersity of PNVCL	50
4.4 Assignment of corresponding FT-IR spectra for NR, PNVCL, and PNVCL-NR	53
4.5 Percentage of indigo carmine loading into NR and PNVCL-NR	66

4.6	Constants of each adsorption isotherm for the adsorption process of indigo carmine onto PNVCL-NR surface	70
4.7	CHN results of NR and DPNR	71
4.8	Assignment of corresponding FT-IR spectra for DPNR, PNVCL, and NVCL- <i>g</i> -DPNR	75
4.9	Assignment of corresponding ¹ H-NMR spectra for DPNR, PNVCL, and NVCL- <i>g</i> -DPNR	78
4.10	Percentage of indigo carmine loading into DPNR and NVCL- <i>g</i> -DPNR	89
4.11	Constants of each adsorption isotherm for the adsorption process of indigo carmine onto NVCL- <i>g</i> -DPNR surface	93
A.1	The amount of each variable parameter for the crosslinking reaction	113
A.2	The amount of each variable parameter for the graft copolymerization	114
B.1	Degree of water swelling of NR	115
B.2	Degree of water swelling of PNVCL-NR (31% gel content)	116
B.3	Degree of water swelling of PNVCL-NR (19% gel content)	117
B.4	Degree of water swelling of DPNR	118
B.5	Degree of water swelling of NVCL- <i>g</i> -DPNR (25% grafting ratio)	119
B.6	Degree of water swelling of NVCL- <i>g</i> -DPNR (15% grafting ratio)	120
C.1	Contact angle of NR	121
C.2	Contact angle of PNVCL-NR (31% gel content)	122
C.3	Contact angle of DPNR	123
C.4	Contact angle of NVCL- <i>g</i> -DPNR (25% grafting ratio)	124
D.1	Parameters for linear plotting in adsorption isotherms of indigo carmine onto PNVCL-NR (31% gel content) surface	125
D.2	Parameters for linear plotting in adsorption isotherms of indigo carmine onto NVCL- <i>g</i> -DPNR (25% grafting ratio) surface	126

LIST OF FIGURES

Figures	Page
1.1 Chemical structure of <i>cis</i> -1,4-polyisoprene	1
1.2 (a) NR products in Thailand, (b) shares of world exports, and (c) price of NR in Thailand	2
1.3 Chemical structures of temperature-responsive polymer of (a) poly(2-isopropyl-2-oxazolines) (PIOZ), (b) poly(dimethyl aminoethyl methacrylate) (PDMAEMA), (c) poly(<i>N</i> -isopropylacrylamide) (PNIPAM), (d) poly(<i>N,N'</i> -diethylacrylamide) (PDEAAM), (e) poly(methyl vinyl ether) (PMVE), and (f) poly(<i>N</i> -vinylcaprolactam) (PNVCL)	3
2.1 Degradation mechanisms of polyisoprene backbone from (a) acidic medium, (b) alkaline and neutral medium, and (c) photo oxidation	8
2.2 Chemical modifications of NR	9
2.3 Decomposition mechanism of BPO	10
2.4 Three allylic positions of NR	11
2.5 Schematic illustration for abstraction and addition reactions of NR	12
2.6 (a) Proposed structure of NR particles in the spherical shape with hydrophobic rubber at core-shell held by proteins in outer layer and phospholipids in inner layer, respectively and (b) layer thickness of the mixed layer between proteins and phospholipids	15
2.7 High speed centrifugation of NR latex	17
2.8 Schematic illustration of deproteinization process using urea treatment	18
2.9 Schematic illustration of phase diagram for polymer solution in (a) LCST and (b) UCST systems	19
2.10 The change in color of polymer solution at below and above LCST	20
2.11 The chain-growth mechanism for synthesis of PNVCL	22

2.12	Schematic illustration of temperature induced phase transition of PNVCL	23
2.13	Several architectures of PNVCL	24
2.14	Water swelling percentage as a function of temperature of SR-g-(NVCL-co-NVIM) (90% grafting ratio)	25
2.15	(a) Effect of the temperature on the swelling percentage of SR-g-(NVCL-co-MAA) in a buffer solution (pH 3) at different grafting ratios and (b) releasing percentage of nystatin from SR-g-(NVCL-co-MAA) at different grafting ratios	26
3.1	Schematic illustration for deproteinization of NR latex by urea treatment	31
4.1	Diagram for preparation of PNVCL	45
4.2	FT-IR spectra of (a) NVCL and (b) PNVCL	46
4.3	¹ H-NMR spectra of (a) NVCL and (b) PNVCL	48
4.4	Diagram for preparation of PNVCL-NR	50
4.5	Synthetic route of polymer radicals on NR and PNVCL molecules through hydrogen abstraction process	51
4.6	Photograph images of (a) insoluble PNVCL-NR in any organic solvents, (b) NR, and (c) PNVCL-NR	52
4.7	FT-IR spectra of (a) NR, (b) PNVCL, and (c) PNVCL-NR (31% gel content)	53
4.8	XPS spectra of NR and PNVCL-NR (31% gel content). The inset shows the multiplex-scan spectra in the N _{1s} region	55
4.9	DSC thermograms of (a) NR, (b) PNVCL, and (c) PNVCL-NR (31% gel content)	56
4.10	TGA thermograms of NR, PNVCL, and PNVCL-NR (31% gel content)	57
4.11	DTG thermograms of NR, PNVCL, and PNVCL-NR (31% gel content)	58
4.12	Effect of PNVCL concentration on gel content	59
4.13	Effect of BPO concentration on gel content	59
4.14	Effect of reaction temperature on gel content	60

4.15	Effect of reaction time on gel content	61
4.16	(a) Crosslink density and (b) degree of swelling of PNVCL-NR as a function of gel content	62
4.17	Degree of swelling of NR and PNVCL-NR (19 and 31% gel contents) in water as a function of temperature	63
4.18	Contact angles of NR and PNVCL-NR (31% gel content) as a function of temperature	64
4.19	UV-visible spectra of standard indigo carmine solution and solutions after immersion of NR and PNVCL-NR (19 and 31% gel contents)	65
4.20	UV-visible spectra of solutions after desorption of indigo carmine from (a) NR, (b) PNVCL-NR (31% gel content), and (c) PNVCL-NR (19% gel content) at different temperatures, and (d) release profiles of indigo carmine from NR and PNVCL-NR samples at $\lambda_{\max} = 610$ nm	67
4.21	Photograph images of NR and PNVCL-NR (31% gel content) after desorption	67
4.22	Linear plots of (a) Langmuir, (b) Freundlich, (c) Temkin, and (d) Dubinin-Radushkevich adsorption isotherms for the adsorption process of indigo carmine onto PNVCL-NR (31% gel content) surface	68
4.23	Plot between equilibrium parameter and initial dye concentration for the adsorption process of indigo carmine onto PNVCL-NR (31% gel content) surface	69
4.24	Diagram for preparation of NVCL- <i>g</i> -DPNR	72
4.25	Locus of the graft copolymerization in the case of AIBN initiator used	73
4.26	Photograph images of (a) DPNR and (b) NVCL- <i>g</i> -DPNR	74
4.27	FT-IR spectra of (a) DPNR, (b) PNVCL, and (c) NVCL- <i>g</i> -DPNR (25% grafting ratio)	75
4.28	¹ H-NMR spectra of (a) DPNR, (b) PNVCL, and (c) NVCL- <i>g</i> -DPNR (25% grafting ratio)	77

4.29	XPS spectra of DPNR and NVCL- <i>g</i> -DPNR (25% grafting ratio). The inset shows the multiplex-scan spectra in the N _{1s} region	79
4.30	DSC thermograms of (a) DPNR, (b) PNVCL, and (c) NVCL- <i>g</i> -DPNR (25% grafting ratio)	80
4.31	TGA thermograms of DPNR, PNVCL, and NVCL- <i>g</i> -DPNR (25% grafting ratio)	81
4.32	DTG thermograms of DPNR, PNVCL, and NVCL- <i>g</i> -DPNR (25% grafting ratio)	82
4.33	Effect of NVCL concentration on grafting ratio	83
4.34	Effect of AIBN concentration on grafting ratio	84
4.35	Effect of reaction temperature on grafting ratio	84
4.36	Effect of reaction time on grafting ratio	85
4.37	Degree of swelling of DPNR and NVCL- <i>g</i> -DPNR (15 and 25% grafting ratios) in water as a function of temperature	86
4.38	Contact angles of DPNR and NVCL- <i>g</i> -DPNR (25% grafting ratio) as a function of temperature	87
4.39	UV-visible spectra of standard indigo carmine solution and solutions after immersion of DPNR and NVCL- <i>g</i> -DPNR (15 and 25% grafting ratios)	88
4.40	Interaction between hydrophilic caprolactam groups of NVCL units in NVCL- <i>g</i> -DPNR with amino groups of indigo carmine	89
4.41	UV-visible spectra of solutions after desorption of indigo carmine from (a) DPNR, (b) NVCL- <i>g</i> -DPNR (25% grafting ratio), and (c) NVCL- <i>g</i> -DPNR (15% grafting ratio) at different temperatures, and (d) release profiles of indigo carmine from DPNR and NVCL- <i>g</i> -DPNR samples at $\lambda_{\max} = 610$ nm	90
4.42	Photograph images of DPNR and NVCL- <i>g</i> -DPNR (25% grafting ratio) after desorption	91
4.43	Linear plots of (a) Langmuir, (b) Freundlich, (c) Temkin, and (d) Dubinin-Radushkevich adsorption isotherms for the adsorption process of indigo carmine onto NVCL- <i>g</i> -DPNR (25% grafting ratio) surface	92

4.44	Plot between equilibrium parameter and initial dye concentration for the adsorption process of indigo carmine onto NVCL- <i>g</i> -DPNR (25% grafting ratio) surface	92
E.1	UV-visible spectra and release profiles (at $\lambda_{\max} = 610$ nm) of solution after desorption of indigo carmine from NR as a function of temperature and time	127
E.2	UV-visible spectra and release profiles (at $\lambda_{\max} = 610$ nm) of solution after desorption of indigo carmine from PNVCL-NR (31% gel content) as a function of temperature and time	128
E.3	UV-visible spectra and release profiles (at $\lambda_{\max} = 610$ nm) of solution after desorption of indigo carmine from PNVCL-NR (19% gel content) as a function of temperature and time	129
E.4	UV-visible spectra and release profiles (at $\lambda_{\max} = 610$ nm) of solution after desorption of indigo carmine from DPNR as a function of temperature and time	130
E.5	UV-visible spectra and release profiles (at $\lambda_{\max} = 610$ nm) of solution after desorption of indigo carmine from NVCL- <i>g</i> -DPNR (25% grafting ratio) as a function of temperature and time	131
E.6	UV-visible spectra and release profiles (at $\lambda_{\max} = 610$ nm) of solution after desorption of indigo carmine from NVCL- <i>g</i> -DPNR (15% grafting ratio) as a function of temperature and time	132

LIST OF ABBREVIATIONS

Symbols/Abbreviations	Terms
FT-IR	Fourier transform infrared spectroscopy
$^1\text{H-NMR}$	^1H nuclear magnetic resonance spectroscopy
XPS	X-ray photoelectron spectroscopy
DSC	Differential scanning calorimetry
TGA	Thermogravimetric analysis
DTG	Derivative thermogravimetric analysis
GPC	Gel permeation chromatography
UV-vis	Ultraviolet-visible spectroscopy
CHN	Carbon hydrogen nitrogen analysis
TEM	Transmission electron microscopy
M_n	Number-average molecular weight
M_w	Weight-average molecular weight
M_z	Z-average molecular weight
\bar{D}	Dispersity
T_g	Glass transition temperature
UV	Ultraviolet
λ	Lambda
α	Alpha
γ	Gamma
ca	Circa
Mg	Magnesium
K	Potassium
R^2	Correlation coefficient
LCST	Lower critical solution temperature
UCST	Upper critical solution temperature
DRC	Dry rubber content

TSC	Total solid content
phr	Parts per hundred of rubber
G	Grafting ratio
NR	Natural rubber
DNR	Dry natural rubber
DPNR	Deproteinized natural rubber
SR	Silicone rubber
PNVCL-NR	Crosslinked material
NVCL- <i>g</i> -DPNR	Grafted material
IPN	Interpenetrating polymer networks
ATRP	Atomic transfer radical polymerization
TiO ₂	Titanium dioxide
GO	Graphene oxide
SDS	Sodium dodecyl sulfate
KOH	Potassium hydroxide
DI	Deionized
CDCl ₃ -d	Deuterated chloroform
THF	Tetrahydrofuran
PNVCL	Poly(<i>N</i> -vinylcaprolactam)
PNIPAM	Poly(<i>N</i> -isopropylacrylamide)
PS	Polystyrene
PAA	Poly(acrylic acid)
PAM	Polyacrylamide
PEG	Poly(ethylene glycol)
PEGMA	Poly(ethylene glycol) methacrylate
PET	Poly(ethylene terephthalate)
PNVP	Poly(<i>N</i> -vinyl-2-pyrrolidone)
PDMAEMA	Poly(dimethyl aminoethyl methacrylate)
PIOZ	Poly(2-isopropyl-2-oxazolines)
PDEAAM	Poly(<i>N,N'</i> -diethylacrylamide)
PMVE	Poly(methyl vinyl ether)

PVC	Poly(vinyl chloride)
NVCL	<i>N</i> -vinylcaprolactam
NVP	<i>N</i> -vinylpyrrolidone
NVIM	<i>N</i> -vinylimidazole
MA	Maleic anhydride
MMA	Methyl methacrylate
MAA	Methacrylic acid
MPC	2-methacryloyloxyethyl phosphorylcholine
DMAEMA	Dimethyl aminoethyl methacrylate
DMAMP	Dimethyl(acryloyloxy methyl) phosphonate
DMMEP	Dimethyl(methacryloyloxy ethyl) phosphonate
DE	Diethyl aminomethyl methacrylate
GMA	Glycidyl methacrylate
HEMA	2-hydroxyethyl methacrylate
BPO	Benzoyl peroxide
DCP	Dicumyl peroxide
AIBN	2,2'-azobisisobutyronitrile
KPS	Potassium persulfate
TEPA	Tetraethylene pentamine
CHP	Cumene hydroperoxide
V70	2,2'-azobis(4-methoxy-2,4-dimethyl valeronitrile)
DEDT-Na	Sodium <i>N,N</i> -diethyldithiocarbamate trihydrate
TBAB	Tetrabutylammonium bromide
3D	Three-dimensional
CQDs	Carbon quantum dots

CHAPTER 1

INTRODUCTION

1.1 State of problems

With regards to the environmental problems, limited materials and petrochemical resources, natural rubber (NR) has received a big deal of interests in the respect towards the utilization of eco-friendly materials. It is a renewable resource obtained from the bark of *Hevea brasiliensis* tree in the form of milky white or pale yellow fluid and its structure contains mostly 100% *cis*-1,4-polyisoprene as illustrated in Figure 1.1 [1]. Obviously, it has attracted wide attention for applications in many industries particularly automobile and glove factory, since it possesses excellent physical properties such as high tensile strength, fatigue resistance, good flexibility at low temperature, and abrasion resistance.

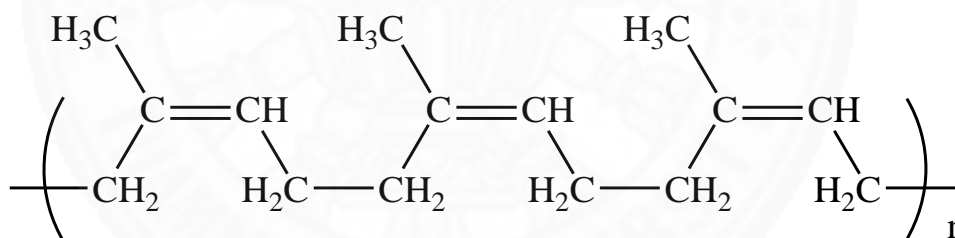


Figure 1.1 Chemical structure of *cis*-1,4-polyisoprene.

Nowadays, Thailand is the world's largest rubber producer and also the exporter of many rubber products such as ribbed smoked sheet, concentrated latex, compound rubber, and block rubber. However, the NR industries as well as rubber producers, suffer from the continued collapse in prices of NR as presented in Figure 1.2 [2-4]. As a result, adding new properties to NR is the brilliant method that sorts out this problem, increases the value, and expands a range of applications of NR.

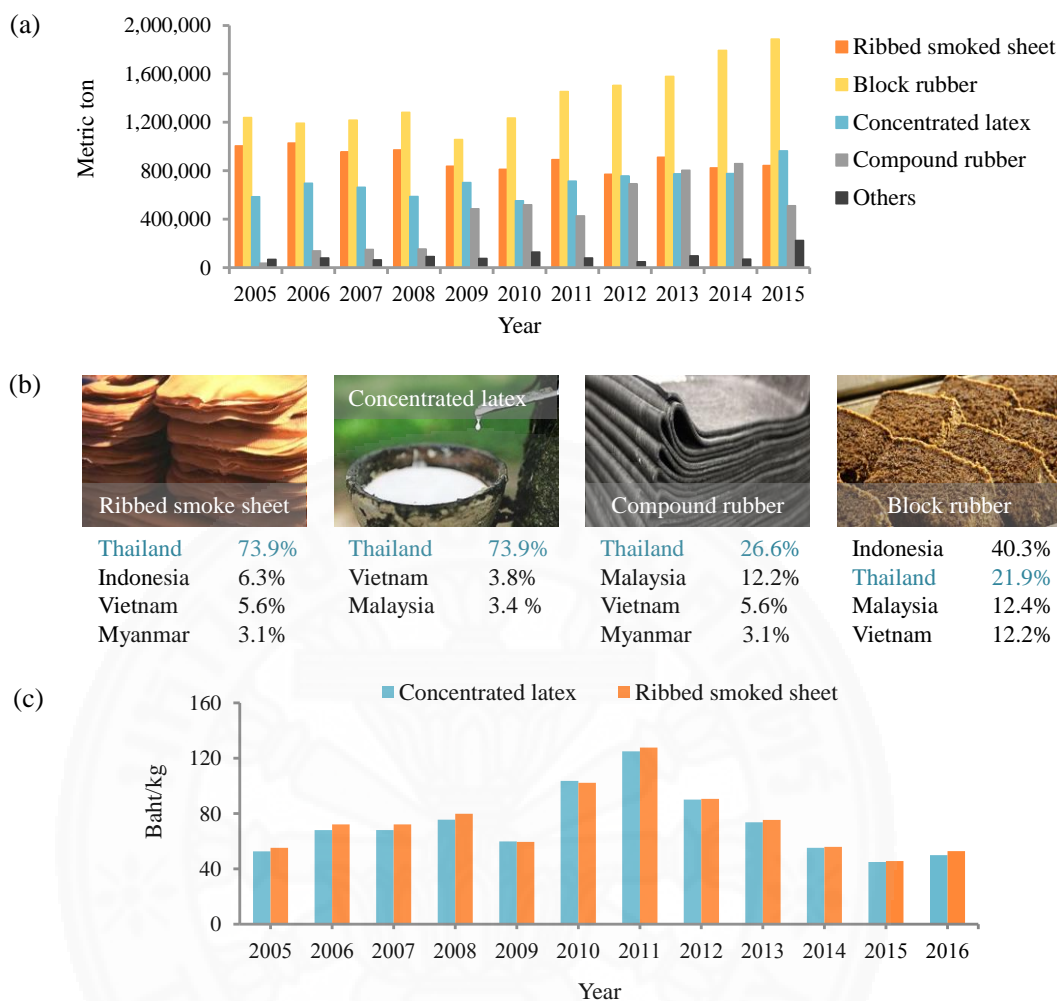


Figure 1.2 (a) NR products in Thailand, (b) shares of world exports, and (c) price of NR in Thailand [2-4].

Among the temperature-responsive polymers as illustrated in Figure 1.3. Poly(*N*-vinylcaprolactam) (PNVCL) is becoming increasingly interesting recently, because it expresses the superior properties over the others in the biomedical fields including benign, good biocompatibility, and biodegradability. Indeed, the higher biocompatibility of PNVCL resulted from its cyclic amide structure. Hence, it is stable against hydrolysis reaction and its hydrolysis does not generate toxic amide, unlike an aliphatic polymer such as poly(*N*-isopropylacrylamide) (PNIPAM) [5,6]. Therefore, the use of PNIPAM in biomedical applications may be suppressed due to its higher toxicity compared to PNVCL. Additionally, PNVCL exhibits the coil-to-

globule transition temperature around 32-34 °C, which is close to human body temperature. This temperature region depends on the molecular weight of the polymer, polymer concentration, and the composition of the solution [7,8]. As a result from its advantages as aforementioned, it is widely used to create novel temperature-responsive materials for widening the range of applications emphasized on biomedical and pharmaceutical fields, such as controlled drug medical devices [9-12], sensors [13,14], and tissue engineering [15,16].

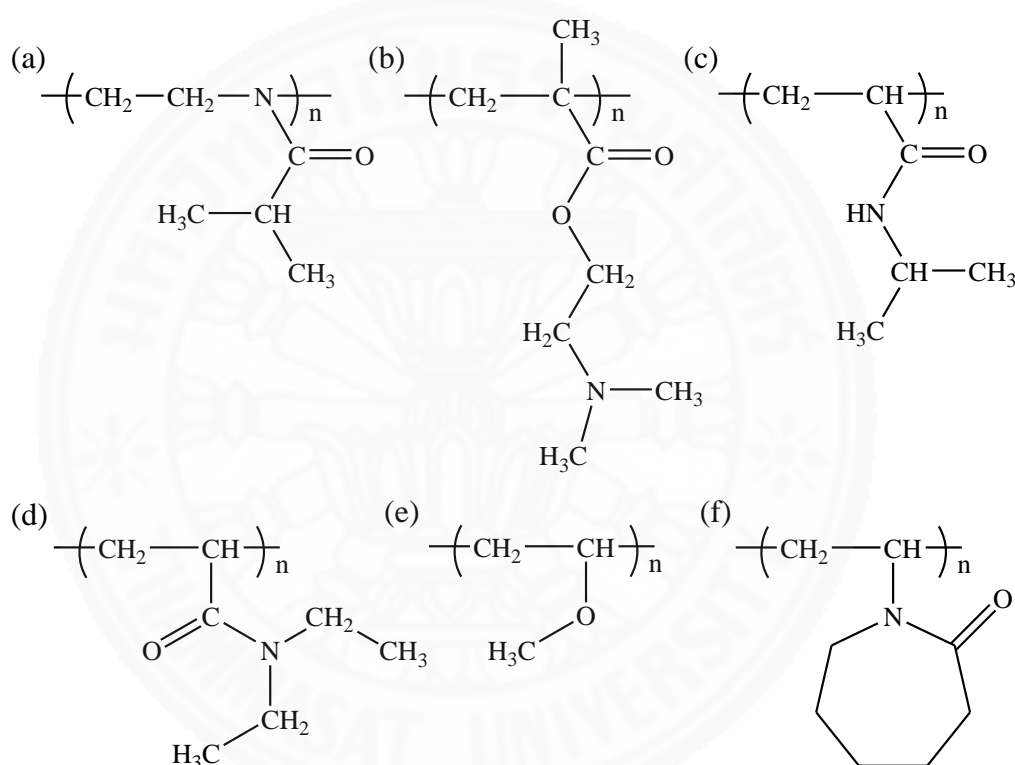


Figure 1.3 Chemical structures of temperature-responsive polymer of (a) poly (2-isopropyl-2-oxazolines) (PIOZ), (b) poly(dimethyl aminoethyl methacrylate) (PDMAEMA), (c) poly(*N*-isopropylacrylamide) (PNIPAM), (d) poly(*N,N'*-diethylacrylamide) (PDEAAM), (e) poly(methyl vinyl ether) (PMVE), and (f) poly (*N*-vinylcaprolactam) (PNVCL).

Herein, we present a facile method for functionalizing *N*-vinylcaprolactam (NVCL) and its polymer which is a temperature-responsive polymer, with NR through crosslinking and graft copolymerization in order to endow the NR with

temperature responsiveness. Although several types of materials have been incorporated with NR, they have only improved the mechanical or chemical properties, while the introduction of responsive functions into NR has never been reported. Therefore, the synthetic NVCL-based thermosensitive materials would enhance a broad variety in valuable applications such as biomedical, pharmaceutical, and sensing fields.

1.2 Research objectives

The objectives of this research work are detailed as follows,

- 1.2.1 To prepare the NVCL-functionalized NR.
- 1.2.2 To study the effect of reaction parameters on reaction efficiency including the monomer and polymer concentrations, initiator concentration, reaction temperature, and reaction time.
- 1.2.3 To characterize the chemical structures, thermal properties, temperature-responsive behaviors, and also adsorption studies.

1.3 Scope and limitations of the study

- 1.3.1 Synthesize the NVCL-functionalized NR materials with temperature responsiveness through crosslinking and graft copolymerization.
- 1.3.2 Study the effect of reaction parameters on reaction efficiency of NVCL-functionalized NR materials.
 - 1.3.2.1 Polymer concentration (in case of crosslinking reaction).
 - 1.3.2.2 Monomer concentration (in case of graft copolymerization).
 - 1.3.2.3 Initiator concentration.
 - 1.3.2.4 Reaction temperature.
 - 1.3.2.5 Reaction time.
- 1.3.3 Characterize the NVCL-functionalized NR materials.
 - 1.3.3.1 Chemical structures.

1.3.3.2 Thermal properties.

1.3.3.3 Temperature-responsive behaviors.

- (1) The water absorption measurement.
- (2) The contact angle determination.
- (3) Dye adsorption and desorption studies.

1.3.3.4 Adsorption studies.

1.3.3.5 Crosslink density (in case of crosslinking reaction).



CHAPTER 2

REVIEW OF LITERATURE

2.1 Natural rubber (NR)

NR is a highly flexible elastomer made from the linkage of isoprene units. Typically, NR molecules consist of unsaturated double bonds with a long chain of *cis*-1,4-polyisoprene polymer. The fresh milky latex acquired from the bark of *Hevea brasiliensis* tree is a naturally colloidal substance dispersed in an aqueous medium, sometimes known as serum. This latex has a range of pH around 6.5-7.0 and density of 0.98 g/mL [17]. Besides, the major components in latex compose of the rubber fraction (ca. 36%) in water (ca. 59%) with some non-rubber components (ca. 5%) including proteins, phospholipids, carbohydrates, and other minor substances such as amino acids and soluble salts of magnesium (Mg) and potassium (K) as tabulated in Table 2.1 [18].

Table 2.1 Components of NR latex [18].

Components	Amount (wt%)
Total solid content (TSC)	41.50
• Dry rubber content (DRC)	36.00
• Proteins	1.60
• Phospholipids	0.60
• Amino acids	0.30
• Neutral lipids	1.00
• Carbohydrates	1.50
• Salts (mainly K and Mg)	0.50
Water	58.50

The widespread uses of NR such as tire, glove, conveyor belt, and several other rubber-based materials, increased tremendously from the past until now due to the fact that it exhibits miscellaneous exceptional properties. One of the essential properties of NR is the high elasticity because of the freely rotating links of its long chain molecules [19]. Also, the crystallization of NR induced by strain brings about the high tensile strength and abrasion resistance [20]. Aside from the properties as stated, the further properties of NR are summarized in Table 2.2.

Table 2.2 Properties of NR [21].

Properties	Proficiency level		
	★★★	★★	★
Elongation	✓		
Tear and cut resistance	✓		
Adhesion to metal	✓		
Gas permeability			✓
Air resistance		✓	
Alcohol resistance		✓	
Water resistance	✓		
Acid and base resistance		✓	

Although NR has many excellent properties as mentioned, the drawbacks of NR remain a serious concern. Owing to their molecules contain the unsaturated double bond in the main chain of polyisoprene, which is deteriorated upon exposure to oxidation, weathering, heat, ozone, and other chemicals or solvents. As shown in Figure 2.1, the unwanted reactions such as crosslinking and chain scission can take place on the polyisoprene backbone [22,23]. Accordingly, various methods have been developed to mend and improve its properties through chemical modifications.

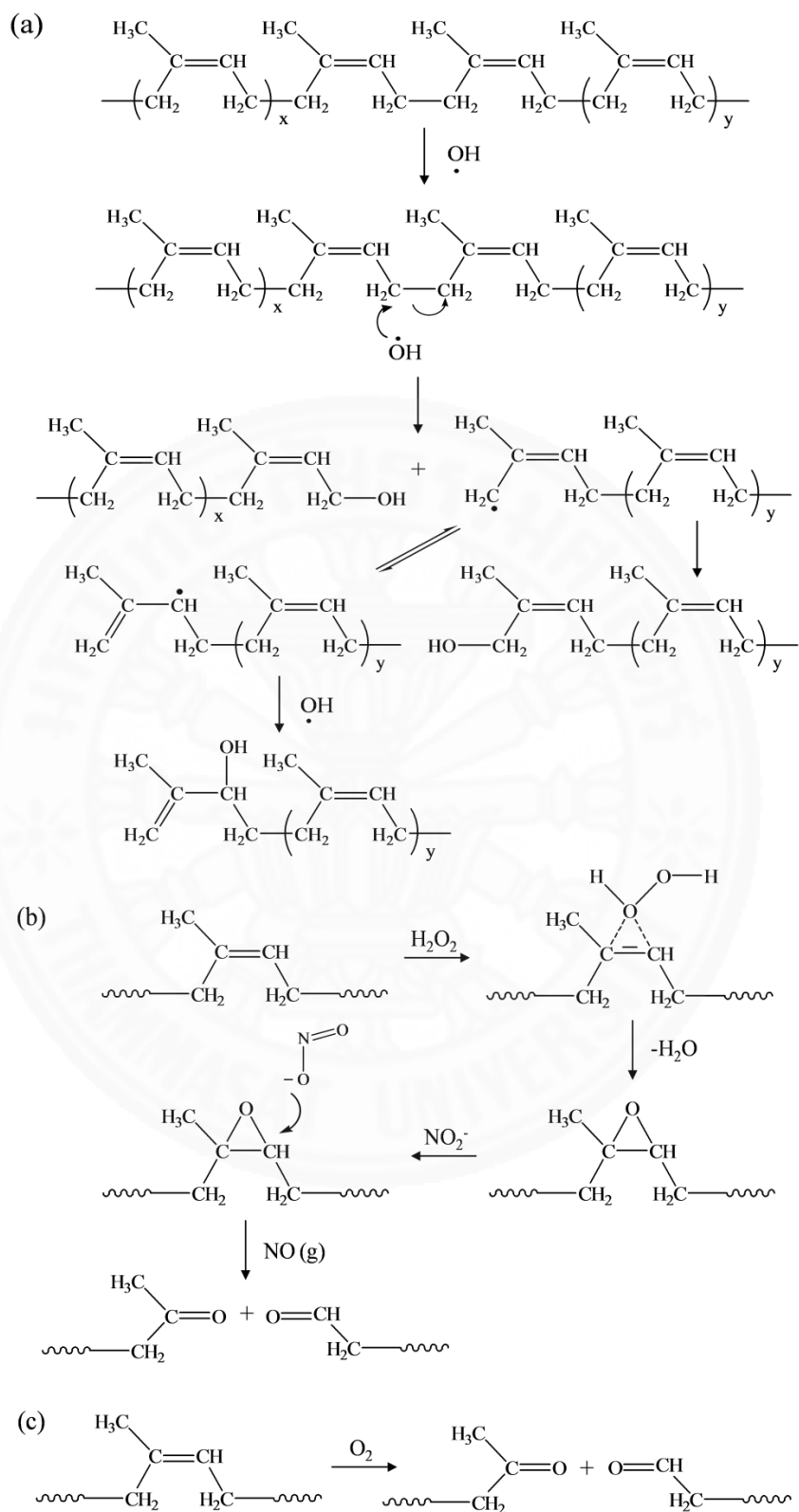


Figure 2.1 Degradation mechanisms of polyisoprene backbone from (a) acidic medium, (b) alkaline and neutral medium, and (c) photo oxidation [22,23].

2.2 Chemical modification of NR

In agreement with the problems of NR as described above, the NR has been not only modified but also introduced with the new functionalities placed on the unsaturated double bonds in polyisoprene molecules as shown in Figure 2.2. One of the straightforward methods is based on the addition reactions such as chlorination [24], hydrogenation [25,26], and bromination [27,28]. Furthermore, the modification of the properties of NR can be performed *via* cyclization [29], epoxidation [30], crosslinking [31-33], and graft copolymerization [34-37].

In this thesis work, we focus on crosslinking and grafting processes, because nowadays both of them are the popular methods that have been extremely utilized to functionalize NR with monomers or polymers in order to fabricate the novel rubber-based materials.

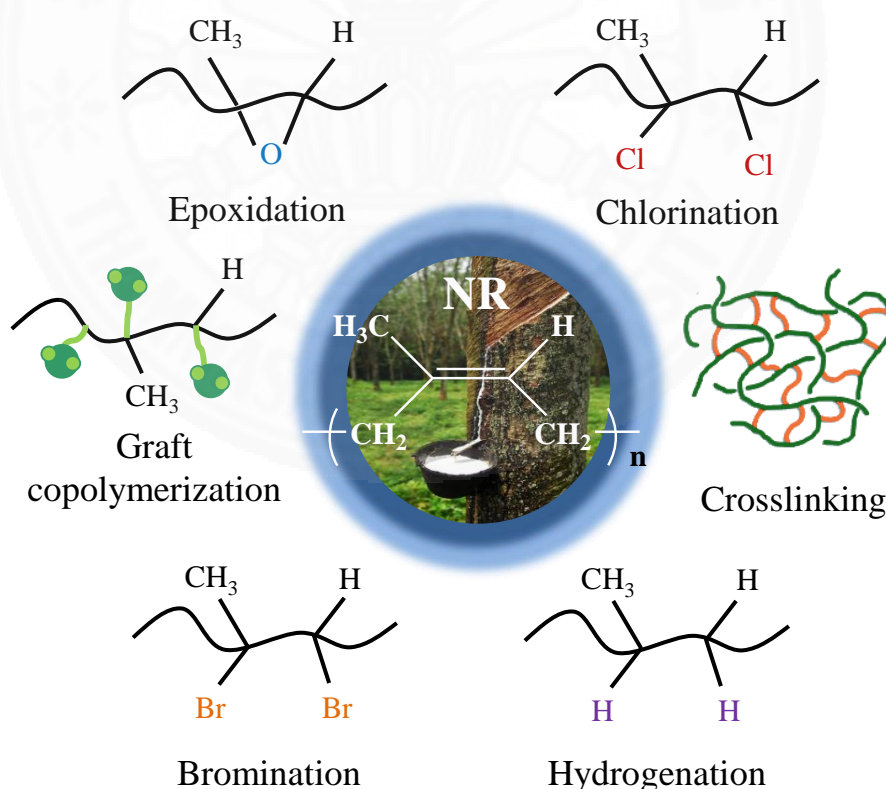


Figure 2.2 Chemical modifications of NR.

2.2.1 Crosslinking reaction of NR

Crosslinking is one of the attractive methods that increases the chemical stability and mechanical strength of the NR. The well-known crosslinking reaction of NR is vulcanization, in which the long chain of *cis*-1,4-polyisoprene molecules become connected all together to form three-dimensional (3D) structure *via* the disulfide linkages. The 3D structure can generate the restriction of the free mobility of the long chain molecules of NR and convert the soft materials into strong ones. Moreover, the enhancement of elasticity, resistance to solvents and chemicals, and an increase in modulus and hardness characteristics over a wide range of temperature are the superior properties which belong to the crosslinked materials.

Based on the preceding works, the formation of insoluble polymer and network structures through crosslinking reaction was accomplished by wide range of techniques. In general, there are several common crosslinking techniques, including radiation crosslinking, sulfur crosslinking, peroxide crosslinking, and silane crosslinking that have been performed to couple various monomers and polymers with NR in order to originate the novel materials with excellent mechanical properties [32,33,38,39]. As stated previously, the sulfur and peroxide crosslinking techniques have always been extensively applied due to they are the simple operation and also give high efficiency to form the network materials, [40,41]. The peroxide initiators such as benzoyl peroxide (BPO) and dicumyl peroxide (DCP), consist of labile oxygen linkage, which usually serves as the source of oxygen-centered free radical species as illustrated in Figure 2.3. These radicals are relatively reactive towards the abstraction of hydrogen atoms from the backbone of the polymer chain.

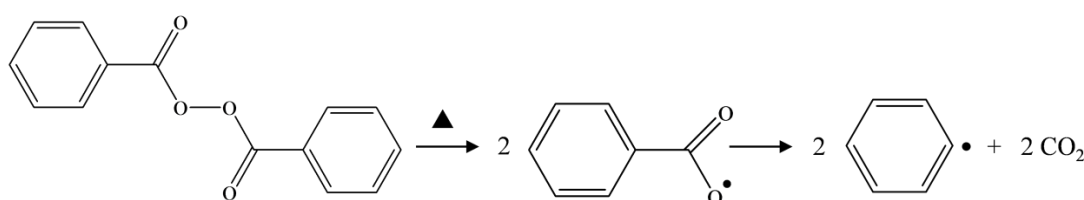


Figure 2.3 Decomposition mechanism of BPO.

In recent decades, the attention was paid onto the use of peroxide substances which play a crucial role as an initiator and also a crosslinker for synthesis of the crosslinked materials. For example, Mathew, A.P. and coworkers studied the preparation and effect of degree of crosslinking on the characteristics of interpenetrating polymer networks (IPN) that combined styrene with NR using various techniques, such as peroxide, conventional, and mixed vulcanization techniques. As a result, it was reported that the peroxide system exhibited the good performance in the case of lowest uptake, compared with the other techniques to fabricate the network materials. [33]. Besides, the similar finding was observed the mechanical properties and morphological features of full-IPN from NR and polystyrene (PS) affected by the quantity of crosslinking agents including 2,2'-azobisisobutyronitrile (AIBN) and peroxide initiators using BPO and DCP. They revealed that the higher amount of crosslinking agent and initiator led to an increase in the mechanical properties of material [32]. In addition to these works, BPO had been vastly applied in other researches for preparation of elastomer-based network materials such as epoxidized-NR [42] and silicone gum [43].

The majority of research works had been studied on the formation of network materials of NR. They reported that the crosslinking reaction of NR was mostly initiated from free radical species through hydrogen abstraction at the allylic site. The reactivities of the three allylic sites in polyisoprene molecules were found to be 11 : 3 : 1 for positions (a) : (b) : (c), respectively (Figure 2.4) [44,45]. Thus, it was postulated that the allylic hydrogen abstraction greatly took place at positions (a) and (b) against (c). This was because the dissociation energy of C-H linkages at the sites (a) and (b) were relatively weak, compared to other positions [46].

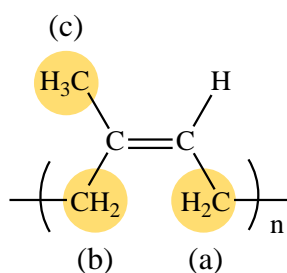


Figure 2.4 Three allylic positions of NR.

2.2.2 Graft copolymerization of NR

Graft copolymerization is a procedure in which secondary monomer or polymer is appended covalently to the backbone of the polymer substrate. Several techniques such as radiation, emulsion, and also solution that have been used for grafting reaction. Graft copolymerization affects the morphology and characteristic of the resulting product which are strongly influenced by the technique, type of monomer or polymer, and compatibility between two substances in the system. There are two main types of technique that are often used to create the graft copolymer of NR, including solution and emulsion polymerization [34,47]. Among them, emulsion polymerization is preferred for grafting reaction, as it will not provide the negative impacts to the environment and human health from the use of organic solvents, as well as NR is spontaneously available in the latex state. Nonetheless, many studies had been reported that the grafting efficiency from the fresh NR latex was not well enough because of the presence of proteins in the latex [48]. Hence, to solve such problem, we should remove the proteins prior to the graft copolymerization.

Generally, the possible grafting modification of NR with a wide range of polymers and monomers may occur in two different pathways including the abstraction of the allylic hydrogen atom and the addition of the radicals into the unsaturated double bond as displayed in Figure 2.5 [49]. The radical species cleave from the initiator can promote the active grafting sites on the rubber backbone through two approaches as stated and then generate the polyisoprene radicals. Subsequently, polymer radicals will interact with desirable polymers or monomers, giving to graft copolymer.

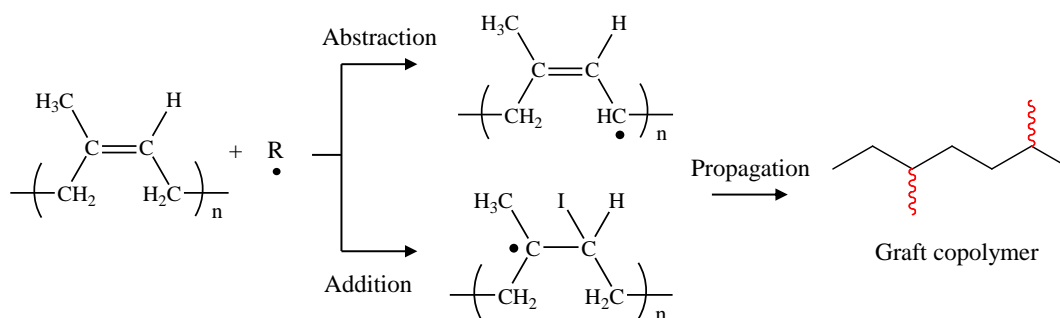


Figure 2.5 Schematic illustration for abstraction and addition reactions of NR.

Previously, there were several works studied on grafting of NR with monomers or polymers with a goal to achieve novel and desirable properties of NR using different types of initiating sources such as ultraviolet (UV) light, high energy radiation, mainly gamma (γ) ray, and chemical initiator as summed up in Table 2.3.

Table 2.3 Research involved the graft copolymerization of NR.

Initiators	Monomers	Applications	References
γ ray	Acrylonitrile	Oil and solvent resistance	[50]
	Styrene	-	[51]
	Butyl acrylate	Film tensile strength resistance	[52]
	Methyl methacrylate (MMA)	-	[53]
	Glycidyl methacrylate (GMA)	Enhancement the tensile strength of NR	[54]
	Diethyl amino methyl methacrylate (DE)		
	2-hydroxyethyl methacrylate (HEMA)		
UV light	MMA	Improving the mechanical properties of NR	[55]
	Polyacrylamide (PAM)	-	[56]
	Poly(ethylene glycol) methacrylate (PEGMA)	Improving the blood compatibility of NR	[57]
	<i>N</i> -vinylpyrrolidone (NVP)		
	2-methacryloyl oxyethyl phosphoryl choline (MPC)		

Table 2.3 (Continued) Research involved the graft copolymerization of NR.

Initiators	Monomers	Applications	References
Chemical initiators			
Cumene hydroperoxide (CHP) and tetraethylene pentamine (TEPA)	MMA	Materials resistant to organic solvents	[58]
	HEMA	Improving the adhesion of plywood	[59]
	Dimethyl aminoethyl methacrylate (DMAEMA)	Rubber-based modification of inorganic fillers	[60]
BPO	Maleic anhydride (MA)	Compatibilizer	[34]
	Copolymers between acrylonitrile and styrene	-	[61]
CHP and (2-methyl butyronitrile), 2,2'-azobis (4-methoxy-2,4-dimethylvalero nitrile) (V70)	Acrylates (methyl, ethyl, butyl, hexyl, and lauryl)	Film with hydrophobic surface and high stretch with no crack	[62]
Sodium <i>N,N</i> -diethyldithio carbamatetri hydrate (DEDT-Na), and tetrabutyl ammonium bromide (TBAB)	Dimethyl (acryloyloxy methyl) phosphonate (DMAMP) and dimethyl (methacryloyl ethyl) phosphonate (DMMEP)	Compatibilizer and flame retardant	[63]
Potassium persulfate (KPS)	Vinyl alcohol	-	[47]

2.3 Deproteinization of NR latex

The structure of NR latex particles had been explored in many studies [64-69]. According to the previous works, the particles of NR were generally spherical that comprised of an apparently homogeneous rubber at the core surrounded by the mixed layer of proteins and phospholipids in the range of thickness ca. 20 nm as shown in Figure 2.6. These components were believed to inhibit coalescence of NR latex particles. Moreover, they proposed that the surface layer of NR consists of mostly proteins about 84% and only 16% of phospholipids.

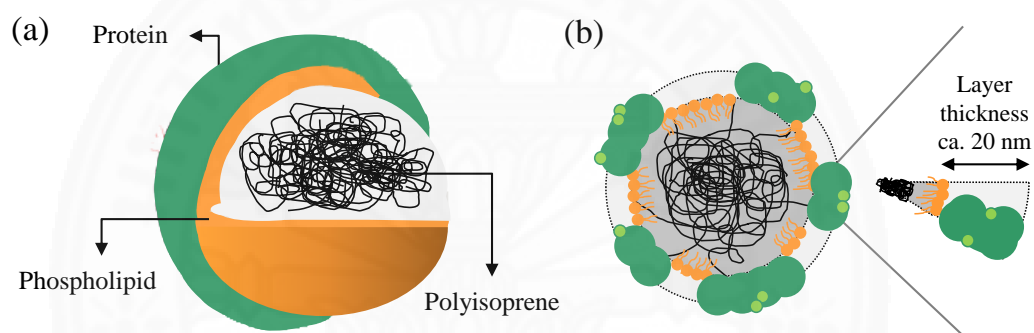


Figure 2.6 (a) Proposed structure of NR particles in the spherical shape with hydrophobic rubber at core-shell held by proteins in outer layer and phospholipids in inner layer, respectively and (b) layer thickness of the mixed layer between proteins and phospholipids [64].

When fresh NR latex is subjected to high-speed centrifugation, there is three major fractions as displayed in Figure 2.7. The rubber fraction is found on the top, the non-rubber particles known as Frey-Wyssling particles and C-serum are suspended between the rubber and bottom phase, and the last is the bottom phase that composed of minor substances. The distribution of centrifuged NR latex and its properties are depicted in Table 2.4.

Table 2.4 Distribution of centrifuged NR latex and its properties [70,71].

Fraction of latex	Percentage of protein concentration	Main compositions	Properties
Rubber particles	27	<ul style="list-style-type: none"> • <i>cis</i>-1,4-polyisoprene • Phospholipids 	<ul style="list-style-type: none"> • High flexibility
Frey Wyssling particles	-	<ul style="list-style-type: none"> • Clusters of carotenoids and luteins 	<ul style="list-style-type: none"> • Less dense than water • Negative zeta potential which immobilized the proteins and phospholipids on the rubber surface • Main reason caused the yellowish rubber upon exposure to environmental conditions
C serum	48	<ul style="list-style-type: none"> • Water soluble proteins, free amino acids, potassium ion, phosphate ion, and carbohydrates 	<ul style="list-style-type: none"> • Protein hydrolysis and buffers pH for stabilization
Bottom fraction	25	<ul style="list-style-type: none"> • Water soluble lipids, ash, inorganic components 	<ul style="list-style-type: none"> • Providing fatty acid from the degradation for stabilization and natural antioxidants

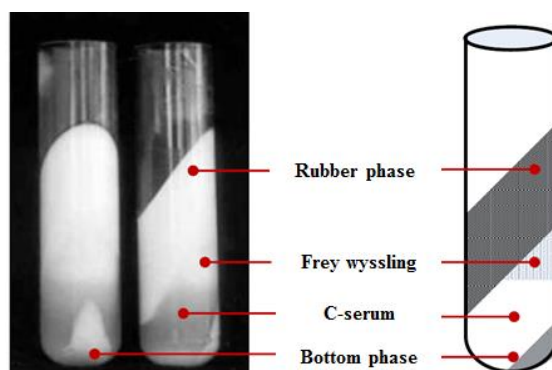


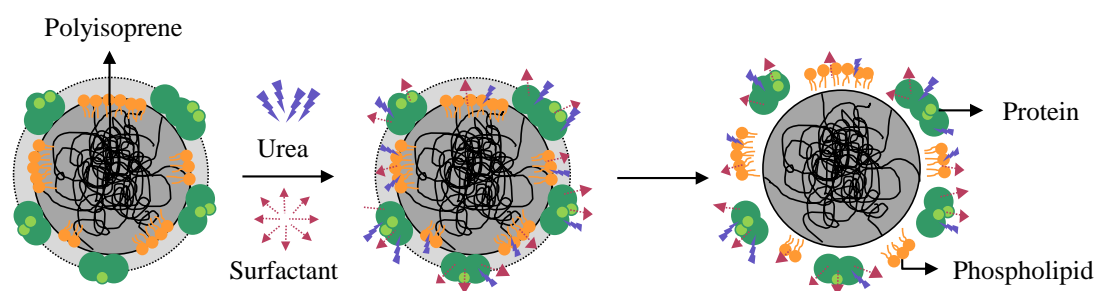
Figure 2.7 High speed centrifugation of NR latex [71].

The removal of proteins in NR latex is the important step due to these proteins reduce the reactivity of NR. Furthermore, recent studies revealed the allergic problems in many latex products, mainly glove resulted from the existence of proteins. The sweat could remove proteins and allow contact with skin, provoking the sensibilization and allergic reactions [72,73]. Besides, it was suggested that proteins would restrain the efficiency of graft copolymerization of NR latex and also generated the undesirable products during the polymerization, such as gel or branched network. According to proteins were also regarded as free radical scavengers and would terminate the free radical species [48,74,75]. Consequently, in most studies the proteins that surrounded the hydrophobic core of NR latex particles were removed prior to grafting operation to achieve the higher grafting efficiency. For example, graft copolymerization of deproteinized natural rubber (DPNR) latex with MMA [48], styrene [74,75], MA [76,77], and butyl acrylate [78] had been reported.

Several approaches had been discovered for removal of proteins in NR latex in order to prepare low proteins latex which also known as DPNR latex, such as saponification [79], surfactant washing [79-81], enzymatic treatment [73,79,81], and urea treatment [80-82]. These findings showed a considerable drop in the nitrogen content in NR latex after treatment, indicating the reduction of proteins as tabulated in Table 2.5. In this regard, urea treatment had caught much attention since it was a simple method, rapid, and remarkably effective owing to the fact that it could decrease the nitrogen content significantly in rubber latex, compared to other methods. Urea could denature proteins *via* hydrogen bonding (Figure 2.8) [83-85].

Table 2.5 Nitrogen content in several types of NR latex [79,81,82].

Specimens	Incubation temperature (K)	Incubation time (h)	Nitrogen content (wt%)
NR latex	-	-	0.380
Fresh NR latex	-	-	0.450
Saponified NR latex	343	3	0.120
Surfactant washed high ammonia NR latex	-	1	0.028
Surfactant washed fresh NR latex	-	1	0.088
Enzymatically deproteinized high ammonia NR latex	305	12	0.017
Enzymatically deproteinized fresh NR latex	305, 310	12	0.014
Urea treated high ammonia NR latex	303	1	0.020
Urea treated fresh NR latex	303	1	0.004

**Figure 2.8** Schematic illustration of deproteinization process using urea treatment.

2.4 Temperature-responsive polymer

Stimuli-responsive materials, also known as advanced materials, can undergo the abrupt changes in properties and morphologies upon exposure to the external stimuli such as magnetic field, electric field, light, pH, and also temperature. Due to the relative ease of control and safety, temperature is an external stimulus that gains much attention to be employed in various responsive systems.

There are two types of temperature-responsive polymers which showed different behaviors as displayed in Figure 2.9. If the polymer is completely miscible in solvent below a reliable temperature, giving a clear polymer solution, defined as lower critical solution temperature (LCST). As the temperature beyond the LCST, the polymer solution becomes turbid due to polymer occurs partial miscibility. On the other hand, if the polymer is soluble above a reliable temperature and their response exhibits vice versa to LCST, defined as upper critical solution temperature (UCST). To clarify this phenomenon, it can be explained by Gibbs equation as shown below [86],

$$\Delta G = \Delta H - T\Delta S \quad (2.1)$$

where G is Gibbs free energy (kJ/mol), H is enthalpy (kJ/mol), S is entropy (J/mol K), and T is temperature (K).

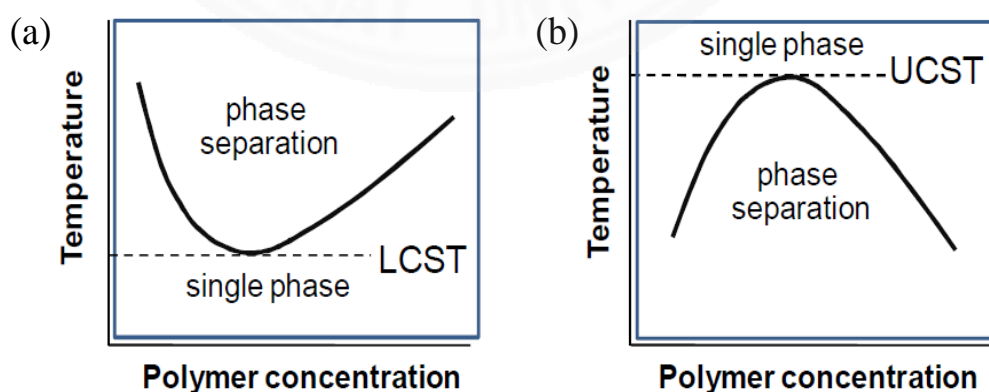


Figure 2.9 Schematic illustration of phase diagram for polymer solution in (a) LCST and (b) UCST systems [87].

The phase transition behavior as aforementioned is attributed to the entropy of the system. Increasing the temperature induces the breakage of interaction between molecules of polymer and solvent (like in the case of broken hydrogen bonding when water is used as a solvent). When the polymer is not in the solution, the solvent molecules are less ordered and then the entropy of the system is increased. Therefore, phase separation occurs immediately as indicated by a change in color of polymer solution (Figure 2.10).

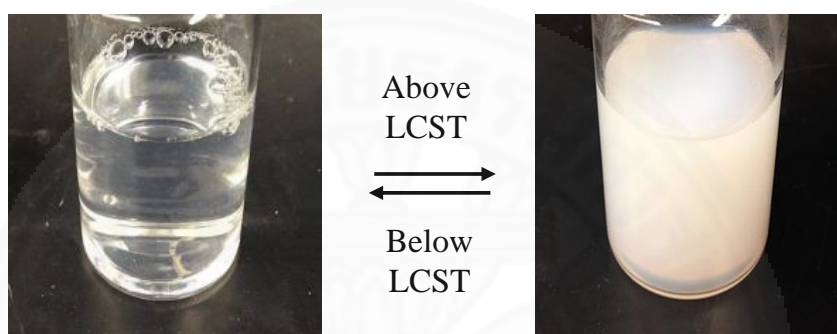


Figure 2.10 The change in color of polymer solution at below and above LCST.

2.4.1 Poly(*N*-vinylcaprolactam) (PNVCL)

PNVCL is one of the well-known temperature-responsive polymers which can be prepared from the free radical polymerization of NVCL through chain-growth mechanism at the vinyl backbone [88]. There are three crucial steps for the synthesis of temperature-responsive PNVCL including initiation, propagation, and termination as illustrated Figure 2.11. In addition, the type of initiator to polymerize NVCL monomer was also proved by Solomon, O.F. and his group [89]. They affirmed that the most effective initiator for free radical polymerization of NVCL was AIBN which is an oil-soluble azo initiator because it yielded high conversion of polymer in the temperature region of 60-80 °C, despite the fact that AIBN was used in the low concentrations.

Typically, PNVCL can be synthesized using several techniques including bulk, emulsion, solution, and radiation polymerization. These techniques for polymerization of NVCL are described below,

Bulk polymerization of NVCL is not productive, since it is difficult to operate the reaction mixture during the polymerization. Upon the reaction is progressed, the viscosity of reaction mixture also instantaneously increased, causing the complete mixing of reaction mixture is hard to accomplish [90].

In addition, NVCL can be polymerized in water but it is impracticable because the temperature-reversible solution behavior of NVCL. NVCL monomer possesses the melting point around 34 °C, so it can miscible in cold water. On the other hand, its polymer is dissolved in cold water but insoluble in water with the temperature beyond its LCST. Accordingly, the reaction to polymerize NVCL should be carried out at the temperature above the melting point of NVCL in terms of an oil-in-water emulsion polymerization [90].

Additionally, the water-soluble polymerization-regulation solvents can be applied to prepare the thermo-sensitive PNVCL such as dioxane, ethanol, methanol, ethylene glycol, and diethylene glycol [90].

To the best of appropriate technique, solution is the most widely applied over the others, due to its simplicity to handle the heat transfer by the solvent and a decrease in the viscosity in the system [7]. Despite, the solution technique provides the excessive advantages, it has also some defects. The main problem of solution polymerization relates to the reaction rate is limited, due to the boiling point of the solvent which is the key that can limit the reaction temperature. For polymerization of NVCL, the organic solvent such as hexane is suitable, but this solvent may act as a regulator or chain transfer agent. Therefore, it must be eliminated prior to processing of the polymer. Otherwise, chain transfer reaction between growing polymer and solvent may occur which can lower the molecular weight of the resulting polymer. However, the molecular weight of the polymer prepared through the solution polymerization depends on the ratio between monomer and solvent as well as the type of the solvent [91].

Based on its structure, PNVCL shows the amphiphilic character from the seven-member of hydrophilic caprolactam ring attached to the hydrophobic carbon backbone. Therefore, it can be soluble in polar and non-polar solvents depending on the conditions.

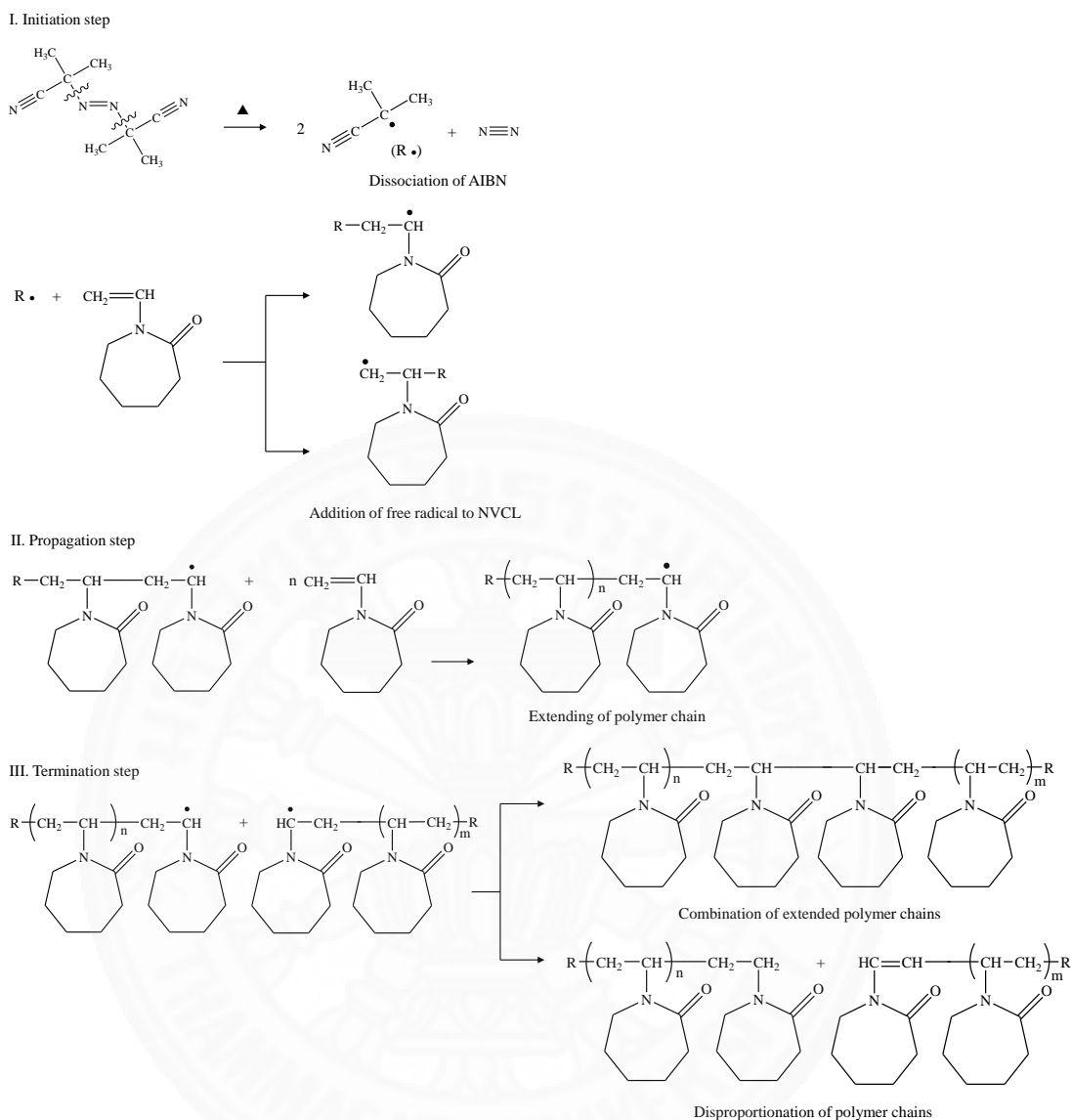


Figure 2.11 The chain-growth mechanism for synthesis of PNVCL [7,88].

At LCST, PNVCL exhibits the soluble-to-insoluble change in an aqueous medium around 32-34 °C, being near the human physiological temperature [7,92,93]. The tunable phase transition of PNVCL involves the hydrogen bonding between amide group of hydrophilic caprolactam ring and water molecule as shown in Figure 2.12. There are two states in the phase separation including hydrophilic state that arises from the interaction between water molecule and amide group of caprolactam ring *via* hydrogen bonding at below LCST and the hydrophobic state

which corresponds to the temperature-induced loss of the hydrogen bonding at above LCST [94].

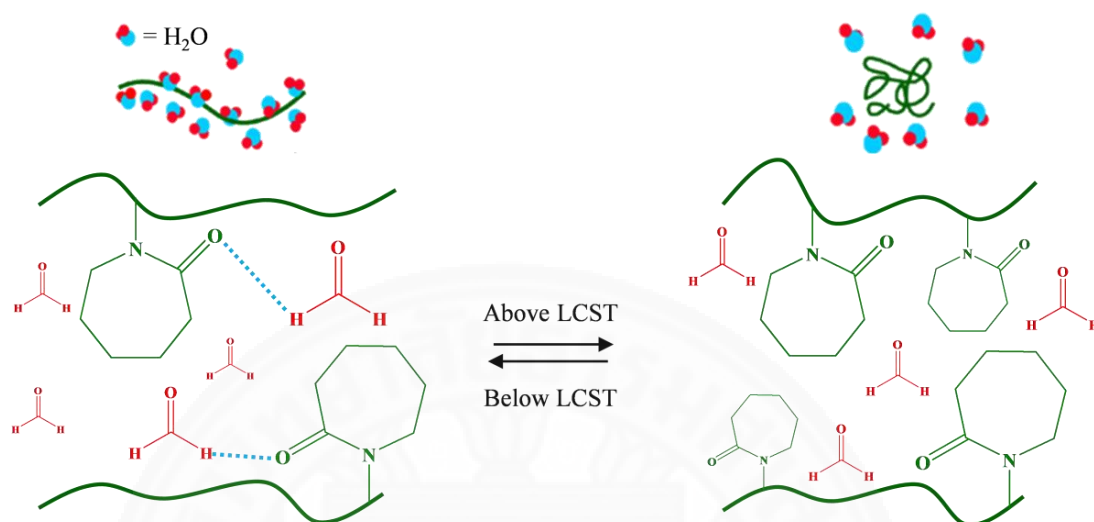


Figure 2.12 Schematic illustration of temperature induced phase transition of PNVCCL.

Although the polymerization of NVCL is more complicated and difficult to form PNVCCL, it still has notable attractiveness than PNIPAM, which is the previously favorite temperature-responsive polymer. In accordance with the structure of PNVCCL that consists of cyclic amide group of caprolactam ring where a nitrogen atom is directly bound to the hydrophobic carbon backbone, its hydrolysis does not provide toxic molecular amides. This is suitable for biomedical applications, unlike in the case of PNIPAM [95]. In addition to its non-toxicity and biodegradability, PNVCCL can be modified in different architectures, such as copolymers, star-shaped polymers, and crosslinked network as shown in Figure 2.13, for desirable applications such as controlled drug medical devices [10,96] and biosensors [97].

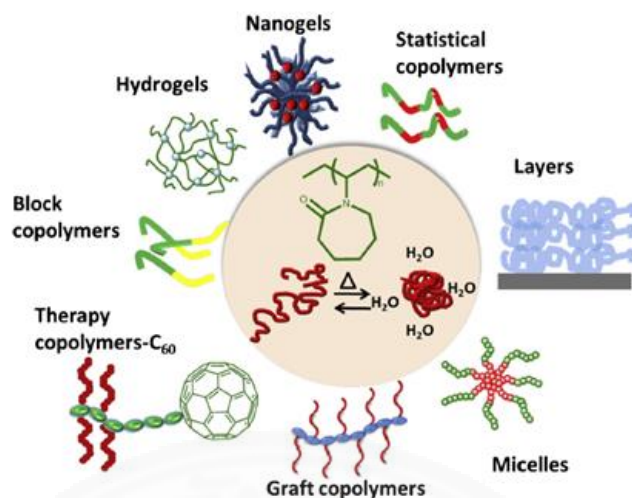


Figure 2.13 Several architectures of PNVCCL [98].

Rejinold, N.S. and coworkers developed a biodegradable thermo-responsive drug carrier from PNVCCL and chitosan. The drug used here was 5-fluorouracil, which is known as a cancer drug. This finding showed that this copolymer possessed the LCST value in the temperature range of 38-45 °C in an aqueous media and it was able to release drug at above that LCST around 40% after 3 days [10].

Kavitha, T. and colleagues reported a novel fluorescent temperature-responsive sensor for proteins adsorption which was made by mixing PNVCCL with carbon quantum dots (CQDs). It could be seen that a novel material presented the LCST around 33 °C and displayed a higher fluorescent intensity at above LCST. This response was believed to be a candidate for biosensing field [97].

Patel, R. and coworkers disclosed the graft copolymerization between PNVCCL and poly(vinyl chloride) (PVC) *via* atomic transfer radical polymerization (ATRP). This graft copolymer was used as a template for the preparation of porous titanium dioxide (TiO₂) thin films [99].

Lequieu, W. and his group also studied the immobilization of PNVCCL onto the surface of poly(ethylene terephthalate) (PET) membrane in order to achieve temperature-sensitive membrane. The behavior of this membrane was confirmed using water permeability upon change in temperature and its water permeability was found a considerable increased when the temperature exceeded the

LCST of the membrane. This outcome was attributed to the shrinkage of polymer chains at the surface of membrane, resulting in an increase in pore diameter [100].

Also, several studies reported the preparation of PNVCL-based copolymers and blends for various applications. For example, PNVCL was coupled with graphene oxide (GO) [5], poly(*N*-vinyl-2-pyrrolidone) (PNVP) [101], poly(ethylene glycol) (PEG) [102], and poly(acrylic acid) (PAA) [103]. However, there were only a few studies that employed the temperature responsiveness to elastomeric materials. For instance, Obando Mora, A. and colleagues synthesized the graft copolymer using γ ray by incorporating the silicone rubber (SR) with the temperature and pH responsiveness from NVCL and *N*-vinylimidazole (NVIM), respectively (Table 2.6). This finding revealed that this material showed sensitivity to the temperature that was influenced by NVCL as indicated through the water swelling experiment (Figure 2.14). The swelling percentage was increased at below LCST and gradually decreased when the temperature beyond its LCST [104].

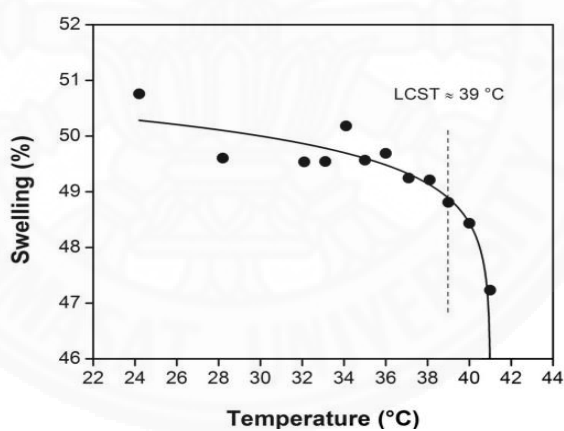


Figure 2.14 Water swelling percentage as a function of temperature of SR-g-(NVCL-co-NVIM) (90% grafting ratio) [104].

Another showed the graft copolymerization of SR with comonomer between NVCL and methacrylic acid (MAA) through γ irradiation (Table 2.6). This copolymer still exhibited the phase transition behavior upon switching the temperature below and above LCST as illustrated in Figure 2.15 (a). Moreover, it had the ability to release the nystatin or antifungal agent at human body temperature for

several hours as shown in Figure 2.15 (b). This confirmed that the modified SR as displayed in this literature was a promising material for drug-eluting medical devices [105].

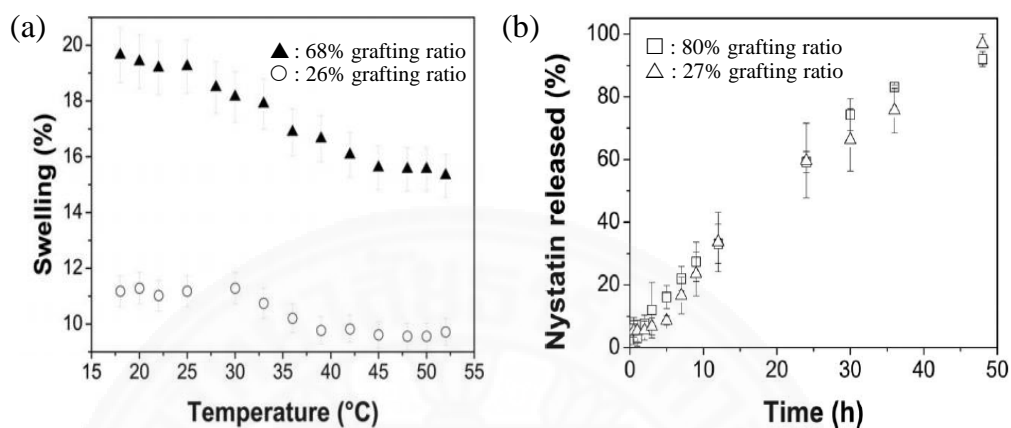


Figure 2.15 (a) Effect of the temperature on the swelling percentage of SR-g-(NVCL-co-MAA) in a buffer solution (pH 3) at different grafting ratios and (b) releasing percentage of nystatin from SR-g-(NVCL-co-MAA) at different grafting ratios [105].

Table 2.6 Comparison between our proposed research and other related studies.

	Obando Mora, A. and coworkers	Melendez Ortiz, H. I. and coworkers	Our proposed work	
1 st polymer	SR	SR	Dry rubber	DPNR latex
2 nd polymer /monomer	NVCL and NVIM	NVCL and MAA	PNVCL	NVCL
Number of synthetic step	1	1	1	1
Processing	γ irradiation	γ irradiation	Free radical crosslinking	Free radical grafting
System	Solution	Solution	Solution	Emulsion

CHAPTER 3

RESEARCH METHODOLOGY

3.1 Materials

3.1.1 Reagents

High ammonia NR latex with 60% DRC was supplied by Department of Agriculture, Thailand. NVCL monomer (assay 98%) was purchased from Sigma Aldrich, Germany. NVCL was purified by recrystallization from hexane at room temperature. It was dissolved in hexane and the resulting solution was filtered several times. Then, the solution was kept in the refrigerator to obtain NVCL crystals. When the pure crystals of NVCL were generated, the solvent was decanted and the purified NVCL was collected at 4 °C. AIBN and BPO (assay 75%) employed as a free radical initiator were manufactured by Acros Organic, China. These initiators were recrystallized using methanol prior to use. Formic acid (assay 85%), toluene (assay 99.8%), glacial acetic acid (assay 99.9%), chloroform (assay 99%), and acetone used as a solvent were obtained from Carlo Erba, China. Diethyl ether (assay 99.7%) applied as a solvent to precipitate PNVCL was supplied by AppliChem Panreac, Germany. Sodium dodecyl sulfate (SDS, assay 98%) utilized as an emulsifier and urea (assay 99.0-100.5%) used as a denaturant agent for deproteinization of NR latex were purchased from Carlo Erba, China. Potassium hydroxide (KOH, assay 85%) applied as a stabilizer was received from Merck, Germany. Indigo carmine used as a drug model was supplied by Acros Organic, Great Britain. Deuterated chloroform ($\text{CDCl}_3\text{-d}$, assay 99.8%) used as a solvent for characterization was received from Cambridge Isotope Laboratories, United States. The deionized (DI) water was employed throughout experiments.

3.2 Methods and preparation

The preparation of NVCL-functionalized NRs as temperature-responsive material was classified into two pathways including crosslinking and graft copolymerization.

3.2.1 Synthesis of crosslinked material (PNVCL-NR)

3.2.1.1 Preparation of PNVCL

PNVCL had been synthesized *via* free radical polymerization of NVCL monomer using AIBN as an initiator. NVCL (3 g), AIBN (0.15 g) and hexane (50 mL) were blended in 100 mL round-bottom flask and then heated in an oil bath at 60 °C for 6 h. After the polymerization, the polymer solution was precipitated with the excess amount of diethyl ether, filtered and dried under vacuum at 60 °C overnight to constant weight. The yield in percentage of temperature-responsive PNVCL was gravimetrically measured using equation 3.1 as shown below,

$$\text{Yield (\%)} = \frac{M_2}{M_1} \times 100 \quad (3.1)$$

where M_1 and M_2 are the masses of monomer and polymer (g), respectively.

3.2.1.2 Preparation of dry rubber

NR latex was coagulated with formic acid (5% v/v) prior to being washed several times with DI water and then dried in an oven at 60 °C overnight. Afterward, the resultant dry natural rubber (DNR) was purified by acetone in soxhlet extraction technique for 24 h to remove any impurities and dried again at 60 °C for 24 h.

3.2.1.3 Preparation of PNVCL-NR

DNR (1 g) was dissolved in chloroform (30 mL). Then PNVCL (50-150 parts per hundred of rubber (phr)) in chloroform (10 mL) and BPO (5-50 phr) in chloroform (5 mL) were slowly added to the DNR solution with continuous stirring. The mixture was heated to a predetermined temperature (75-95 °C) for a specified length of time (12-36 h). The variable parameters for the crosslinking reaction under this research work were enumerated in Table 3.1. After

being cooled to room temperature (30 °C), the crude polymer product was washed with plenty of chloroform and dried in an oven for 24 h. The resulting crosslinked material was purified by a soxhlet extraction in acetone for 24 h in order to remove any contaminants and dried at 60 °C overnight until the weight was unchanged. The gel content percentage of crosslinked material was calculated as follows,

$$\text{Gel content (\%)} = \frac{W_2 - W_1}{W_1} \times 100 \quad (3.2)$$

where W_1 and W_2 are the weights of the rubbers before and after crosslinking reaction (g), respectively.

Table 3.1 Variable parameters used for preparation of PNVCL-NR.

Parameters	Quantities	
	phr	g
Main ingredients		
• DNR	100	1.00
• PNVCL	50, 100, 150	0.50, 1.00, 1.50
Initiator		
• BPO	5, 10, 50	0.05, 0.10, 0.50
Reaction temperature (°C)	75, 85, 95	
Reaction time (h)	12, 24, 36	

3.2.1.4 Investigation of crosslink density

Crosslinked material (~0.1 g) was incubated in toluene (10 mL) and kept in the dark for 1 week at room temperature. After immersion, the swollen rubber was removed and blotted with filter paper before weighing. The crosslink density was determined using the Flory-Rehner Equation as follows [106],

$$p_c = -\frac{1}{2V_s} \frac{\ln(1-V_r^0) + V_r^0 + \chi(V_r^0)^2}{(V_r^0)^{1/3} - \frac{V_r^0}{2}} \quad (3.3)$$

where p_c is the crosslink density (mol/m^3), V_s is the molar volume of toluene ($1.069 \times 10^{-4} \text{ m}^3/\text{mol}$) at 25°C , χ is the interaction parameter ($0.44 + 0.18V_r^0$), and V_r^0 is the volume fraction of rubber in the swollen gel, which can be computed by the following equation,

$$V_r^0 = \frac{1}{1 + \frac{\rho_r}{\rho_s} \left(\frac{W_s - W_D}{W_D} \right)} \quad (3.4)$$

where ρ_s and ρ_r are the densities of toluene (0.87 g/mL) and rubber (0.92 g/mL), and W_s and W_D are the weights of swollen and dried rubbers (g), respectively.

3.2.2 Synthesis of grafted material (NVCL-g-DPNR)

3.2.2.1 Preparation of DPNR latex

The schematic diagram for removal the proteins was shown in Figure 3.1. NR latex (100 g) used in this study was commercial high ammonia latex (60% DRC). The incubation of the latex was conducted with 0.1 wt% urea (0.2 g) in the presence of 1 wt% SDS (2 g) dissolved in DI water (100 g). After incubation for 1 h with continuous stirring at room temperature, the obtained latex was purified by centrifugation at 10,000 rpm for 1 h at 25°C . The cream fraction was re-dispersed in 1 wt% SDS solution and washed twice by centrifugation to prepare DPNR latex (32% DRC). To calculate the DRC percentage, DPNR latex was coagulated with acetone, dried in an oven at 60°C overnight to a definite weight, and then calculated the DRC according to the equation 3.5,

$$\text{DRC (\%)} = \frac{W_2}{W_1} \times 100 \quad (3.5)$$

where W_1 and W_2 are the weights of DPNR latex and coagulated DPNR rubber (g), respectively.

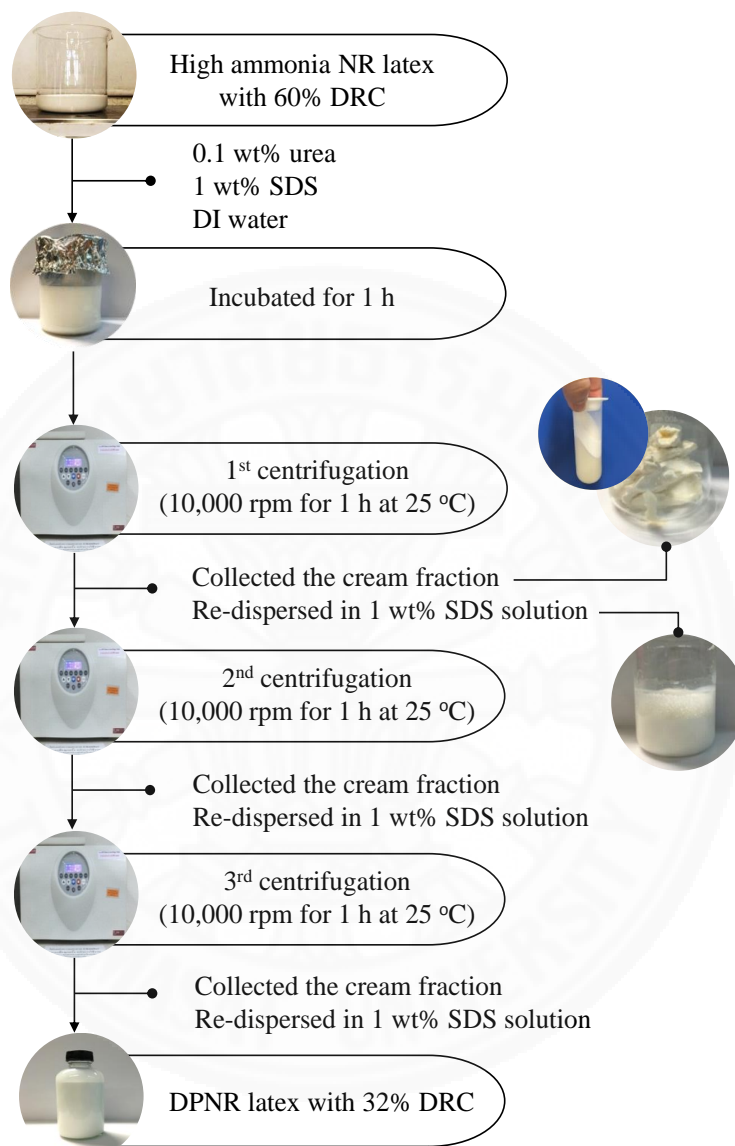


Figure 3.1 Schematic illustration for deproteinization of NR latex by urea treatment.

3.2.2.2 Preparation of NVCL-g-DP NR

A solution of SDS (0.15 g) as an emulsifier and KOH (0.15 g) used to maintain pH in the presence of DI water were mixed with DPNR latex (5 g) in 100 mL round-bottom flask. Subsequently, NVCL (50-150 phr with

respect to DRC) was added continually and then the reaction mixture was maintained at 80 °C for at least 30 min with continuous stirring. Next, AIBN (5-15 phr with respect to DRC) as an initiator was dissolved with a slight amount of toluene and slowly charged into the reactor. The polymerization reaction was allowed to progress at the desired temperature (80-100 °C) and specified length of time (4-8 h). The recipes and variable parameters for the grafting reaction under this current work were summarized in Table 3.2. After being cooled to room temperature, the reaction mixture was coagulated using 5 wt% acetic acid solution and dried at 60 °C for 24 h. The prepared graft copolymer was subjected to extraction with acetone for 24 h to remove homopolymers and unreacted monomers, followed by drying under vacuum at 60 °C overnight. After drying, NVCL-*g*-DPNR was dissolved with CDCl₃-d to investigate the efficiency of grafting using ¹H nuclear magnetic resonance (¹H-NMR) intensity. Grafting ratio (G) was determined from ¹H-NMR spectra by the equation as follows,

$$G (\%) = \frac{I_{4.4}}{I_{5.2}} \times 100 \quad (3.6)$$

where $I_{4.4}$ is the integrated signal area of the proton in –CH–N group at α -position of the caprolactam ring in NVCL units and $I_{5.2}$ is the integrated signal area of the unsaturated methyne proton (=CH) of the polyisoprene backbones.

Table 3.2 Variable parameters used for preparation of NVCL-*g*-DPNR.

Parameters	Quantities	
	phr	g
Main ingredients		
• DPNR latex	100	1.60*
• NVCL	50, 100, 150	0.80, 1.60, 2.40
Initiator		
• AIBN	5, 10, 15	0.08, 0.16, 0.24

Table 3.2 (Continued) Variable parameters used for preparation of NVCL-*g*-DPNR.

Parameters	Quantities	
	phr	g*
Emulsifier		
• SDS	9.37	0.15
Stabilizer		
• KOH	9.37	0.15
Reaction temperature (°C)	80, 90, 100	
Reaction time (h)	4, 6, 8	

* Weight of DPNR latex with 32% DRC computed from dried rubber 5 g.

3.2.3 Investigation of temperature-responsive behaviors

3.2.3.1 The water absorption measurement

The modified and unmodified rubbers (~0.1 g) were cut into small pieces (1x1 cm²) and compressed to remove air bubbles and also reduced porosity by sandwiching between two glass slides, followed by heating at 60 °C for 24 h. Then, rubber samples were immersed in DI water contained in vials and placed in a controlled temperature water bath for 3 h in the temperature range of 28-38 °C. After wiping the rubber surface with tissue paper, the samples were weighted and calculated the swelling percentage to determine the LCST value from the equation as shown below,

$$\text{Swelling (\%)} = \frac{W_2 - W_1}{W_1} \times 100 \quad (3.7)$$

where W_1 and W_2 are the weights of the specimens before and after immersion (g), respectively.

3.2.3.2 The contact angle determination

The rubber samples were cut into small pieces (1x1 cm²) and removed air bubbles to achieve the smooth surface. Before measuring the water contact angle, the rubber samples were heated for 30 min at desired temperature between 28-38 °C on the heater of controlled temperature contact angle meter. The size of water droplet was applied as 8 µL and the measurement was repeated 3 times at the different positions on the samples in each temperature in order to obtain an average contact angle.

3.2.3.3 Dye adsorption and desorption studies

Indigo carmine was chosen to represent an anionic drug model. The rubber samples (~0.1 g) with the sample size around 1x1 cm² were immersed in an aqueous solution of indigo carmine (10 ppm) for 1 week at room temperature. After 1 week of immersion, the rubber samples were removed and dried in an oven at 60 °C for 24 h. The amount of dye loading was computed by the following equation,

$$\text{Dye loading (\%)} = \frac{W_2}{W_1} \times 100 \quad (3.8)$$

where W_1 is the weight of rubber sample before dye loading (g) and W_2 is the weight of dye in rubber sample after dye loading (g), respectively.

To determine the desorption process, the rubber samples were incubated in DI water and placed in a controlled temperature water bath at a range of temperature between 28-38 °C for 3 h. Subsequently, aliquots were withdrawn for measurement using ultraviolet-visible (UV-vis) spectroscopy in the wavelength range of 400-700 nm.

3.2.4 Adsorption studies

A stock solution of 50 ppm was prepared by dissolving indigo carmine (0.05 g) in DI water (1 L). The working solutions (10-50 ppm) were prepared by diluting the stock solution with DI water. The equilibrium adsorption of indigo carmine was carried out by introducing the rubber samples (~0.2 g) with 10 mL of different concentrations of working solutions from 10-50 ppm in vials. Then, these vials were sealed and placed on a shaker at room temperature for 1 week. The concentration of the residual dye was measured using UV-visible spectroscopy at a λ_{max} corresponding to the maximum adsorption of the dye solution ($\lambda_{\text{max}} = 610 \text{ nm}$). Calibration curve was made up between absorbance and dye concentration to obtain absorbance-concentration profile. The amount of adsorbed indigo carmine onto the rubber sample at equilibrium (q_e , mg/g) was calculated based on a mass balance equation as given by [107],

$$q_e = \frac{(C_i - C_e)V}{W} \quad (3.9)$$

where C_i is the initial concentration of indigo carmine in the solution (mg/L), C_e is the final or equilibrium concentration of indigo carmine in the solution (mg/L), V is the volume of the solution (L), and W is the weight of rubber sample (g).

3.2.4.1 Equilibrium adsorption isotherm models

To elucidate the adsorption studies, four of the predominant adsorption models were applied to describe the equilibrium adsorption mechanism between indigo carmine molecules (adsorbate) and surface of modified rubbers (adsorbent) by comparing the correlation coefficient (R^2) of each model which was acquired from the linear relationship in the mathematical equations as summarized in Table 3.7. The adsorption data were fitted into four notable adsorption isotherms as follows,

(1) Langmuir adsorption isotherm

This adsorption isotherm describes the monolayer coverage of adsorbate molecules occurred on the adsorbent surface. It assumes that the active site on the surface of adsorbent is homogeneous which can absorb only one adsorbate [108]. The Langmuir adsorption is calculated from the equation as follows,

$$q_e = \frac{Q_0 K_L C_e}{1 + K_L C_e} \quad (3.10)$$

The Langmuir adsorption equation can be described by the linearized form as presented below,

$$\frac{1}{q_e} = \frac{1}{Q_0} + \frac{1}{Q_0 K_L C_e} \quad (3.11)$$

where q_e is the amount of adsorbate per gram of adsorbent at equilibrium (mg/g), Q_0 is the maximum monolayer coverage capacity (mg/g), K_L is the Langmuir isotherm constant (L/mg), and C_e is the equilibrium concentration of adsorbate (mg/L).

The values of Q_0 and K_L of Langmuir adsorption isotherm are computed from the slope and intercept of the linear plot by plotting between $1/q_e$ and $1/C_e$. The important parameter of this isotherm is equilibrium parameter (R_L) which is the unitless constant. This parameter explains the favorability of the adsorbate to the adsorbent and the nature of adsorption process as depicted in Table 3.3. It can be determined from the following equation [109],

$$R_L = \frac{1}{1 + K_L C_i} \quad (3.12)$$

where K_L is the Langmuir isotherm constant (L/mg) and C_i is the initial concentration of adsorbate (mg/L).

Table 3.3 Type of adsorption process depending on the equilibrium parameter of the Langmuir adsorption isotherm [110-112].

R_L value (dimensionless)	Type of isotherm
$R_L > 1$	Unfavorable
$R_L = 1$	Linear
$0 < R_L < 1$	Favorable
$R_L = 0$	Irreversible

(2) Freundlich adsorption isotherm

The Freundlich adsorption isotherm explains the multilayer adsorption with an interaction between adsorbed molecules take place on the heterogeneous surface of the adsorbent [108]. Based on the assumption, this adsorption isotherm can be defined by the following equation,

$$q_e = K_f C_e^{1/n} \quad (3.13)$$

The expression of the Freundlich equation in terms of linear form can be derived by taking the logarithm as given by equation 3.14,

$$\log q_e = \log K_f + \frac{1}{n} \log C_e \quad (3.14)$$

where q_e is the amount of adsorbate per gram of adsorbent at equilibrium (mg/g), K_f is the Freundlich isotherm constant (mg/g), C_e is the equilibrium concentration of adsorbate (mg/L), and n is the adsorption intensity (dimensionless).

Based on the linear regression equation of Freundlich adsorption isotherm as aforementioned, the characteristic constants of n and K_f are estimated from the slope and intercept that correspond with linear plot of $\log q_e$ against $\log C_e$. Furthermore, the requisite parameter of Freundlich isotherm may be displayed in terms of n parameter which is dimensionless parameter, indicating that the type of isotherm and also mechanism of adsorption as listed in Table 3.4.

Table 3.4 Type of adsorption process depending on the adsorption intensity of the Freundlich adsorption isotherm [108,111].

n value (dimensionless)	Type of isotherm	Type of adsorption
$n < 1$	Unfavorable	Chemisorption
$n > 1$	Favorable	Physisorption

(3) Temkin adsorption isotherm

The Temkin adsorption isotherm involves an indirect phenomena such as the heat of adsorption [110], which results from the adsorption nature. This model can be examined by the following equation,

$$q_e = \frac{RT}{b_T} \ln(A_T C_e) = B \ln(A_T C_e) \quad (3.15)$$

Then, the equation 3.15 can be rearranged to achieve a linear form as presented below,

$$q_e = B \ln A_T + B \ln C_e \quad (3.16)$$

where q_e is the amount of adsorbate per gram of adsorbent at equilibrium (mg/g), C_e is the equilibrium concentration of adsorbate (mg/L), R is the universal gas constant

(8.314 J/mol K), T is the absolute temperature (K), A_T is the Temkin isotherm equilibrium binding constant (L/mg), b_T is the Temkin isotherm constant (dimensionless), and B (RT/b_T) is a constant related to the heat of adsorption (J/mol).

Both constants of B and A_T of linear regression equation of Temkin adsorption isotherm will greatly impact the information about the experimental data and can be calculated from the slope and intercept of the linear plot between q_e and $\ln C_e$. Moreover, the B parameter represents the type of adsorption between physisorption and chemisorption as displayed in Table 3.5.

Table 3.5 Type of adsorption process depending on the B constant corresponded with heat of adsorption of the Temkin adsorption isotherm [113-115].

B value (kJ/mol)	Type of adsorption
$B < 20$	Physisorption
$B > 20$	Chemisorption

(4) Dubinin-Radushkevich adsorption isotherm

The Dubinin-Radushkevich isotherm reports the adsorption mechanism of adsorbate molecules on both homogeneous and heterogeneous surfaces of adsorbent, depending on pore filling mechanism [110]. This adsorption model is generally defined as follows,

$$q_e = (q_s) \exp(-K_{ad} \epsilon^2) \quad (3.17)$$

The linear form of Dubinin-Radushkevich isotherm regression can be written as follows,

$$\ln q_e = \ln(q_s) - (K_{ad}\epsilon^2) \quad (3.18)$$

where q_e is the amount of adsorbate per gram of adsorbent at equilibrium (mg/g), q_s is the theoretical isotherm saturation capacity (mg/g), K_{ad} is the Dubinin-Radushkevich isotherm constant (mol^2/kJ^2), and ϵ is the Dubinin-Radushkevich isotherm constant (dimensionless) which can be calculated according to the following equation,

$$\epsilon = RT \ln \left[1 + \frac{1}{C_e} \right] \quad (3.19)$$

where R is the universal gas constant (8.314 J/mol K), T is the absolute temperature (K), and C_e is the equilibrium concentration of adsorbate (mg/L).

The linear plot of $\ln q_e$ versus ϵ^2 reveals the information about the slope and intercept in terms of K_{ad} and q_s , respectively. For the Dubinin-Radushkevich isotherm, the mean sorption energy (E , kJ/mol) is the crucial parameter used to discriminate the physical and chemical adsorptions of adsorbate molecules as enumerated in Table 3.6. It can be calculated by the following equation,

$$E = \left[\frac{1}{\sqrt{2K_{ad}}} \right] \quad (3.20)$$

where K_{ad} is the Dubinin-Radushkevich isotherm constant (mol^2/kJ^2).

Table 3.6 Type of adsorption process depending on the mean sorption energy of the Dubinin-Radushkevich adsorption isotherm [115,116].

E value (kJ/mol)	Type of adsorption
$E < 8$	Physisorption
$E > 8$	Chemisorption

Table 3.7 Mathematical equations used for each adsorption isotherm [117].

Isotherm	Nonlinear form	Linear form	Plot
Langmuir	$q_e = \frac{Q_0 K_L C_e}{1 + K_L C_e}$	$\frac{1}{q_e} = \frac{1}{Q_0} + \frac{1}{Q_0 K_L C_e}$	$\frac{1}{q_e}$ VS $\frac{1}{C_e}$
Freundlich	$q_e = K_f C_e^{1/n}$	$\log q_e = \log K_f + \frac{1}{n} \log C_e$	$\log q_e$ VS $\log C_e$
Temkin	$q_e = \frac{RT}{b_T} \ln(A_T C_e)$	$q_e = B \ln A_T + B \ln C_e$	q_e VS $\ln C_e$
Dubinin-Radushkevich	$q_e = (q_s) \exp(-K_{ad} \varepsilon^2)$	$\ln q_e = \ln(q_s) - (K_{ad} \varepsilon^2)$	$\ln q_e$ VS ε^2

3.3 Characterization

The NVCL-functionalized NRs were characterized using several types of techniques as shown below,

3.3.1 Fourier transform infrared spectroscopy (FT-IR)

The chemical structures and functional groups of the materials were characterized using a Perkin Elmer FT-IR spectrophotometer (Spectrum GX model). These materials were dissolved with $CDCl_3$ -d and placed on NaCl salt windows. The FT-IR spectra were taken in the range of 300 - 3800 cm^{-1} .

3.3.2 1H nuclear magnetic resonance spectroscopy (1H -NMR)

1H -NMR spectroscopy was used to further confirm the chemical structure in the molecule of materials. 1H -NMR spectra of the materials were taken from AVANCE Bruker NMR Spectrometer and $CDCl_3$ -d was used as a solvent. Chemical shift was reported in the unit of ppm.

3.3.3 X-ray photoelectron spectroscopy (XPS)

The chemical compositions on the surface of the materials were determined using an XPS spectrometer (AXIS ULTRA^{DLD}, Kratos analytical, Manchester, UK). The base pressure in the XPS analysis chamber was about 5×10^{-9} torr. The materials were excited using X-ray hybrid mode at a $700 \times 300 \mu\text{m}$ spot area with monochromatic Al $K_{\alpha 1,2}$ radiation at 1.4 keV. The X-ray anode was run at 15 kV 10 mA 150 W. The photoelectrons were detected by a hemispherical analyzer positioned at an angle of 45° with respect to the sample surface.

3.3.4 Differential scanning calorimetry (DSC)

The glass transition temperature (T_g) of the materials was characterized using a DSC 822e Mettler Toledo calorimeter. These specimens were heated in a range of temperature from -80 to 300°C with a scanning rate of $10^\circ\text{C}/\text{min}$ under inert nitrogen atmosphere.

3.3.5 Thermogravimetric analysis (TGA)

The thermal stability of the materials was recorded using a TGA/SDTA 851e Mettler Toledo analyzer. The materials were heated in a measured temperature range of 30 - 600°C at the heating rate of $10^\circ\text{C}/\text{min}$ under nitrogen atmosphere.

In addition, TGA technique provides the information about the thermal property in terms of weight loss but it difficult to interpret. Therefore, the interpretation of the TGA result is better made using the first derivative weight curve which is derived from the derivative thermogravimetric analysis (DTG).

3.3.6 Gel permeation chromatography (GPC)

Molecular weights of the polymer and its dispersity were measured by GPC using Waters e2695 separations modules. PS was used as a standard and tetrahydrofuran (THF) was employed as a solvent for dissolving the polymer. The flow rate was 1 mL/min.

3.3.7 Ultraviolet-visible spectroscopy (UV-vis)

UV-visible spectra of the specimens were investigated using a UV-1700 PharmaSpec UV-visible spectrometer in the wavelength of 400-700 nm range.

3.3.8 The contact angle determination

Prior to the determination of water contact angle, the materials (1x1 cm²) were prepared in thin film by sandwiching them with two glass slide and heated at 60 °C for overnight. Water contact angle of the materials was measured using an OCA35 Dataphysics contact angle meter. The size of the water droplet was 8 µL. During the operation, the materials were heated by the heater in a controlled temperature contact angle meter around 30 min at a region of temperature from 28-38 °C. The measurement was carried out in triplicate at different positions to obtain the average values.

3.3.9 Carbon nitrogen and hydrogen analysis (CHN)

Before the operation, the rubber latex samples were dried by placing on a petri dish as a thin film and then cut into small pieces (1x1 cm²). The content of carbon, hydrogen, and nitrogen elements in these rubber samples was examined using a Perkin-Elmer 2400 Series CHNS/O analyzer.

3.3.10 Centrifugation

Prior to graft copolymerization, proteins were removed from high ammonia NR latex in order to achieve the higher grafting efficiency of graft copolymer. These proteins were separated from rubber particles by centrifugation 3 times at 10,000 rpm for 1 h at 25 °C using a Velocity 14R refrigerated centrifuge (Dynamica).



CHAPTER 4

RESULTS AND DISCUSSION

4.1 Synthesis and characterization of PNVCL-NR

4.1.1 Preparation of PNVCL

4.1.1.1 Morphological observation of PNVCL

PNVCL was prepared through free radical polymerization by solution technique of NVCL in the presence of AIBN as an initiator using hexane as a solvent. For solution polymerization of NVCL, hexane was used as a solvent due to both AIBN and NVCL were soluble in it. Obviously, this polymerization progressed at the vinyl group of NVCL monomer. The obtained PNVCL was a white powder that was soluble in both water and organic solvents, resulting from its amphiphilic character [7,8]. As presented in Figure 4.1, the appearance of PNVCL differed from its monomer due to the change in conformation of molecules.

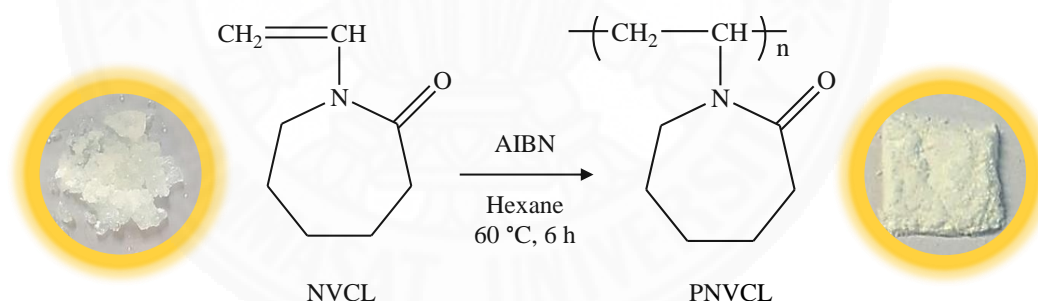


Figure 4.1 Diagram for preparation of PNVCL.

4.1.1.2 Chemical structure and characteristics of PNVCL

(1) FT-IR analysis of PNVCL

The FT-IR spectra of NVCL and PNVCL were shown in Figure 4.2. After the polymerization came to a completion, new and broad peak were observed in the spectrum of PNVCL at 3509 cm^{-1} . This broad peak corresponded to O-H stretching which arose from the unique property of PNVCL that readily absorbed

water in the air. There was no change in the position of N-H stretching which located at 3287 cm^{-1} , but it became broader in the spectrum of PNVCL. Meanwhile, the peaks at 1673 and 3114 cm^{-1} belonged to C=C stretching and C-H stretching of vinyl group ($=\text{CH}$ and $=\text{CH}_2$) were only found in the spectrum of NVCL and disappeared after polymerization. These changes were might be due to the alternation of intermolecular distance upon polymerization, yielding the chair conformation of caprolactam group in their molecule was changed [7,8]. The additional peaks of NVCL and PNVCL were tabulated in Table 4.1.

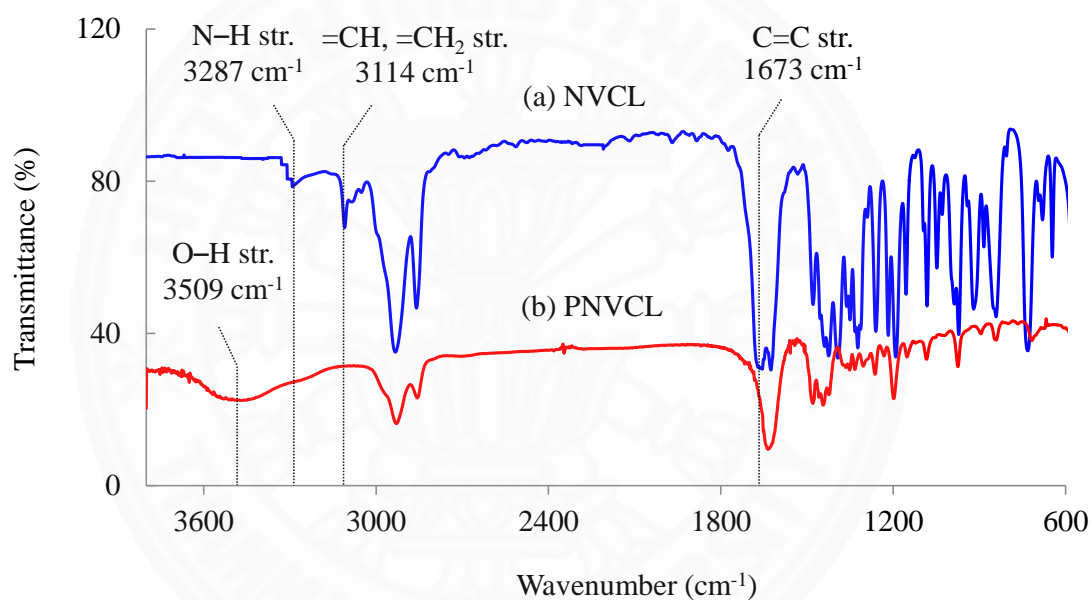


Figure 4.2 FT-IR spectra of (a) NVCL and (b) PNVCL.

Table 4.1 Assignment of corresponding FT-IR spectra for NVCL and PNVCL.

Functional group	Wavenumber (cm^{-1})	
	NVCL	PNVCL
O-H stretching	-	3509
N-H stretching	3287	3287

Table 4.1 (Continued) Assignment of corresponding FT-IR spectra for NVCL and PNVCL.

Functional group	Wavenumber (cm ⁻¹)	
	NVCL	PNVCL
Aliphatic C–H stretching	2943, 2865	2937, 2864
C–N stretching	1475	1485
C=O stretching	1650	1643
–CH ₂ bending	1440	1447
C=C stretching	1673	-
=CH and =CH ₂ stretching	3114	-
=CH and =CH ₂ bending	923	-

(2) ¹H-NMR analysis of PNVCL

¹H-NMR technique was used to confirm the formation of thermo-sensitive PNVCL as depicted in Table 4.2. In the ¹H-NMR spectrum of NVCL as displayed in Figure 4.3 (a) showed six different peaks of the protons which located in the structure of monomer. The chemical shift at 1.5 ppm could be assigned to the protons in –CH₂ (H_a) of the caprolactam ring. The assigned protons in –CH₂–CO (H_b) and –CH₂–N (H_c) were found at 2.4 and 3.4 ppm, respectively. Besides, the protons in the vinyl group of NVCL monomer appeared at 4.2, 4.3, and 7.4 ppm which belonged to =CH (H_d), =CH (H_e), and =CH–N (H_f), respectively. While, the H_f in =CH–N group appearing in the germinal position exhibited the highest chemical shift [7].

The ¹H-NMR spectrum of PNVCL was given in Figure 4.3 (b) expressed a broad spectrum of four peaks that influenced by the change after polymerization. The chemical shifts of protons in –CH₂ group were observed at

1.0-1.8 ppm (H_a), 2.4 ppm (H_b), and 3.1 ppm (H_c), respectively. Moreover, the peak at 4.4 ppm was assigned to the proton in $-CH-N$ (H_d). However, the characteristic peaks corresponded to vinyl group vanished [7,8].

According to the appearance of resulting polymer, FT-IR, and 1H -NMR results certainly confirmed the polymerization of NVCL.

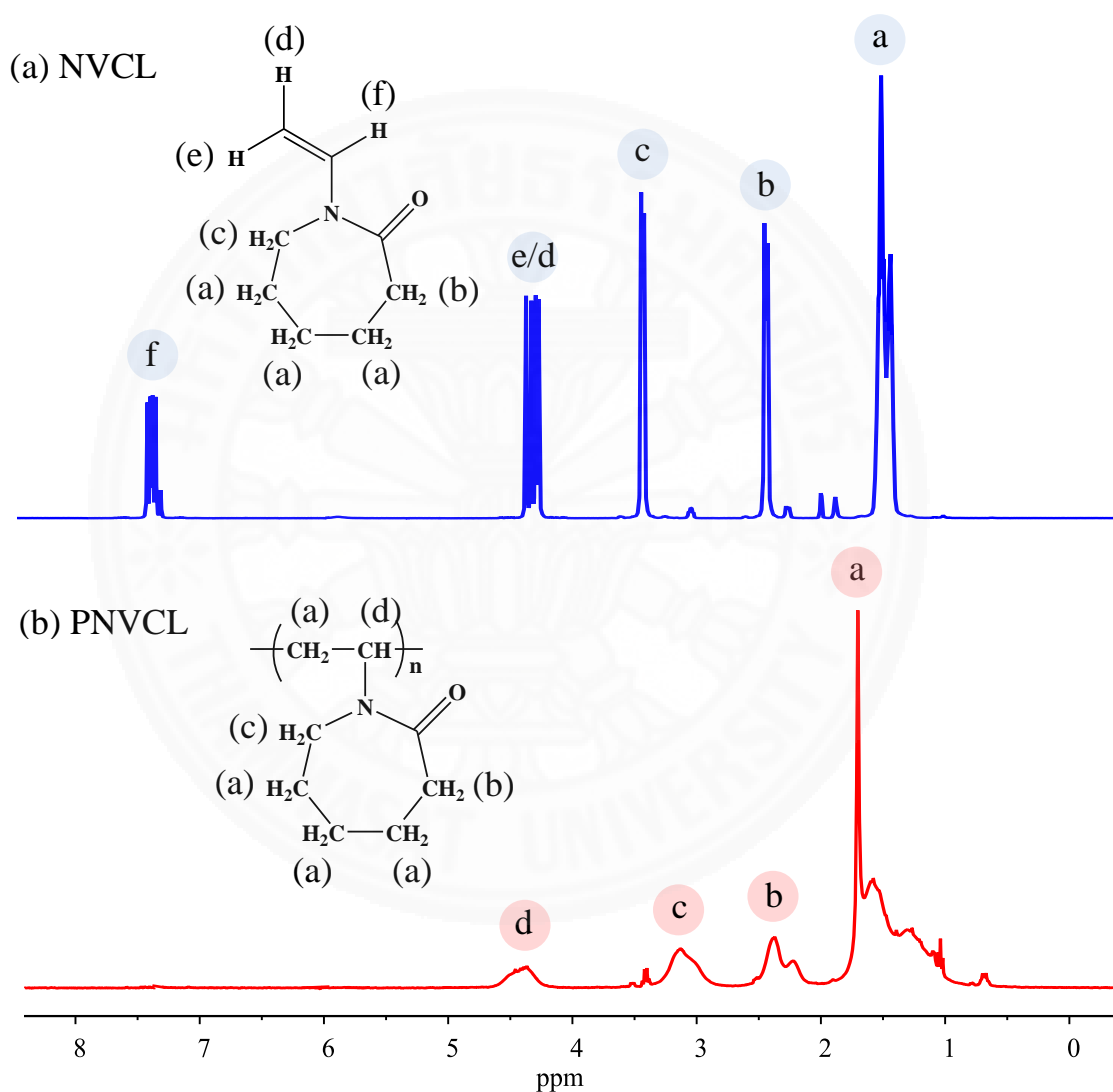


Figure 4.3 1H -NMR spectra of (a) NVCL and (b) PNVCL.

Table 4.2 Assignment of corresponding $^1\text{H-NMR}$ spectra for NVCL and PNVCL.

Proton position	Chemical shift (ppm)	Functional group
(a) NVCL		
H _a	1.5	(-CH ₂) ₃ (6H)
H _b	2.4	-CH ₂ -CO (2H)
H _c	3.4	-CH ₂ -N (2H)
H _d	4.2	=CH (1H)
H _e	4.3	=CH (1H)
H _f	7.4	=CH-N (1H)
(b) PNVCL		
H _a	1.0-1.8	(-CH ₂) ₄ (8H)
H _b	2.4	-CH ₂ -CO (2H)
H _c	3.1	-CH ₂ -N (2H)
H _d	4.4	-CH-N (1H)

4.1.1.3 Molecular weight determination of PNVCL

Average molecular weights of PNVCL and its dispersity were analyzed using GPC technique with THF as a solvent and PS as a standard. The GPC results of PNVCL as listed in Table 4.3 exhibited the number-averaged (M_n), weight-averaged (M_w), and z-averaged (M_z) molecular weights of 940, 1200, and 1500 g/mol, respectively. Moreover, the dispersity (\mathcal{D} , M_w/M_n) was found to be 1.3.

Based on this study, the solution technique was performed to polymerize the NVCL monomer because the heat transfer could be controlled easily which prevented the accumulation of heat as well as the presence of solvent gave the reduction in viscosity upon the polymerization was continually proceeded. Although this technique provided many strong points as stated, it had also some disadvantages. In this polymerization, hexane was found to be a suitable solvent but it had acceptable chain transfer characteristic which might result in a limitation in molecular weight of PNVCL as presented in this work.

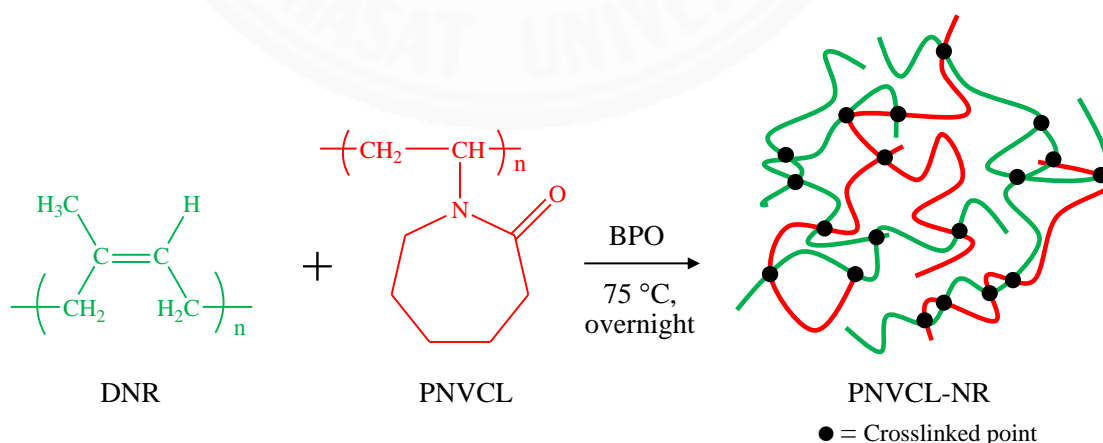
Table 4.3 Average molecular weights and dispersity of PNVCL.

Molecular weights (g/mol)			Đ
M_n	M_w	M_z	
940	1200	1500	1.3

4.1.2 Preparation of PNVCL-NR

4.1.2.1 Morphological observation of PNVCL-NR

The synthesis of crosslinked material between dry rubber and PNVCL was carried out using BPO as an initiator and chloroform as a solvent because both of them were miscible in this solvent (Figure 4.4). In this section, the yellowish dry rubber was used instead of the latex due to it could be facilely controlled without using any chemicals including emulsifier and also stabilizer which frequently applied to maintain the latex form of the rubber. Furthermore, there was no problem about the solubility of PNVCL under the solution system because the as-prepared PNVCL expressed the amphiphilic character, giving it could dissolve easily in both water and organic solvents as mentioned.

**Figure 4.4** Diagram for preparation of PNVCL-NR.

The formation of PNVCL-NR sample was believed to proceed by two plausible steps including the free radicals from the decomposition of BPO initiated the active sites at the allylic positions of rubber backbones as well as at the tertiary C-H bonds in the PNVCL molecules *via* hydrogen abstraction process (Figure 4.5) and another which related to the interaction between both polymer radical species, generating the crosslinked material [118].

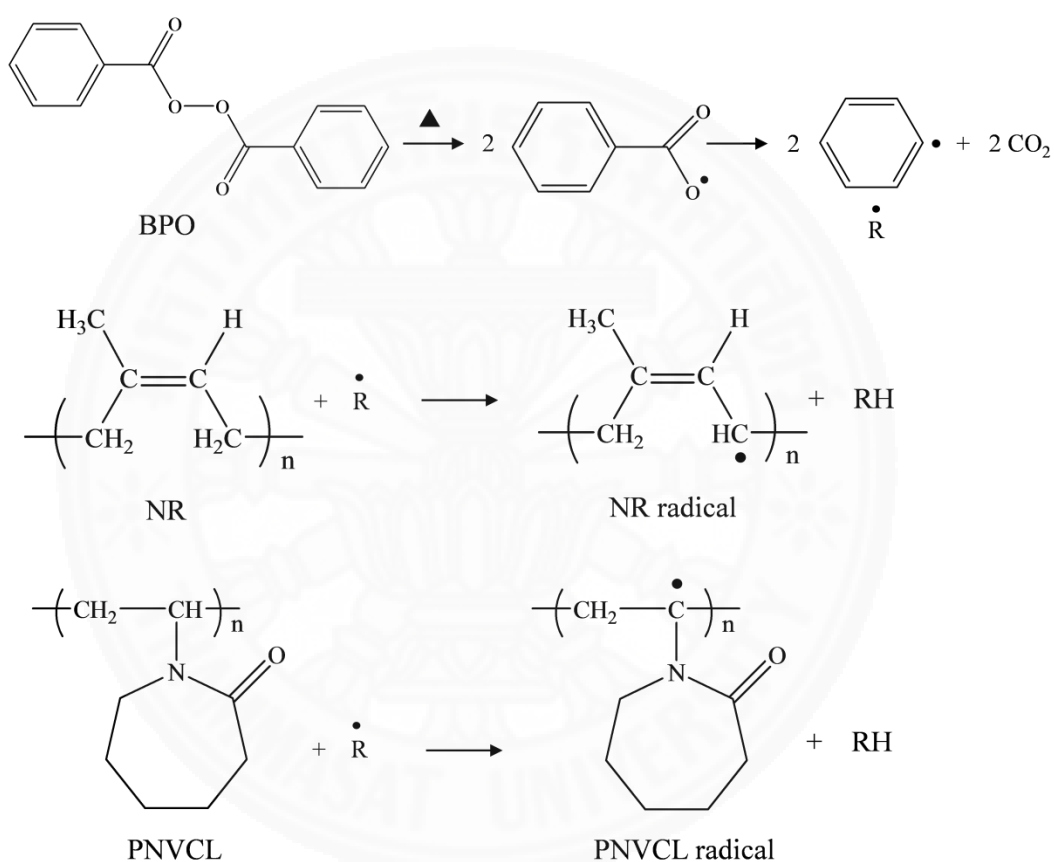


Figure 4.5 Synthetic route of polymer radicals on NR and PNVCL molecules through hydrogen abstraction process.

After the polymerization, an insoluble polymer or gel was formed which indicated that the formation of crosslinked material [119]. Another evidence could be further confirmed this finding which was derived from the immersion of PNVCL-NR sample in many types of solvents such as formic acid, chloroform, toluene and acetone as displayed in Figure 4.6 (a). It was also clearly

observed that the resulting product could absorb the solvents and then only be swollen but did not even dissolve. This feature was due to the polymeric chains within the obtained PNVCL-NR were covalently tied each other. As shown in Figure 4.6 (b) and (c), the appearance of PNVCL-NR was unlike the pristine NR as it showed the dark yellow with sticky character. The change of color could be considered as NR and PNVCL were blended together. According to these results markedly claimed that the network material was successfully prepared in this approach.

Thereafter, the as-prepared PNVCL-NR was characterized using many techniques. Based on the fact that the PNVCL-NR material hardly dissolved in organic solvents as aforementioned, thus it could not investigate the characteristic using $^1\text{H-NMR}$ technique.

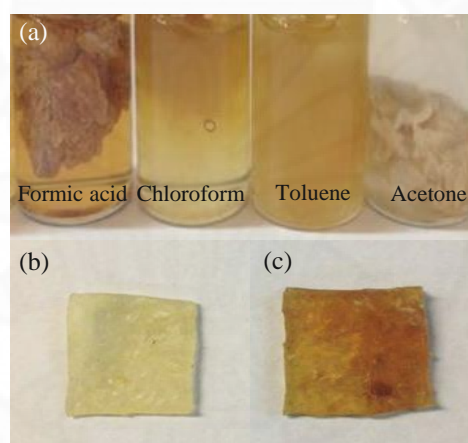


Figure 4.6 Photograph images of (a) insoluble PNVCL-NR in any organic solvents, (b) NR, and (c) PNVCL-NR.

4.1.2.2 Chemical structure and characteristics of PNVCL-NR

(1) FT-IR analysis of PNVCL-NR

The FT-IR spectrum of PNVCL-NR sample as demonstrated in Figure 4.7 showed the characteristic signals of both NR and PNVCL domains. The signals at 3473 and 3285 cm^{-1} assigned to the stretching vibration of O–H and N–H bands of the caprolactam ring. Moreover, the peaks of C=O and C–N stretching of PNVCL within the crosslinked material were observed at 1634 and 1482 cm^{-1} ,

respectively [7,8]. Nevertheless, the NR component showed the signals at 1375 and 923 cm^{-1} , which corresponded to C–H bending of $-\text{CH}_3$ and C=C bending, respectively [35,76,120]. These results confirmed that NR and PNVCL were presented within the crosslinked material. Additionally, the further signature signals of FT-IR spectra for NR, PNVCL, and PNVCL-NR were shown in Table 4.4.

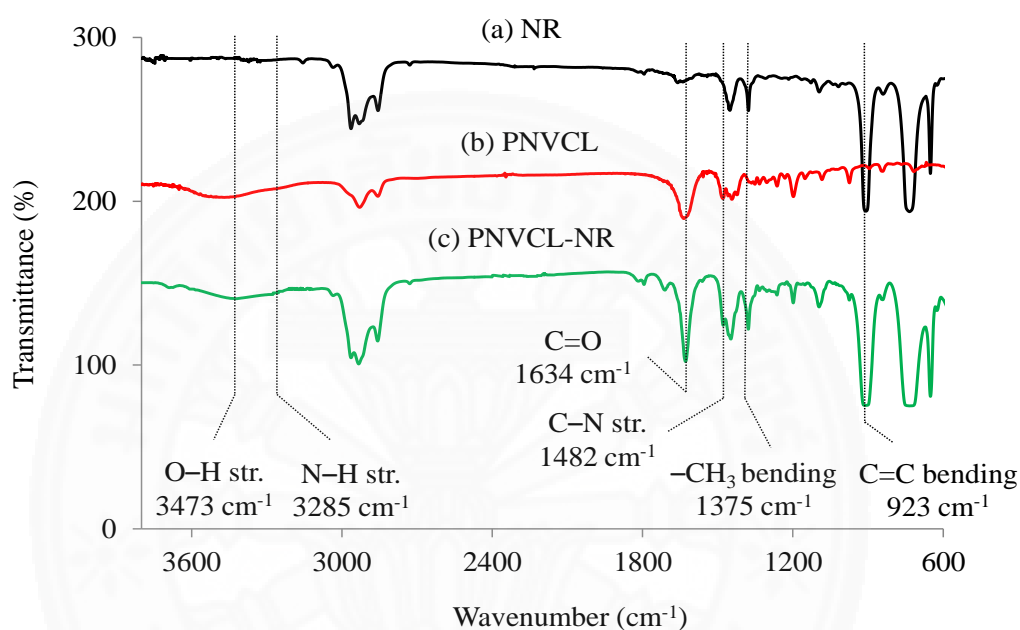


Figure 4.7 FT-IR spectra of (a) NR, (b) PNVCL, and (c) PNVCL-NR (31% gel content).

Table 4.4 Assignment of corresponding FT-IR spectra for NR, PNVCL, and PNVCL-NR.

Functional group	Wavenumber (cm^{-1})		
	NR	PNVCL	PNVCL-NR
O–H stretching	-	3509	3473
N–H stretching	-	3287	3285
Aliphatic C–H stretching	2953, 2863	2937, 2864	2942, 2865

Table 4.4 (Continued) Assignment of corresponding FT-IR spectra for NR, PNVCL, and PNVCL-NR.

Functional group	Wavenumber (cm ⁻¹)		
	NR	PNVCL	PNVCL-NR
C=C stretching	1676	-	1724
C=O stretching	-	1643	1634
C-N stretching	-	1485	1482
-CH ₂ bending	1457	1447	1458
-CH ₃ bending	1379	-	1375
C=C bending	930	-	923

(2) XPS analysis of PNVCL-NR

In order to guarantee the synthesis of crosslinked material, XPS technique was chosen to give the information about the chemical compositions at the surface of measured specimens. XPS spectra of both NR and PNVCL were illustrated in Figure 4.8. We found the signals of O_{1s}, C_{1s}, Si_{2s}, and Si_{2p} at 532, 285, 153, and 102 eV, respectively. As expected, the presence of carbon signals resulted from the intrinsic hydrocarbon domain in the rubber materials, while silicon signals arose from the silicon substrate used in the measurement. However, only the PNVCL-NR sample showed a strong N_{1s} signal at 399 eV with the increasing in atomic percentage of nitrogen around 2.13%, indicating the presence of PNVCL in the crosslinked structure. By contrast, small N_{1s} peak was negligible in the spectrum of pristine NR sample, which might be corresponded to the protein's residue.

Based on the formation of insoluble product and the evidences from FT-IR and XPS techniques thus affirmed the formation of crosslinked material between dry rubber and PNVCL.

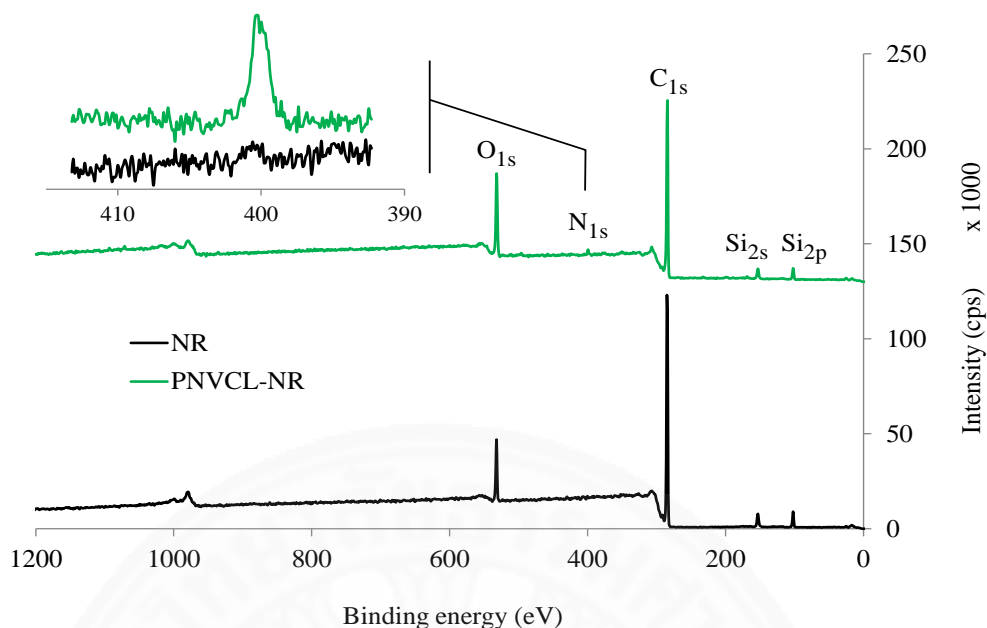


Figure 4.8 XPS spectra of NR and PNVCL-NR (31% gel content). The inset shows the multiplex-scan spectra in the N_{1s} region.

4.1.2.3 Thermal properties of PNVCL-NR

(1) DSC analysis of PNVCL-NR

DSC was conducted to examine the thermal behavior of the specimens by heating them at the temperature range between -80 and 300 °C under inert nitrogen atmosphere with a heating rate of 10 °C/min. From Figure 4.9, DSC thermograms illustrated the T_g value of each specimen from the midpoint of transition step. In this thesis work the T_g of pristine NR was found about -58.9 °C. While the other literature works presented the T_g of NR as -47.0 °C [121], -65.1 °C [35], and -73.0 °C [122]. Moreover, the T_g value at 184.1 °C belonged to the PNVCL was observed in the current research, which apparently slight higher than the preceding works that reported the T_g of PNVCL at 147.0 °C [123,124] and 174.6 °C [8]. Many reasons include the unique properties of the prepared product (such as molecular weight) as well as sample preparation could result in the differences in T_g value of the samples [35]. However, the synthesized PNVCL-NR sample presented only one of T_g value at approximately 133.0 °C. It could be assumed the formation of novel

copolymer because it exhibited the new T_g value which located between the T_g of pristine NR and PNVCL. The occurrence of one T_g value in this resultant material indicated that the two polymer domains were compatible and presented only single phase. Moreover, this result agreed with the earlier work that was reported by Gordon, M. and coworkers [125]. They noticed that the random copolymer regularly showed the T_g between those of the correspondent homopolymers.

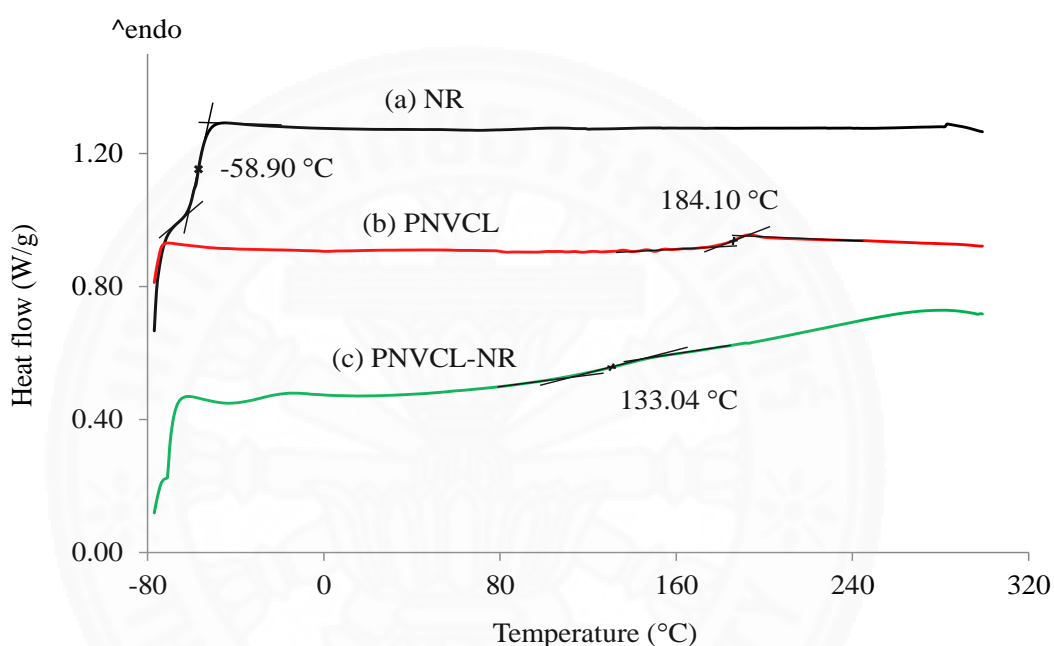


Figure 4.9 DSC thermograms of (a) NR, (b) PNVCL, and (c) PNVCL-NR (31% gel content).

(2) TGA analysis of PNVCL-NR

To clarify the thermal property and components of the specimens, it was also investigated using TGA technique from 30 to 600 °C under the nitrogen atmosphere at a ramp rate of 10 °C/min. According to the TGA and its first derivative curve which also known as DTG as illustrated in Figure 4.10 and 4.11, each sample showed its own decomposition behavior upon the region of temperature in accordance with its component. Thermogram of intrinsic NR presented only one stage of weight loss around 300-480 °C (99.52%). This was because of the

degradation of hydrocarbon composition. Meanwhile, PNVCL showed two-main steps of thermal decomposition at about 40-120 °C and up to 380 °C. The first step of weight loss associated with the dehydration of specimen and another one that attributed to the breakage of amide functional group of caprolactam ring [7]. In the case of PNVCL-NR sample, the minimal weight decrease (7.49%) started at 90 °C and continued up to around 310 °C related to the elimination of absorbed moisture. Besides, it underwent the maximum weight loss (63.80%) in the second stage at around 310-420 °C, similar to the thermal degradation of pristine NR. After approximately 420 °C, the final weight loss (27.76%) indicated the thermal degradation of PNVCL. By considering the decomposition temperatures with around 50% weight loss of each specimen from the intermediate point of two lines were observed at 387, 443, and 391 °C which belonged to NR, PNVCL, and PNVCL-NR samples, respectively. From the data as mentioned previously, the thermal stability of PNVCL-NR almost resembled those of NR, but it was slightly more stable due to the presence of PNVCL. Also, this result could be confirmed the existence of both NR and PNVCL in the PNVCL-NR material.

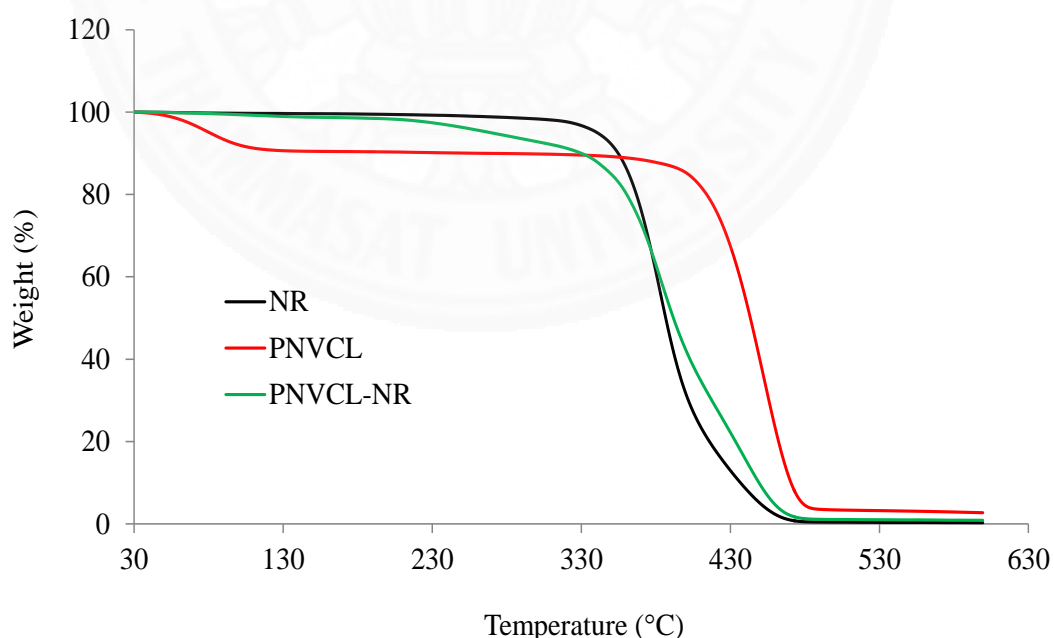


Figure 4.10 TGA thermograms of NR, PNVCL, and PNVCL-NR (31% gel content).

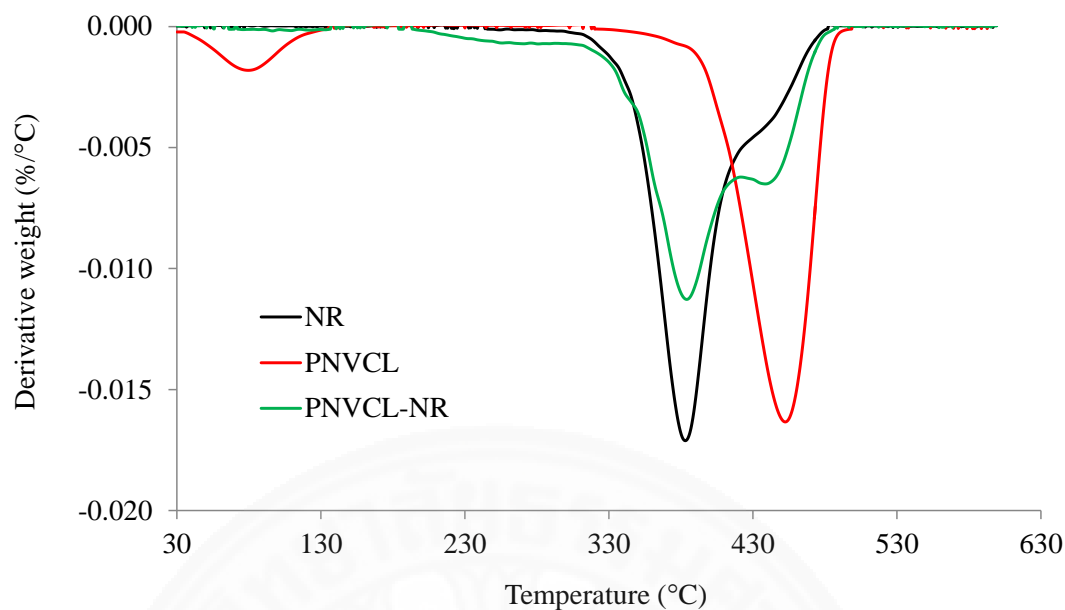


Figure 4.11 DTG thermograms of NR, PNVCL, and PNVCL-NR (31% gel content).

4.1.2.4 Effect of reaction parameters on gel content of PNVCL-NR

(1) Effect of polymer concentration

The gel content in percentage as a function of PNVCL concentration was measured using an initiator concentration of 10 phr, a reaction temperature of 75 °C, and a reaction time of 24 h. It was seen that, when the PNVCL concentration was increased from 50 to 150 phr, the gel content in percentage linearly increased from 36 to 85% as displayed in Figure 4.12. The increase in gel content under this condition might be due to a large number of PNVCL molecules providing a higher probability of PNVCL radicals from the abstraction at labile hydrogen atoms *via* free radicals to react with the polyisoprene backbone at the active sites.

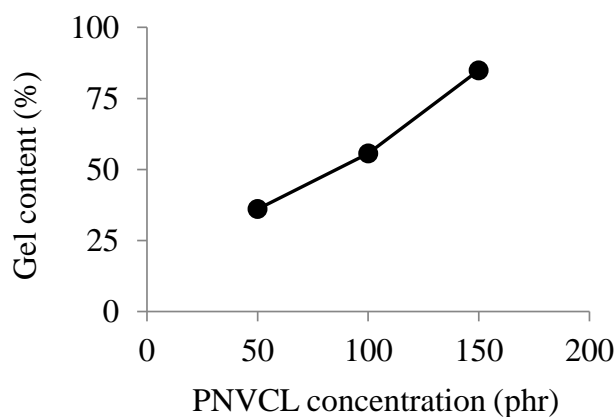


Figure 4.12 Effect of PNVCL concentration on gel content.

(2) Effect of initiator concentration

The effect of BPO concentration on gel content was studied using a PNVCL concentration of 100 phr, a reaction temperature of 75 °C, and a reaction time of 24 h. When the BPO concentration was increased from 5 to 50 phr, the gel content showed an increasing trend from 51 to 67% as illustrated in Figure 4.13. This phenomenon could be explained that the abundant free radicals produced by the dissociation of BPO promoted the formation of reactive sites on both PNVCL and rubber backbone [61]. Hence, more active radicals yielded higher gel content.

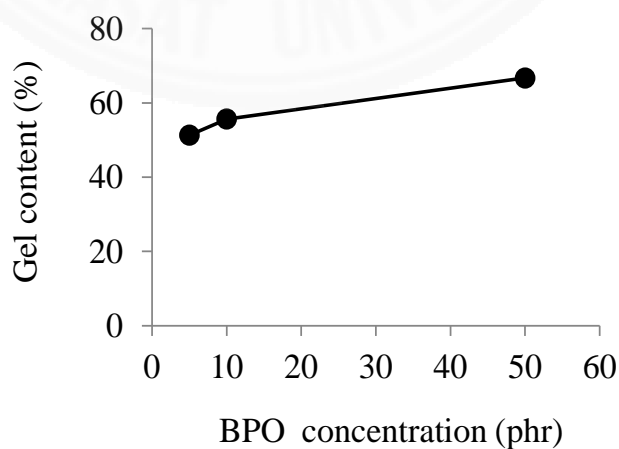


Figure 4.13 Effect of BPO concentration on gel content.

(3) Effect of reaction temperature

To investigate the effect of reaction temperature on the percentage of gel content, the reaction was carried out using a PNVCL concentration of 100 phr, a BPO concentration of 10 phr, and a reaction time of 24 h. As shown in Figure 4.14, when the temperature was increased from 75 to 95 °C, which is an optimum temperature range for BPO and PNVCL, the gel content gradually fell from 56 to 26%. This was due to the higher temperature could generate the numerous free radicals from the very rapid degradation of BPO and then these radicals might recombine, leading to the initiator proficiency was depleted which related to the lower amount of active species [36]. Thus, the decreasing of gel content was also observed.

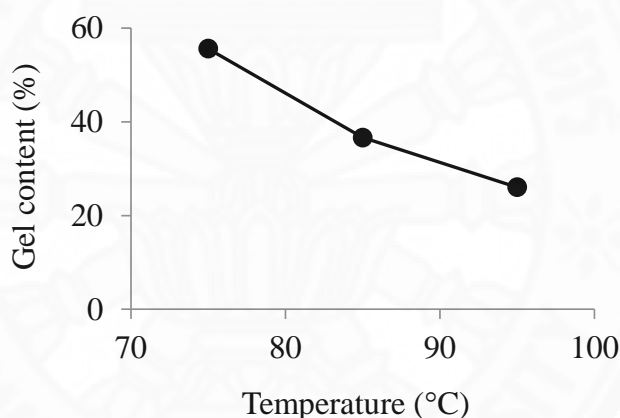


Figure 4.14 Effect of reaction temperature on gel content.

(4) Effect of reaction time

The effect of reaction time on the gel content was examined using a PNVCL concentration of 100 phr, a BPO concentration of 10 phr, and a reaction temperature of 75 °C. It was seen that as the reaction time was extended from 12 to 36 h, there was a considerable increase in the percentage of gel content from 21 to almost 100% as displayed in Figure 4.15. This outcome could be explained that a prolong reaction time brought about the higher probability for PNVCL radicals to interact with the reactive sites on polyisoprene backbone [34]. Therefore, the gel content was greatly progressed with the use of longer period of reaction time.

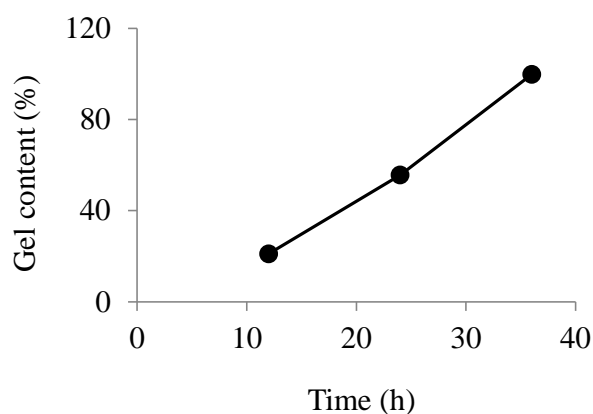


Figure 4.15 Effect of reaction time on gel content.

4.1.2.5 Investigation of crosslink density of PNVCL-NR

The crosslink density of the crosslinked material was determined from equilibrium swelling in toluene using the Flory-Rehner equation. As could be noticed, the gel content was proportional to the crosslink density. When increasing the percentage of gel content from 26 to 80%, the crosslink density also climbed up gradually from 2 to 7 mol/m³ as shown in Figure 4.16 (a). This behavior was anticipated that a much higher concentration of PNVCL led to chain entanglement in the rubber network, resulting in a progressive increase in restriction of polymeric chain mobility [126,127].

By contrast, the higher gel content gave rise to decrease in the degree of swelling as displayed in Figure 4.16 (b). At the gel content of 26%, the swelling percentage was found to be approximately 1932%. While the swelling percentage lowered to 954% at the gel content of 80%. The reasonable result suggested that the polymeric chains of network material with lower gel content were still flexible enough for solvent to readily move inside the network, causing the extension of the polymer chains as indicated by the growth of swelling percentage [128]. On the other hand, at higher gel content of the material, this network material had polymer chains with less flexible which could act as the barrier to prevent the solvent from penetrating into the rubber material, resulting in minimum solvent uptake.

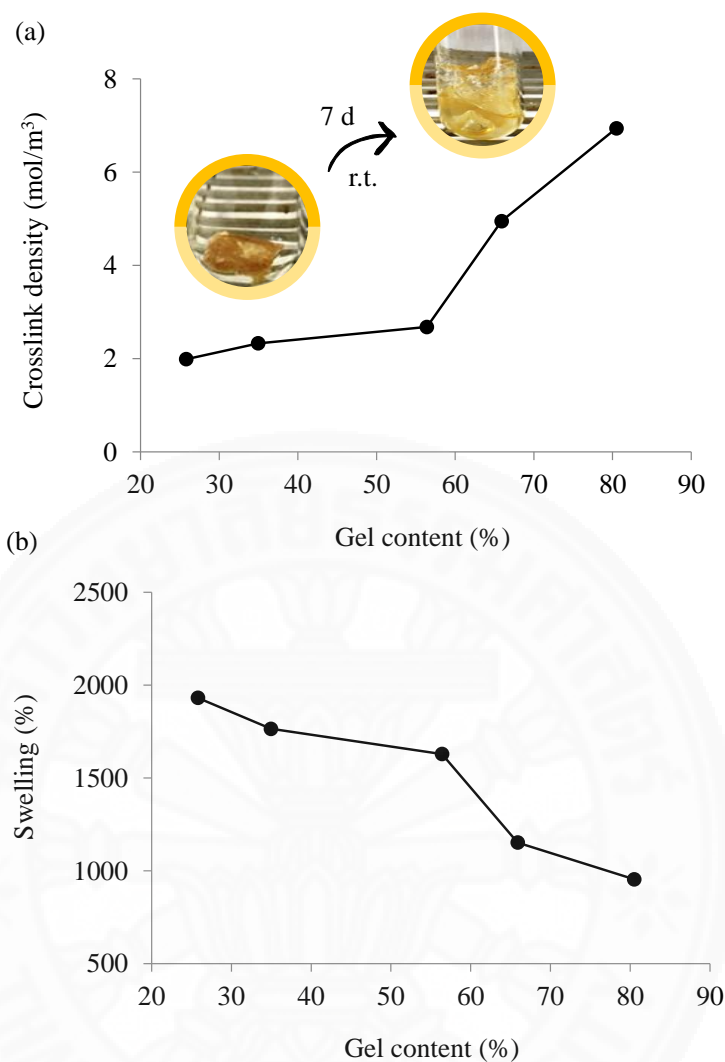


Figure 4.16 (a) Crosslink density and (b) degree of swelling of PNVCN-NR as a function of gel content.

4.1.2.6 Investigation of temperature-responsive behaviors of PNVCN-NR

(1) The water absorption measurement of PNVCN-NR

The temperature-responsive behaviors of pristine NR and PNVCN-NR were characterized using water swelling experiment at the temperature interval of 28-38 °C for 3 h. As shown in Figure 4.17, at the temperature below 34 °C, the crosslinked samples with the gel contents of 19 and 31% swelled to approximately

10 and 16% of their original weights or around 5 and 8 times more than the NR sample, respectively. Regarding the degree of swelling of both PNVCL-NR samples were found to higher than NR, because of the presence of hydrophilic NVCL moieties in the crosslinked materials that linked with water molecules *via* hydrogen bonding. This interaction was predominant at low temperature.

In contrast, as the temperature exceeded 32 °C, the swelling percentage of the PNVCL-NR samples reduced immediately. Also, the shrinkage of these samples was observed in agreement with the temperature-induced disappearance of hydrogen bonding with molecules of water and enhancement the hydrophobic character of caprolactam groups [93]. However, there was no change in the swelling percentage of NR sample across the measured temperature range. As a result, it could be distinctly implied that PNVCL-NR samples exhibited the coil-to-globule transition behavior in the range of 32-34 °C. This value was regarded as LCST, which was similar to the soluble-to-insoluble temperature of PNVCL [7,8]. Furthermore, this finding additionally revealed that the presence of NR and network structure in the PNVCL-NR samples did not significantly affect the LCST of the PNVCL molecules. This was consistent with the reports on other thermosensitive-based crosslinked materials [129-131].

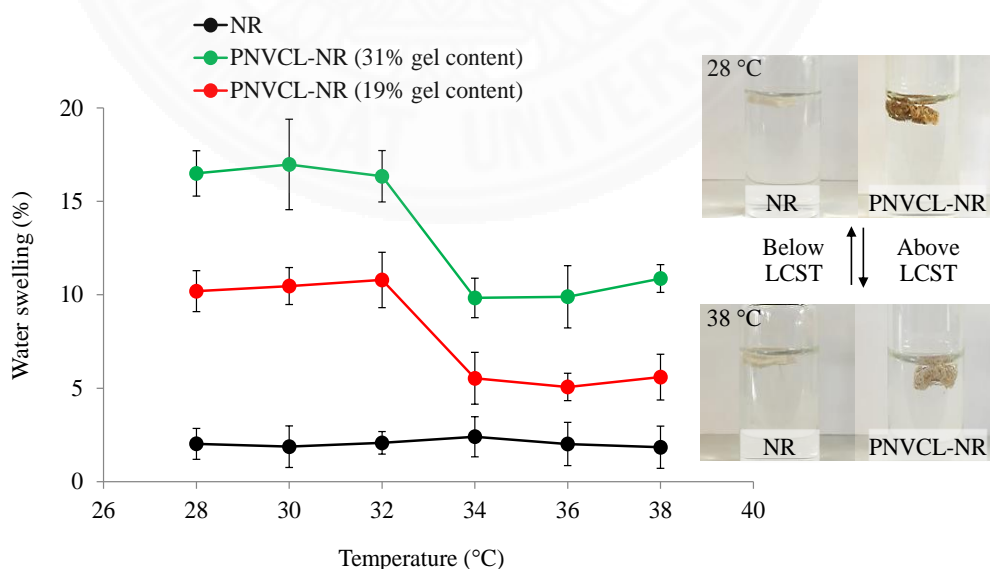


Figure 4.17 Degree of swelling of NR and PNVCL-NR (19 and 31% gel contents) in water as a function of temperature.

(2) The contact angle determination of PNVCL-NR

The water contact angle was also measured to identify the LCST character of the samples by heating the samples in controlled temperature contact angle meter at the temperature range from 28 to 38 °C. From the contact angle values as illustrated in Figure 4.18, it was found that the contact angle of the NR sample remained approximately at 104-108° through the measured temperature range. As expected, the NR showed the hydrophobic characteristic. Meanwhile, the contact angle of PNVCL-NR sample was lower than those of NR because of the presence of hydrophilic NVCL units. Increasing the temperature from 32 to 34 °C resulted in an increase in contact angle of PNVCL-NR from 77 to 97°, indicating an increase in hydrophobicity of NVCL units. This outcome was governed by the broken hydrogen linkages between the water molecules and NVCL units within the PNVCL-NR sample. Besides, the sudden change of PNVCL-NR at the temperature range between 32-34 °C, confirmed the LCST value of this material which agreed with the result from the water absorption measurement.

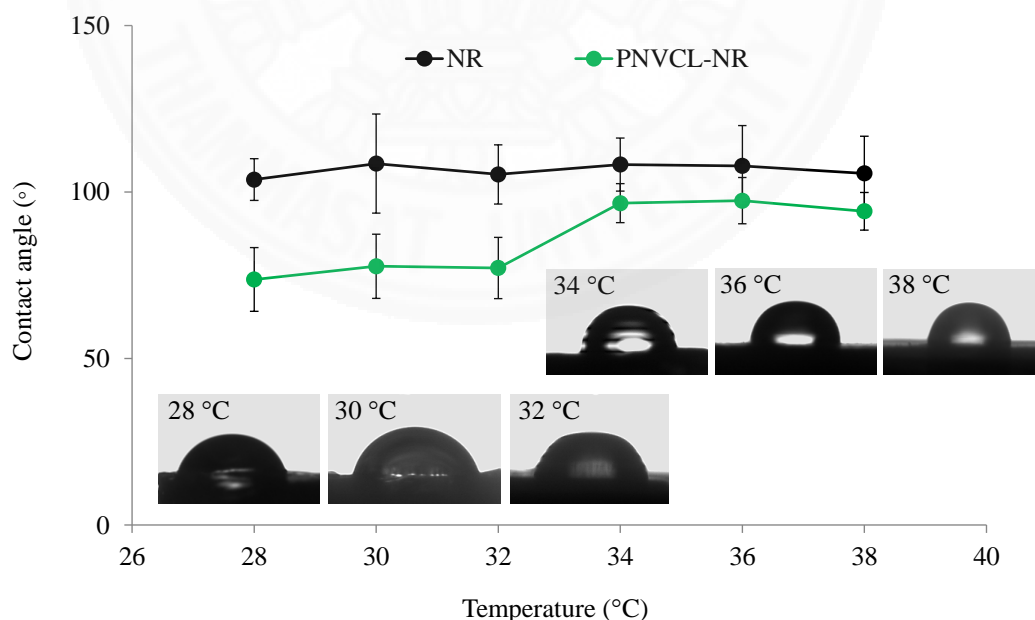


Figure 4.18 Contact angles of NR and PNVCL-NR (31% gel content) as a function of temperature.

(3) Dye adsorption and desorption studies of PNVCL-NR

To utilize the temperature responsive function of the PNVCL-NR samples, the adsorption and desorption as a function of temperature were determined using indigo carmine as the drug model. Indigo carmine was selected due to its non-toxic, high soluble in an aqueous medium as well as it exhibits the strong absorbance in the visible region. After the rubber samples were immersed in the indigo carmine solution for 1 week at room temperature, the crosslinked samples were found to absorb more dyes than the pristine NR, as illustrated by a greater reduction in dye absorbance and the change of color as shown in Figure 4.19. Fortunately, the PNVCL-NR sample with higher gel content absorbed more indigo carmine than the sample with lower gel content, as indicated by the larger decrease in absorbance in the UV-visible spectra and the amount of dye loading which was estimated by the weight difference before and after dye loading as presented in Table 4.5. This fascinating behavior was possibly attributed to the larger number of amide functional groups of caprolactam ring within the crosslinked structure, leading to more hydrogen bonding with the amino groups of the indigo carmine molecules [132].

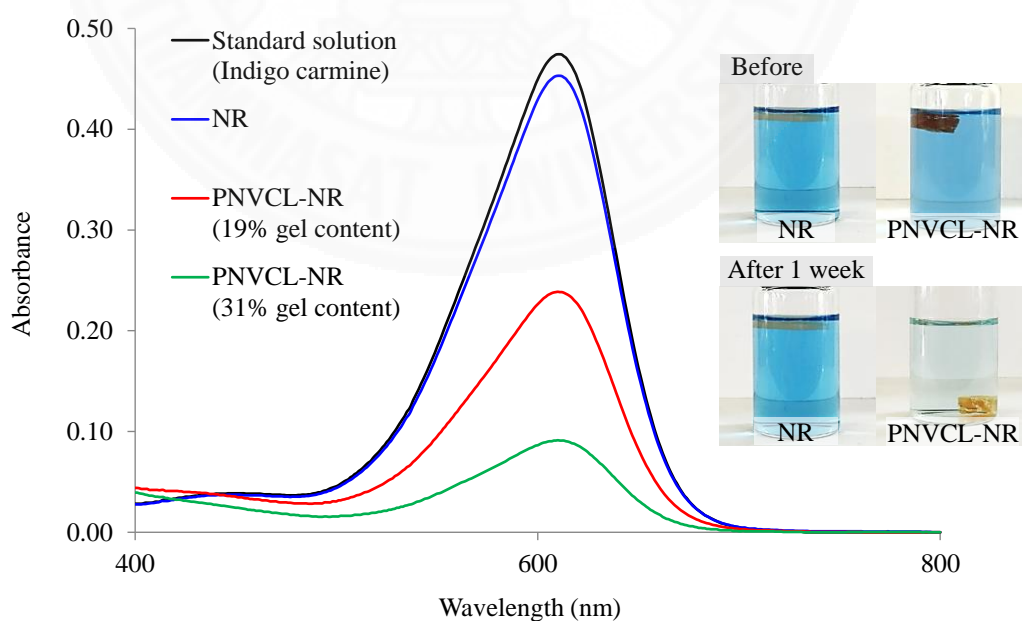


Figure 4.19 UV-visible spectra of standard indigo carmine solution and solutions after immersion of NR and PNVCL-NR (19 and 31% gel contents).

Table 4.5 Percentage of indigo carmine loading into NR and PNVCL-NR.

Sample name	Percentage of indigo carmine loading
NR	0.11
PNVCL-NR (19% gel content)	3.69
PNVCL-NR (31% gel content)	8.81

After dye adsorption, the rubber samples were removed, dried, and soaked in an aqueous solution at the range of temperature between 28 and 38 °C for 3 h. The UV-visible spectra and release profiles of indigo carmine from both rubber samples at above and below the LCST were presented in Figure 4.20. Apparently, at the temperature below 34 °C, it was seen that both crosslinked materials still held dyes on their molecules through hydrogen bonding between hydrophilic moieties of caprolactam groups in PNVCL-NR samples and amino groups of indigo carmine. Furthermore, the absorbance of PNVCL-NR samples at this temperature range was found to higher than NR. This was due to some of dyes on the surface of PNVCL-NR samples were released into the solution.

Once the temperature was raised above 32 °C, the PNVCL-NR samples contracted and then discharged the entrapped dyes into an aqueous media, as confirmed by the increasing absorbance and darker blue solution as shown in Figure 4.20 and 4.21, respectively. This behavior corresponded to the collapse of the PNVCL chains in the crosslinked materials at above its nature LCST [133,134]. Similarly, the PNVCL-NR with 31% gel content could release more dyes than the sample with 19% gel content, because more dyes were available on the sample with higher gel content that related to it had numerous hydrogen bonding between hydrophilic segments of NVCL units containing in the PNVCL-NR with amino groups of indigo carmine. During this experiment, the absorbance of indigo carmine from the NR sample did not change over the measured temperature range. This result assured that only PNVCL-NR samples could be the temperature-responsive material in biomedical and sensing applications.

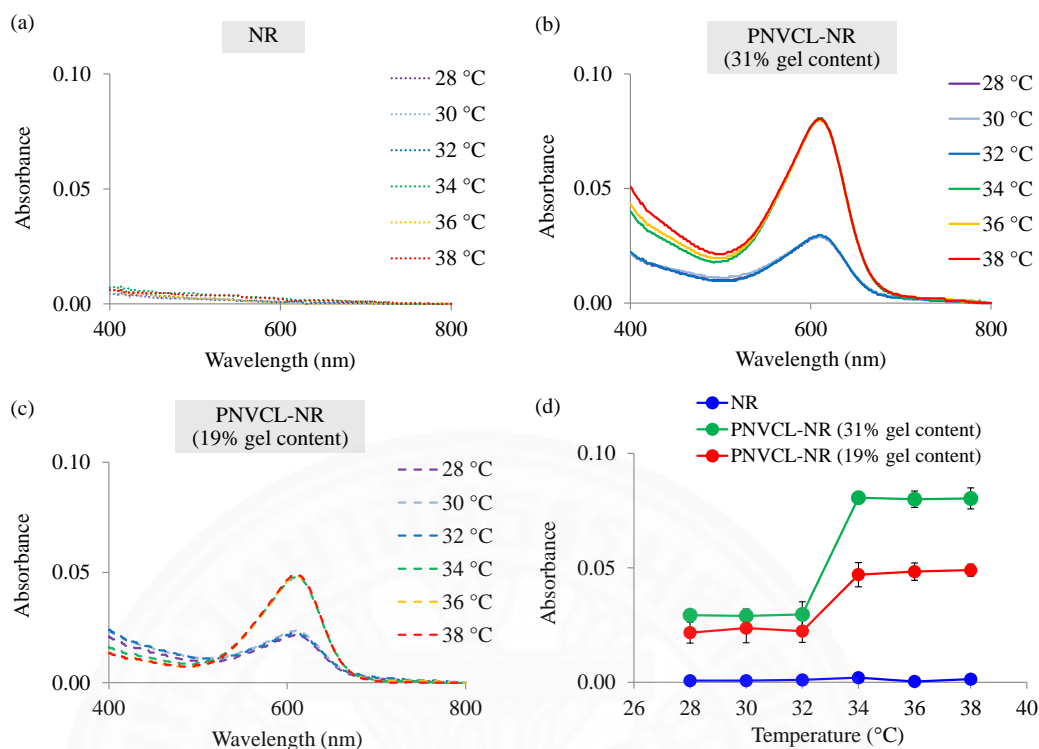


Figure 4.20 UV-visible spectra of solutions after desorption of indigo carmine from (a) NR, (b) PNVCL-NR (31% gel content), and (c) PNVCL-NR (19% gel content) at different temperatures, and (d) release profiles of indigo carmine from NR and PNVCL-NR samples at $\lambda_{\max} = 610$ nm.

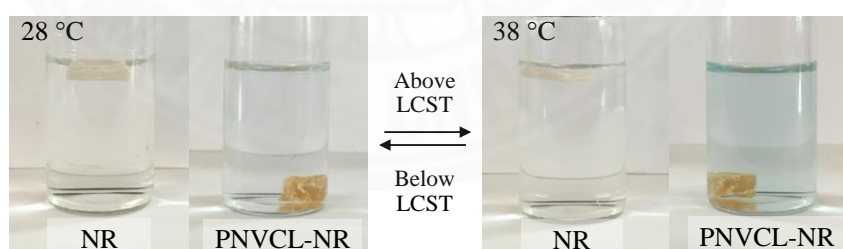


Figure 4.21 Photograph images of NR and PNVCL-NR (31% gel content) after desorption.

4.1.2.7 Adsorption studies of PNVCL-NR

In this part studies on the interaction between indigo carmine molecules and the surface of PNVCL-NR samples. The equilibrium adsorption

process was done by introducing the PNVCL-NR samples into different concentrations of indigo carmine solution in the range of 10-50 ppm for 1 week at room temperature. Also, the determination of adsorption mechanism was performed on the basis of comparing the correlation coefficient or R^2 of four well-known isotherm models including Langmuir, Freundlich, Temkin, and Dubinin-Radushkevich isotherms.

On the basis of R^2 which was achieved from the linear plot between q_e and C_e values of these models as demonstrated in Figure 4.22, the Langmuir model showed the highest value of R^2 as 0.80, which was the best suitable isotherm among the four adsorption models. This result indicated that a monolayer adsorption of indigo carmine was more likely to take place on the surface of PNVCL-NR samples with Q_0 or maximum monolayer coverage capacity around 0.91 mg/g [107,117].

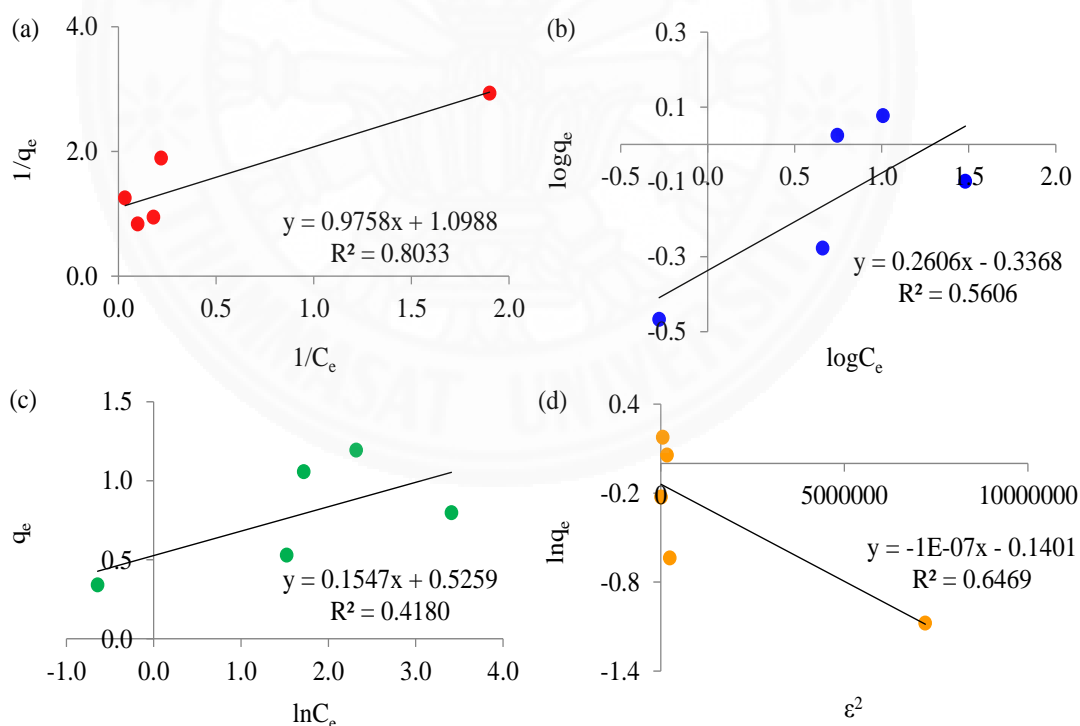


Figure 4.22 Linear plots of (a) Langmuir, (b) Freundlich, (c) Temkin, and (d) Dubinin-Radushkevich adsorption isotherms for the adsorption process of indigo carmine onto PNVCL-NR (31% gel content) surface.

In addition to the R^2 values, there were the characteristic parameters from each model which provided the several essential information related to adsorption mechanism as depicted in Table 4.6. From the Langmuir adsorption model, the R_L parameter known as the unitless constant which applied to forecast the nature of adsorption between dye molecules and PNVCL-NR surface. As shown in Figure 4.23, the R_L value was observed in the region of 0.02-0.08 with different concentrations of indigo carmine solution from 10-50 ppm, representing that the adsorption of indigo carmine on the outer surface of PNVCL-NR samples was the favorable process ($0 < R_L < 1$) [110,111]. In addition, the lower R_L at higher initial dye concentration referred that the adsorption was found to be more favorable at higher concentration. The degree of favorability was generally involved with the irreversibility of the system, providing a qualitative assessment of the interaction between PNVCL-NR and dyes. The R_L approached zero with the increase of initial dye concentration (the completely ideal irreversible case) rather than the unity (the completely reversible case).

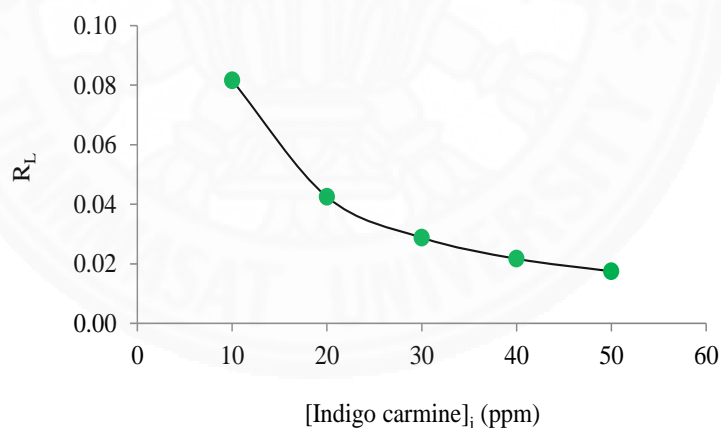


Figure 4.23 Plot between equilibrium parameter and initial dye concentration for the adsorption process of indigo carmine onto PNVCL-NR (31% gel content) surface.

Although the R^2 of the Freundlich isotherm model was not the best value for describing the adsorption mechanism. The n parameter from this model remained useful to explain the favorability of adsorption process. Under this experiment, the n value ($n = 3.84$) exhibited the higher value than the unity ($n > 1$),

it markedly denoted that the indigo carmine was favorably physical absorbed onto the PNVCL-NR surface [108,135].

The B parameter from the Temkin isotherm could describe the type of adsorption from the parameter involved the heat of sorption. As a result, the B value was computed to be 0.15 J/mol, suggesting that the adsorption process was naturally physical sorption owing to its value below than 20 kJ/mol [113-115].

In accordance with the value of E constant from the Dubinin-Radushkevich isotherm gave the information about chemical and physical adsorption. The E value was reported to be 2.24 kJ/mol that lower than 8 kJ/mol, revealing the physisorption mechanism of indigo carmine would play an essential role on the outmost surface of PNVCL-NR [116,136,137].

Obviously, the data from n, B, and E values from each isotherm as stated formerly could guarantee that the adsorption process between indigo carmine molecules and PNVCL-NR surface was dominated by the physical sorption.

Table 4.6 Constants of each adsorption isotherm for the adsorption process of indigo carmine onto PNVCL-NR surface.

Langmuir constants				Freundlich constants			
Q_0 (mg/g)	K_L (L/mg)	R_L	R^2	1/n	n	K_f (mg/g)	R^2
0.91	1.13	0.02-0.08	0.80	0.26	3.84	0.46	0.56
Temkin constants				Dubinin-Radushkevich constants			
b_T	A_T (L/mg)	B (J/mol)	R^2	q_s (mg/g)	K_{ad} (mol ² /kJ ²)	E (kJ/mol)	R^2
16292.11	29.95	0.15	0.42	0.87	1×10^{-7}	2.24	0.65

4.2 Synthesis and characterization of NVCL-g-DPNR

4.2.1 Preparation of DPNR latex

The removal of proteins from NR latex is the indispensable step before graft copolymerization, since proteins surrounding the rubber particles can act as the free radical scavengers which limit the reaction to occur effectively and also originate the unpleasant compounds such as the branch or network materials. It was found that the deproteinization of NR would improve the grafting efficiency as insisted in previous reports [48,76]. Therefore, in this work the proteins were separated using urea treatment because this method was simple, rapid, and gave high proficiency [82]. Urea also known as denaturant agent which changes the conformation of proteins through hydrogen bonding with either peptide backbone or polar/apolar side chains of proteins [138]. Indeed, if the proteins exist on the rubber surface *via* physical interactions, it perhaps possible to eliminate the proteins from latex phase after denaturation process [81]. Besides, SDS serves as the surfactant that can enhance the colloidal stability in the latex system and further facilitate in the denaturation step. From the CHN data in Table 4.7 displayed the decrease in the nitrogen content in DPNR sample almost half compared to the untreated NR sample, while the percentages of carbon and hydrogen remained almost the same. Consequently, from our results could be inferred that the proteins were denatured with urea and then solubilized with SDS [139], hence those proteins would productively extract from rubber latex after centrifugation.

Table 4.7 CHN results of NR and DPNR.

Sample name	Average		
	%C	%H	%N
NR	84.79	12.68	0.76
DPNR	84.19	12.88	0.43

4.2.2 Preparation of NVCL-g-DPNR

4.2.2.1 Morphological observation of NVCL-g-DPNR

NVCL-g-DPNR was successfully prepared *via* free radical graft copolymerization in an aqueous media between DPNR latex and NVCL monomer using AIBN as a free radical initiator as displayed in Figure 4.24.

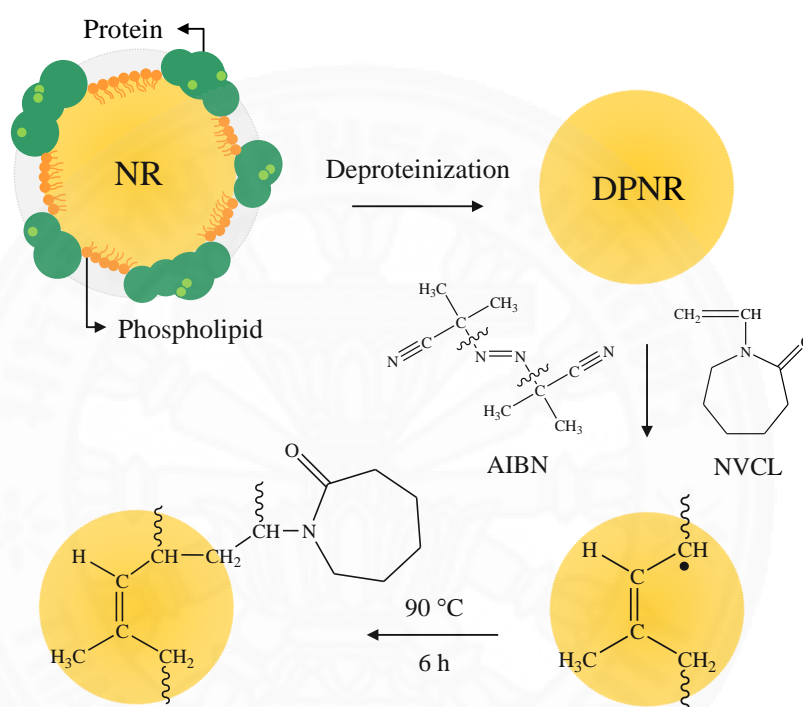


Figure 4.24 Diagram for preparation of NVCL-g-DPNR.

In this pathway, the water media was served as the solvent in the emulsion state for grafting the NVCL monomer onto rubber backbone due to its own good properties including environmental friendliness and generally available. As expected, this feasible process did not give the serious issues to the environment, human health, and production cost. This was due to avoiding the extensive usage of organic solvents, unlike in the case of solution system. Another advantage of this technique involved with the NR that was naturally available in the latex phase which would further facilitate to directly perform the grafting modification with NVCL monomer.

The formation of the grafted material progressed *via* two main procedures including a reaction between radical species from the decomposition of AIBN initiator with DPNR molecules through the abstraction of labile hydrogen atom in the α -methylene group to build the polyisoprenyl radicals and another related to the reaction of polymer radicals with NVCL monomer, generating the NVCL-g-DPNR [47,140,141].

When initiation by oil-soluble azo initiator or AIBN was used, it was predicted that the radicals should take place entirely within the rubber particle, which was the desirable locus of polymerization since AIBN structure contains a non-polar moiety which easily dissolved in a non-polar part of NR, leading to the generation of graft copolymer inside the rubber particle as shown in Figure 4.25 [38].

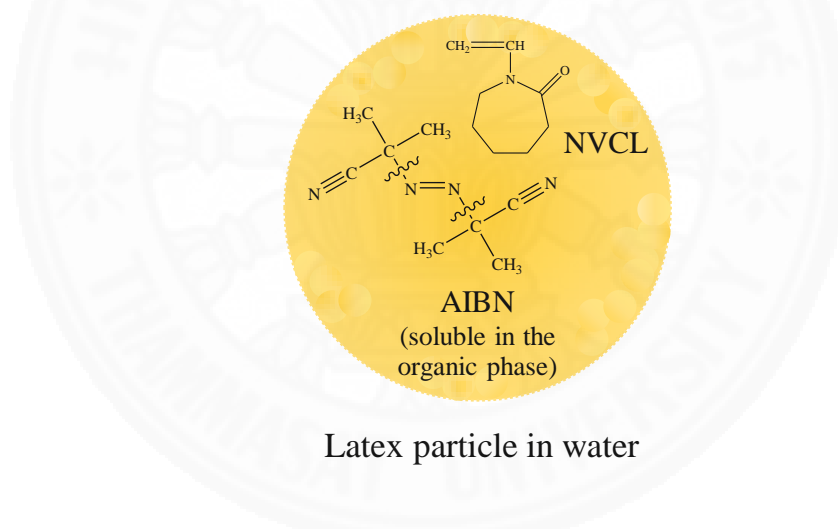


Figure 4.25 Locus of the graft copolymerization in the case of AIBN initiator used.

Certainly, the appearance of DPNR sample was a clear solid, whereas NVCL-g-DPNR material was a yellowish solid and stiffer than the DPNR as illustrated in Figure 4.26. The difference in color and characteristic could be indicated that the NVCL monomer was grafted onto rubber backbone.

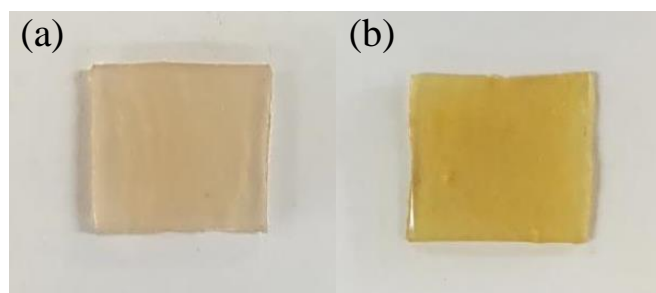


Figure 4.26 Photograph images of (a) DPNR and (b) NVCL-*g*-DPNR.

The thermo-sensitive modified rubber *via* grafting reaction was subsequently characterized in order to determine the chemical structure, thermal properties, temperature-responsive behaviors, as well as the adsorption studies using many techniques as presented below,

4.2.2.2 Chemical structure and characteristics of NVCL-*g*-DPNR

(1) FT-IR analysis of NVCL-*g*-DPNR

The FT-IR technique was used to characterize the chemical structure of rubber materials. Figure 4.27 presents the FT-IR spectrum of NVCL-*g*-DPNR which composed of the signature signals of DPNR and PNVCL. The peaks at 3442, 3274, 1634, and 1481 cm^{-1} were attributed to the stretching vibrations of O–H, N–H, C=O, and C–N bands of the PNVCL component, respectively [7,8]. While, the signals of C–H bending of $-\text{CH}_3$ and C=C bending of the polyisoprene domain within graft copolymer were observed at 1379 and 902 cm^{-1} , respectively [76,120]. The FT-IR results were consistent with our report in the previous section. Moreover, the further corresponding signals in FT-IR spectra of DPNR, PNVCL, and NVCL-*g*-DPNR were enumerated in Table 4.8.

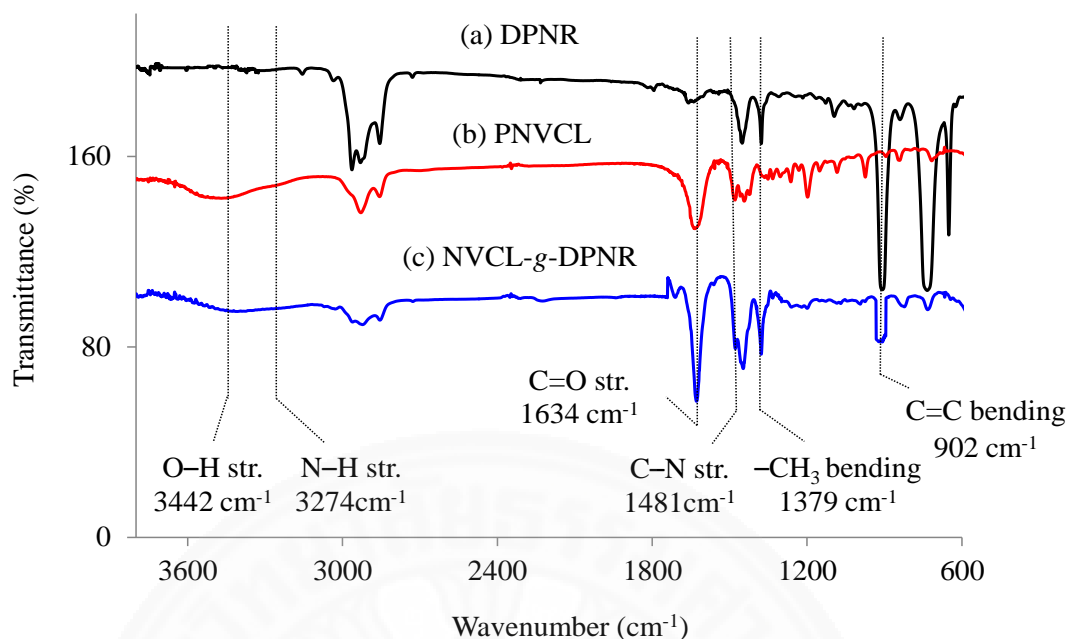


Figure 4.27 FT-IR spectra of (a) DPNR, (b) PNVCL, and (c) NVCL-g-DPNR (25% grafting ratio).

Table 4.8 Assignment of corresponding FT-IR spectra for DPNR, PNVCL, and NVCL-g-DPNR.

Functional group	Wavenumber (cm ⁻¹)		
	DPNR	PNVCL	NVCL-g-DPNR
O-H stretching	-	3509	3442
N-H stretching	-	3287	3274
Aliphatic C-H stretching	2955, 2864	2937, 2864	2946, 2877
C=C stretching	1679	-	1723
C=O stretching	-	1643	1634
C-N stretching	-	1485	1481
-CH ₂ bending	1462	1447	1456

Table 4.8 (Continued) Assignment of corresponding FT-IR spectra for DPNR, PNVCL, and NVCL-*g*-DPNR.

Functional group	Wavenumber (cm ⁻¹)		
	DPNR	PNVCL	NVCL- <i>g</i> -DPNR
-CH ₃ bending	1375	-	1379
C=C bending	938	-	902

(2) ¹H-NMR analysis of NVCL-*g*-DPNR

The ¹H-NMR technique was also applied to further detect the chemical structure of grafted material as demonstrated in Figure 4.28 and Table 4.9. The spectrum of DPNR showed resonance signals at 5.2, 2.1, and 1.7 ppm which were assigned to the unsaturated methyne proton (=CH), methylene protons (-CH₂), and methyl protons (-CH₃), respectively [59,76,142]. Furthermore, PNVCL exhibited essential signals at 4.4, 3.1, 2.4, and 1.0-1.8 ppm which corresponded to the protons in -CH-N, -CH₂-N, -CH₂-CO, and -CH₂ groups, respectively [7,8]. For NVCL-*g*-DPNR sample contained both signals of DPNR and NVCL units such as the signal at 5.2 ppm that was corresponded with the methyne proton (=CH) of the isoprene units and the important peak at 4.4 ppm which was attributed to the proton in -CH-N group of the NVCL units. Both signals as mentioned were used to calculate the grafting ratio, which was found to be 25% as presented in the following equation,

$$\begin{aligned}
 G (\%) &= \frac{I_{4.4}}{I_{5.2}} \times 100 \\
 &= \frac{0.25}{1.00} \times 100 \\
 &= 25 \%
 \end{aligned}$$

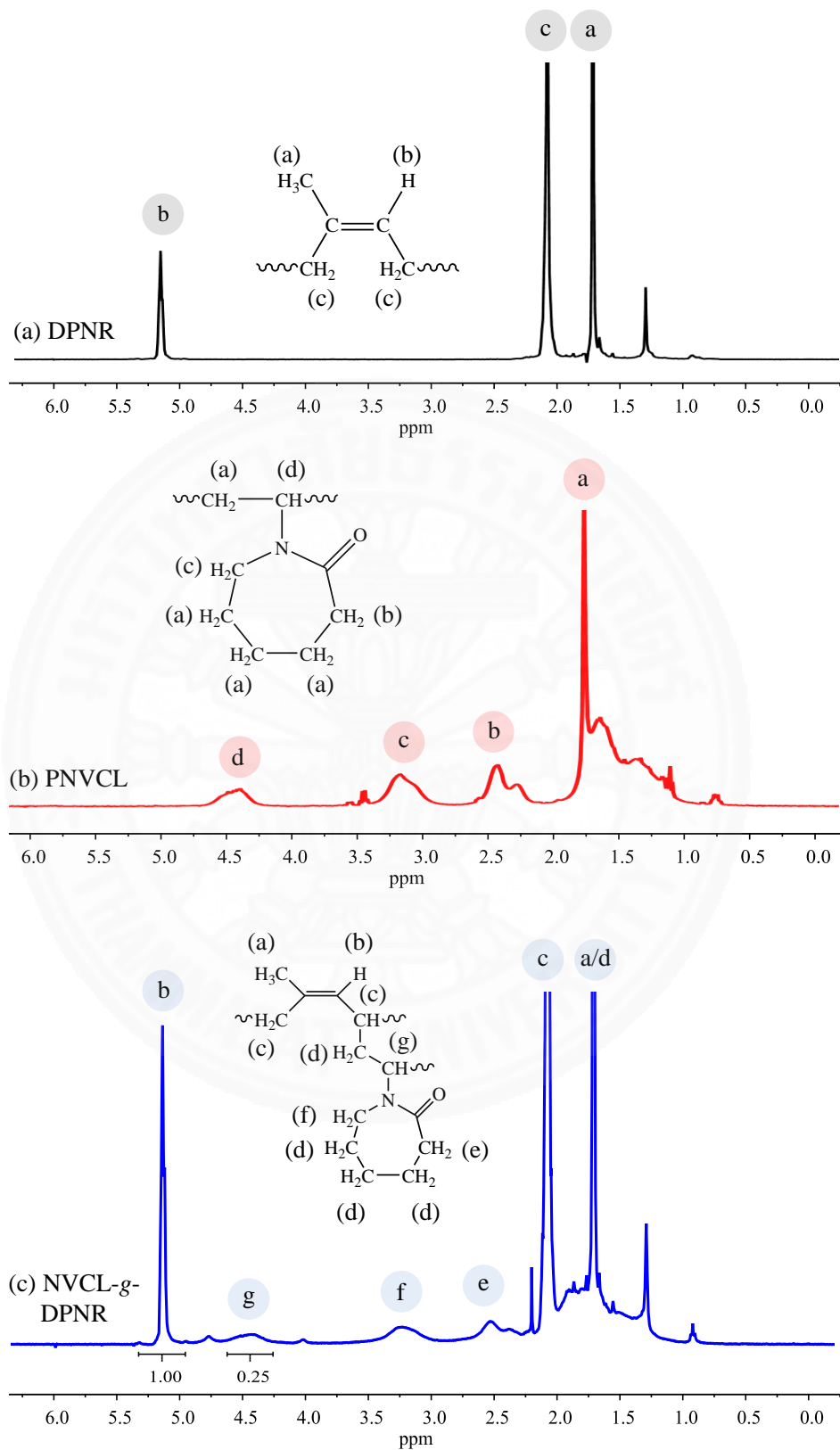


Figure 4.28 $^1\text{H-NMR}$ spectra of (a) DPNR, (b) PNVCL, and (c) NVCL-g-DPNR (25% grafting ratio).

Table 4.9 Assignment of corresponding $^1\text{H-NMR}$ spectra for DPNR, PNVCL, and NVCL-*g*-DPNR.

Proton position	Chemical shift (ppm)	Functional group
(a) DPNR		
H _a	1.7	–CH ₃ (3H)
H _b	5.2	=CH (1H)
H _c	2.1	(–CH ₂) ₂ (4H)
(b) PNVCL		
H _a	1.0-1.8	(–CH ₂) ₄ (8H)
H _b	2.4	–CH ₂ –CO (2H)
H _c	3.1	–CH ₂ –N (2H)
H _d	4.4	–CH–N (1H)
(c) NVCL-<i>g</i>-DPNR		
H _a	1.7	–CH ₃ (3H)
H _b	5.2	=CH (1H)
H _c	2.1	(–CH ₂) _{2-0.5} (3H, loss 1H)
H _d	1.0-1.8	(–CH ₂) ₄ (8H)
H _e	2.5	–CH ₂ –CO (2H)
H _f	3.2	–CH ₂ –N (2H)
H _g	4.4	–CH–N (1H)

(3) XPS analysis of NVCL-*g*-DPNR

The XPS spectra of DPNR and NVCL-*g*-DPNR showed the signals of O_{1s}, C_{1s}, Si_{2s}, and Si_{2p} at 532, 285, 153, and 102 eV, respectively (Figure 4.29). The presence of silicon signals due to the silicon substrate used in the measurement. Nevertheless, the XPS spectrum of NVCL-*g*-DPNR reported a notably greater in the N_{1s} signal at 399 eV with 2.72% of nitrogen concentration, showing the

existence of caprolactam groups of NVCL units in the graft copolymer. In contrast, the N_{1s} signal was unimportant in DPNR sample.

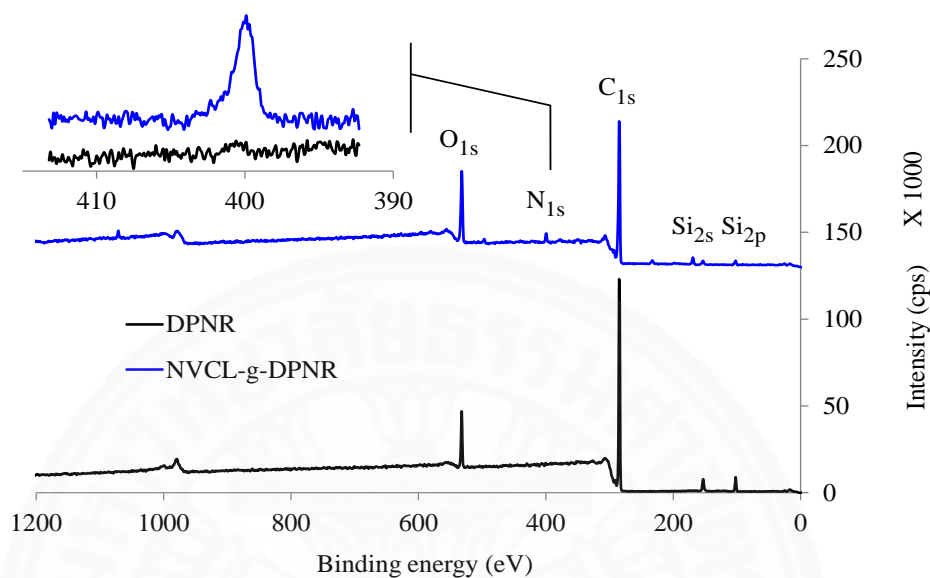


Figure 4.29 XPS spectra of DPNR and NVCL-*g*-DPNR (25% grafting ratio). The inset shows the multiplex-scan spectra in the N_{1s} region.

4.2.2.3 Thermal properties of NVCL-*g*-DPNR

(1) DSC analysis of NVCL-*g*-DPNR

The thermal property of samples was evaluated using DSC technique at the measured temperature interval from -80 to 300 °C under inert nitrogen atmosphere with a heating rate of 10 °C/min. The DSC curves as demonstrated in Figure 4.30 exhibited the T_g values of DPNR and PNVCCL samples at about -63.7 °C [121,122] and 184.1 °C [8,123,124], respectively. As stated in the previous section, the differences in T_g value of the measured samples could be related to many factors including the sample preparation, measurement condition, and also properties of the evaluated sample [35]. Interestingly, the thermogram of NVCL-*g*-DPNR showed two endothermic peaks derived from the intersection point of two lines includes slope and baseline of the peaks around -60.3 °C attributed to the T_g value of DPNR sample and at 175.7 °C corresponded to the T_g value of PNVCCL

component. This particularly implied that the obtained grafted material consists of amorphous domains of DPNR and NVCL units. Literally, T_g value was affected by the size of the side groups and the chain mobility. The increase in T_g of DPNR in graft copolymer was due to the chain stiffening because the existence of NVCL units which led to the reduction in free volume of the main chain. Consequently, the T_g of DPNR component in NVCL-*g*-DPNR was found to higher than the T_g of pure DPNR.

In the case of block or graft copolymer with adequate length of polymer chain, there could be more than one T_g values from the constituent units [125]. Therefore, this clearly confirmed the formation of graft copolymer whereas the resulting crosslinked product as mentioned earlier exhibited only one T_g value.

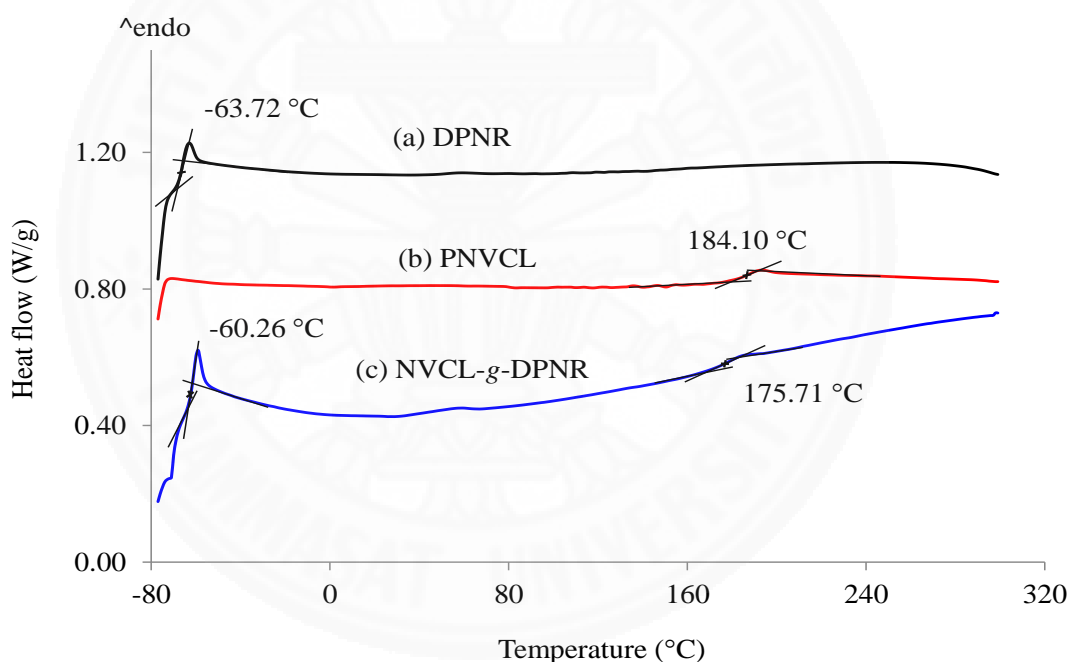


Figure 4.30 DSC thermograms of (a) DPNR, (b) PNVCL, and (c) NVCL-*g*-DPNR (25% grafting ratio).

(2) TGA analysis of NVCL-*g*-DPNR

To characterize the thermal stability, the TGA test was carried out in a temperature range of 30-600 °C under nitrogen atmosphere at the heat rate of 10 °C/min. As appeared in Figure 4.31 and 4.32, the TGA and DTG curves of

DPNR sample showed the one-step of thermal degradation at approximately 300-490 °C. This decrease came from the decomposition of polymer chains of rubber material. In addition, the PNVCL sample occurred the thermal decomposition in the two regions at about 40-120 °C and beyond 380 °C. The first period attributed to the absence of moisture. While, the second being related to the cracking of cyclic amide of caprolactam rings within PNVCL structure [7]. As can be seen the curve of the graft copolymer, the first period lowered at 290 °C was associated with the dehydration of specimen with initial weight loss about 5.50%. Moreover, the second stage exhibited the dramatical drop of weight as 53.48% and it took place in the region of 290-420 °C related to the degradation of polyisoprene. The last stage attributed to the decomposition of PNVCL around 38.23% which completely decomposed after 420 °C. Also, the decomposition temperatures of 50% weight loss for DPNR, PNVCL, and NVCL-g-DPNR samples underwent at the temperature around 390, 443, and 401 °C, respectively. This outcome guaranteed that NVCL grafting could improve the thermal stability of the DPNR main chain. Apparently, this result also confirmed the presence of both DPNR and NVCL units in the NVCL-g-DPNR sample.

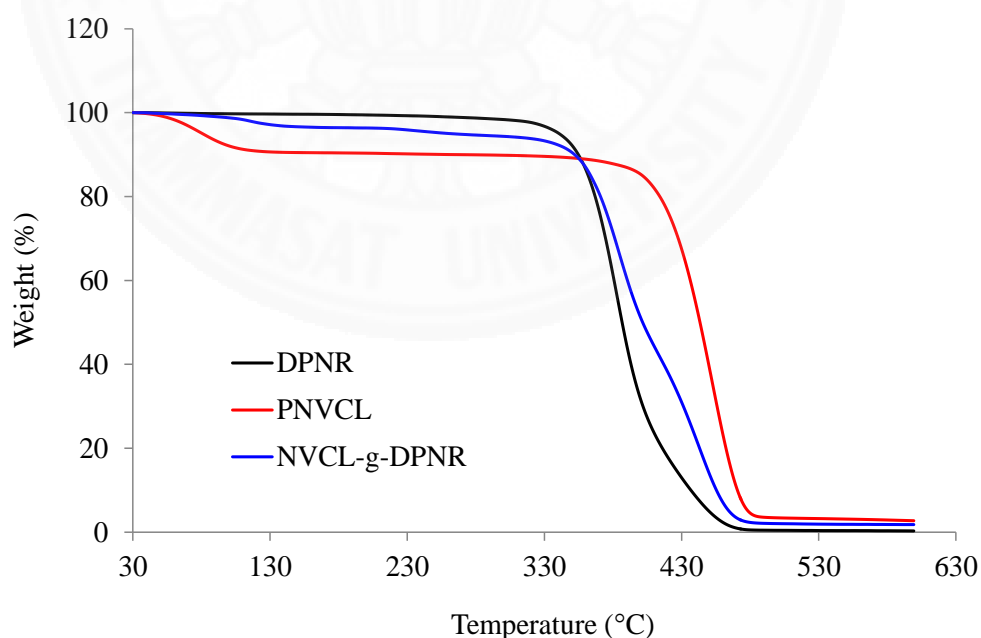


Figure 4.31 TGA thermograms of DPNR, PNVCL, and NVCL-g-DPNR (25% grafting ratio).

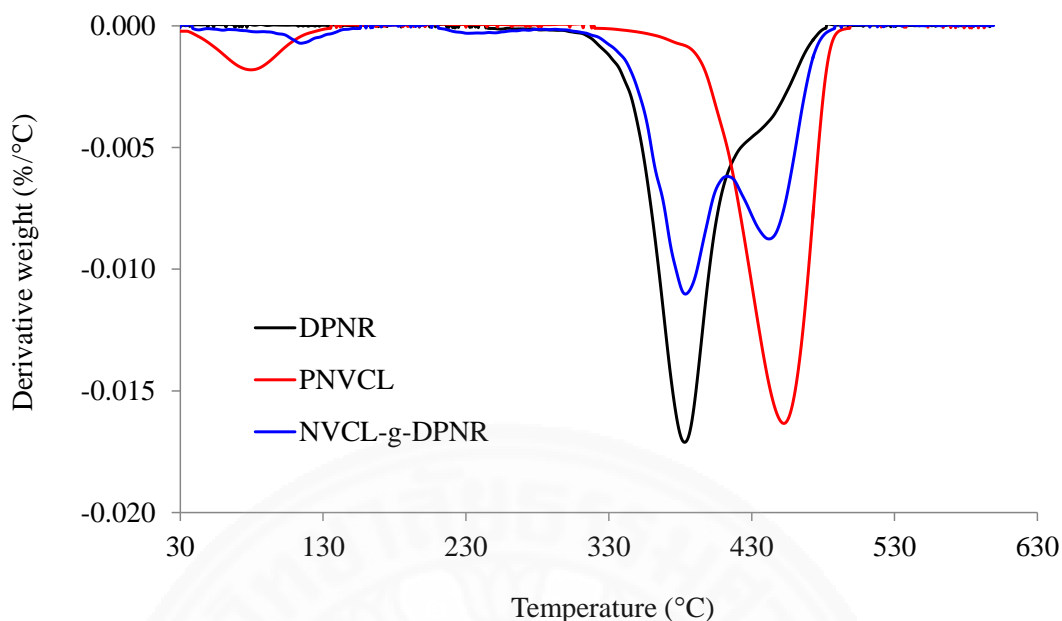


Figure 4.32 DTG thermograms of DPNR, PNVCL, and NVCL-*g*-DPNR (25% grafting ratio).

4.2.2.4 Effect of reaction parameters on grafting ratio of NVCL-*g*-DPNR

(1) Effect of monomer concentration

To explore the effect of NVCL concentration on the grafting ratio, the reaction was carried out using an AIBN concentration of 10 phr, a reaction temperature at 90 °C, and a reaction time of 6 h. It was found that, as the NVCL concentration was raised extremely from 50 to 150 phr, the grafting ratio increased from 11 to 38% as illustrated in Figure 4.33. This result indicated that the greater number of NVCL brought about the higher probability of NVCL radicals to disperse with the rubber phase for grafting at the reactive sites onto DPNR substrate [77]. Therefore, the percentage of grafting ratio also increased under this condition.

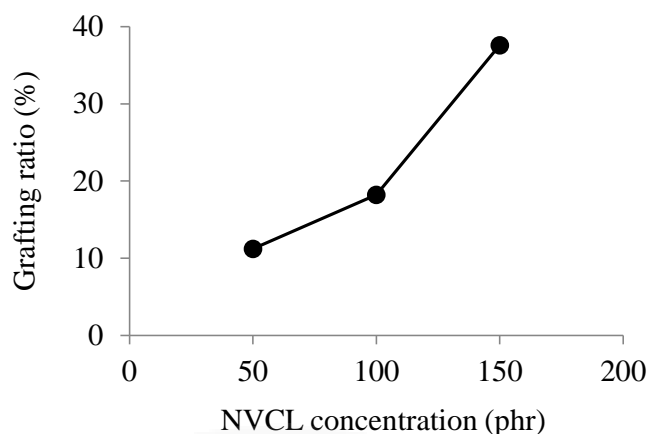


Figure 4.33 Effect of NVCL concentration on grafting ratio.

(2) Effect of initiator concentration

For the effect of AIBN concentration on grafting ratio, an NVCL concentration of 100 phr, a reaction temperature at 90 °C, and a reaction time of 6 h were used. When the AIBN concentration was enhanced from 5 to 15 phr, the grafting ratio gradually decreased from 21 to 10% as given in Figure 4.34. Increasing the initiator concentration resulted in a lower grafting ratio. We assume that the higher initiator concentration, generating more active sites on the DPNR backbone and also in the NVCL monomer. However, these free radicals of monomer might preferentially react with each other rather than grafting onto the DPNR backbone, producing a free homopolymer. Another reason possibly due to higher content of radicals might be performing as scavengers, which could reduce the reactive species in the system *via* recombination process. As a result, the grafting ratio was dropped with any further increase in the initiator concentration [35,143].

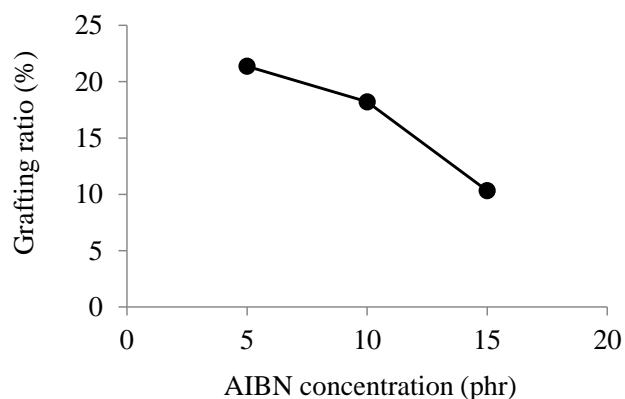


Figure 4.34 Effect of AIBN concentration on grafting ratio.

(3) Effect of reaction temperature

The effect of reaction temperature on grafting ratio was investigated using an NVCL concentration of 100 phr, an AIBN concentration of 10 phr, and a reaction time of 6 h. It could be seen that when the reaction temperature was lifted up from 80 to 100 °C, which is the optimum working range for AIBN [144,145], the grafting ratio sudden diminished from 51 to 11% as shown in Figure 4.35. These results claimed that the dissociation of AIBN upon higher temperature was plausible to give more free radicals. Then, after these radicals transferred to create the active sites on both NVCL and rubber backbone, partial active radicals might undergo either chain transfer reaction or termination, yielding the reduction in active species. [61,143]. Hence, the grafting ratio did not increase under this system.

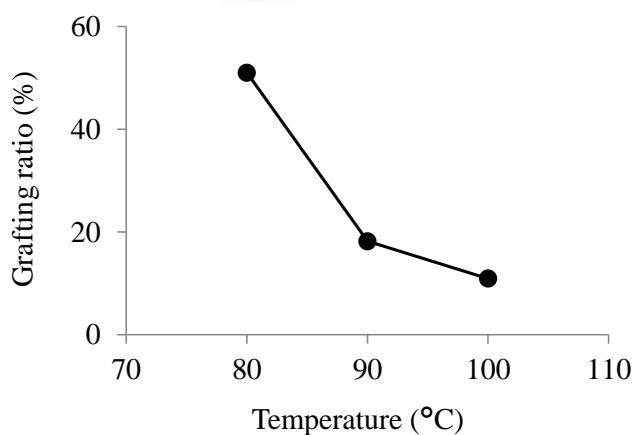


Figure 4.35 Effect of reaction temperature on grafting ratio.

(4) Effect of reaction time

With the respect to the effect of reaction time on grafting ratio, the reaction was performed using an NVCL concentration of 100 phr, an AIBN concentration of 10 phr, and a reaction temperature of 90 °C. As the reaction time was increased from 4 to 8 h, the grafting ratio considerably lowered from 29 to 6% as presented in Figure 4.36. It could be suggested that the use of a longer reaction time caused a progressive decrease of grafted DPNR sample and might be increased the free PNVCL. This was due to a prolong period of time affected the recombination of the NVCL radicals or perhaps limited active sites for grating which available on the polyisoprene substrate. Accordingly, a longer reaction time under this condition might lead to reduction of the NVCL-*g*-DPNR product [36].

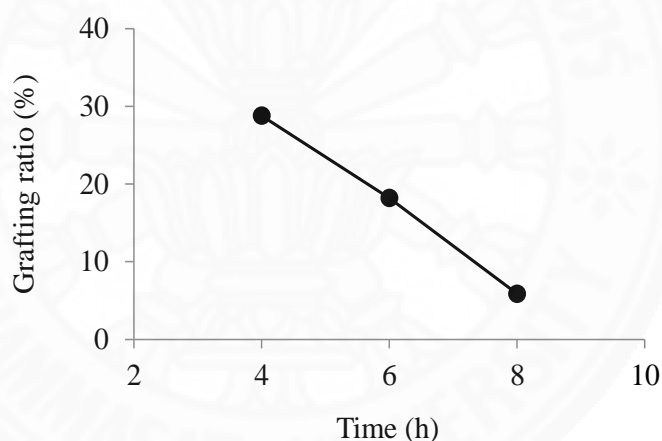


Figure 4.36 Effect of reaction time on grafting ratio.

4.2.2.5 Investigation of temperature-responsive behaviors of NVCL-*g*-DPNR

(1) The water absorption measurement of NVCL-*g*-DPNR

To gain an insight into the temperature-responsive behavior of NVCL-*g*-DPNR, the swelling experiment in an aqueous media was conducted at evaluated temperature range of 28-38 °C. In Figure 4.37, at the temperature region of 28-32 °C, NVCL-*g*-DPNR with higher grafting ratio swelled by 26% of its original

weight or about 10 times more than the DPNR sample, due to the presence of hydrophilic NVCL units that bound to the water molecules *via* hydrogen bonding. Under this temperature range, the appearance of NVCL-*g*-DPNR sample started to be swollen compared to pristine DPNR in agreement with the degree of swelling results. In addition, it could be distinctly noted that the NVCL-*g*-DPNR sample with 25% grafting ratio demonstrated the higher swelling percentage than the sample with 15% grafting ratio. This was because of the excessive hydrogen bonding with water molecules belonged to the sample with higher grafting ratio.

In contrast, the swelling percentage of both NVCL-*g*-DPNR samples became dramatically decreased when the temperature was raised up to 32 °C. This immediate drop in the swelling percentage of NVCL-*g*-DPNR was affected by the LCST behavior of the thermo-sensitive NVCL units in which the polymer chains could aggregate and then expel the water molecules at above LCST [105].

Nevertheless, there was no appreciable change in the swelling percentage of DPNR sample throughout the temperature range. From this result, it could be concluded that the NVCL-*g*-DPNR sample exhibited the LCST in the region of 32-34 °C. This LCST value was similar to the phase separation temperature of PNVCL.

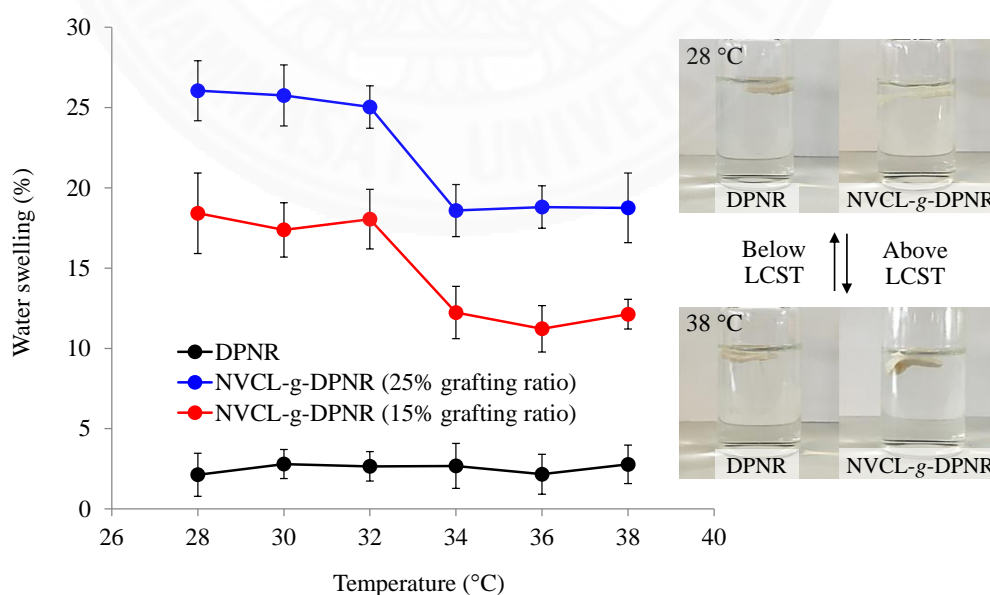


Figure 4.37 Degree of swelling of DPNR and NVCL-*g*-DPNR (15 and 25% grafting ratios) in water as a function of temperature.

(2) The contact angle determination of NVCL-*g*-DPNR

The contact angle of the rubber samples was measured to further elucidate the temperature responsiveness using a controlled temperature contact angle meter in the temperature range between 28 and 38 °C (Figure 4.38). Raising the temperature from 32 to 34 °C caused an increase in the contact angle of NVCL-*g*-DPNR from 59 to 78°. This growth was attributed to the increase in hydrophobicity of the NVCL units as a result of hydrogen bond breakage between the water molecules and caprolactam groups of NVCL units within the obtained grafted material. However, the contact angle of the DPNR sample remained constant around 104-109° throughout the measured temperature range. Thus, it could be inferred that the NVCL-*g*-DPNR sample displayed an LCST behavior about 32-34 °C, which agreed well with the results from the water swelling experiment.

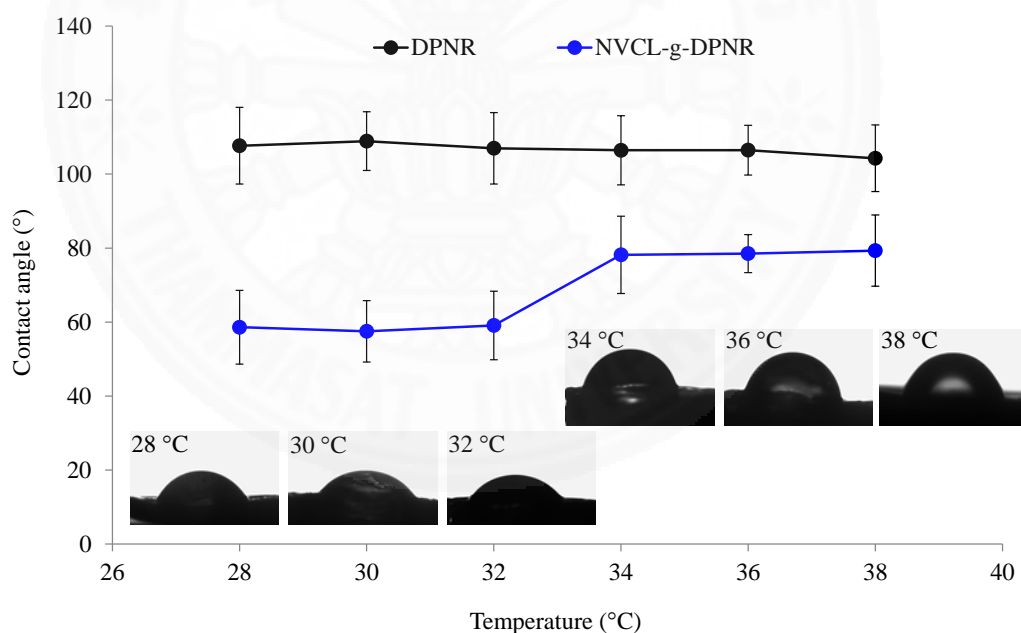


Figure 4.38 Contact angles of DPNR and NVCL-*g*-DPNR (25% grafting ratio) as a function of temperature.

(3) Dye adsorption and desorption studies of NVCL-*g*-DPNR

The additional evidence to stimulate the proving of temperature-responsive behavior of the grafted samples was investigated *via* dye adsorption and desorption studies which were carried out using the indigo carmine as a representative drug. Upon immersing the rubber samples into the indigo carmine solution for 1 week at room temperature, NVCL-*g*-DPNR samples were found to absorb more dyes than the DPNR sample. This result was observed by the decreasing of dye absorbance in UV-visible spectra and the change in color as displayed in Figure 4.39, as well as the amount of dye loading as listed in Table 4.10. Furthermore, the graft copolymer with grafting ratio of 25% showed more absorption of dyes than the sample with grafting ratio of 15%, because the graft material with higher grafting ratio had the abundant hydrogen bonding between hydrophilic amide functional groups of NVCL units and the amino groups of the indigo carmine as demonstrated in Figure 4.40 [132]. In contrast, DPNR sample could not trap dyes because there was no interaction with dye molecules, as confirmed by the almost unchanged in dye absorbance.

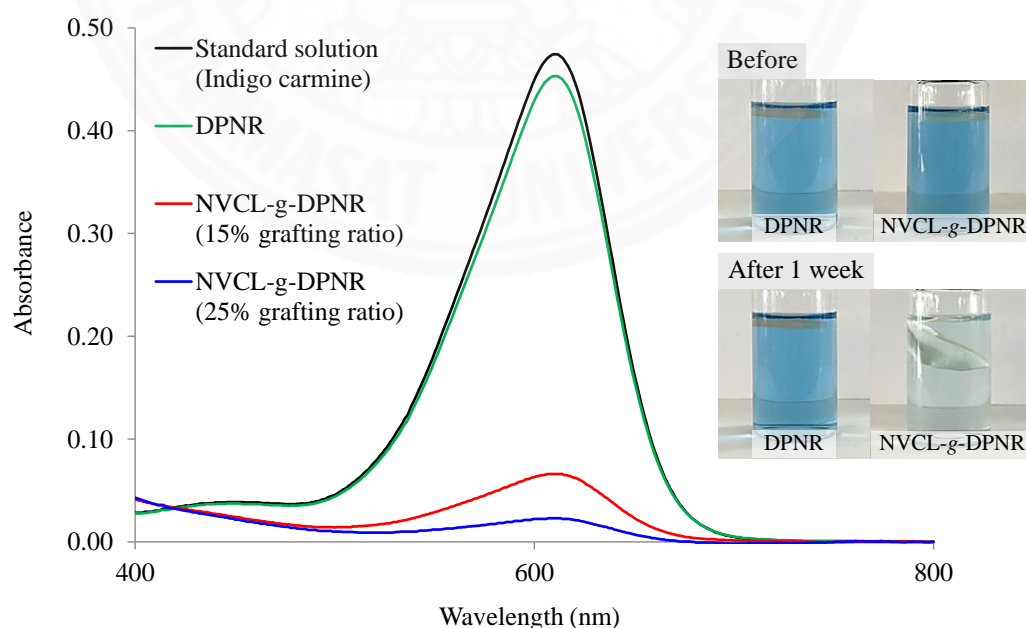


Figure 4.39 UV-visible spectra of standard indigo carmine solution and solutions after immersion of DPNR and NVCL-*g*-DPNR (15 and 25% grafting ratios).

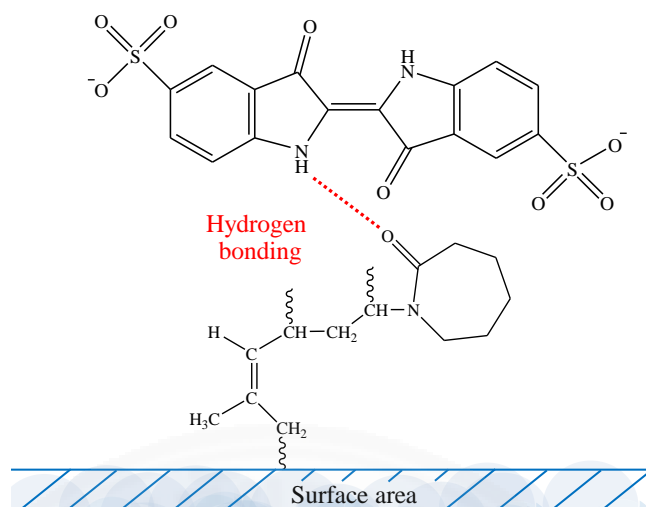


Figure 4.40 Interaction between hydrophilic caprolactam groups of NVCL units in NVCL-*g*-DPNR with amino groups of indigo carmine.

Table 4.10 Percentage of indigo carmine loading into DPNR and NVCL-*g*-DPNR.

Sample name	Percentage of indigo carmine loading
DPNR	0.26
NVCL- <i>g</i> -DPNR (15% grafting ratio)	11.60
NVCL- <i>g</i> -DPNR (25% grafting ratio)	13.52

In drug release studies were accomplished at the temperature below and above LCST in order to explore the thermo-sensitive nature of all rubber samples in an aqueous medium for 3 h. Figure 4.41 shows the UV-visible spectra and release profiles of indigo carmine from different rubber samples (pristine DPNR and NVCL-*g*-DPNR) along the temperature range of 28-38 °C. At the temperature below 34 °C, the dye molecules still absorbed on the NVCL-*g*-DPNR samples through hydrogen bonding as mentioned. The higher absorbance of dye at this range of temperature was attributed to the presence of dyes which ripped from the NVCL-*g*-DPNR samples whereas almost none was on the DPNR sample.

Upon increasing the solution temperature exceeded 32 °C, corresponding to the LCST nature of NVCL units, the entrapped dyes were released from NVCL-*g*-DPNR samples, as indicated by an increase in UV-visible absorbance. These dyes were ejected because of the PNVCCL chains within grafted materials were collapsed as induced by the temperature up to the LCST of NVCL units [133,134]. Similarly, the grafted sample with 25% grafting ratio released more dyes than the grafted sample with 15% grafting ratio due to the sample with higher grafting ratio contained more dyes on their molecules.

By looking the absorbance of the DPNR sample, it could be observed that, there was no tremendous difference at all measured temperature range. Photographs of dye desorption of DPNR and NVCL-*g*-DPNR samples were presented in Figure 4.42. The NVCL-*g*-DPNR released the dye when the temperature was raised above the LCST as shown by the change of color, whereas the solution color of the DPNR sample was almost unchanged. Hence, it was worth mentioning that the graft copolymer was potentially able to use as temperature-responsive material.

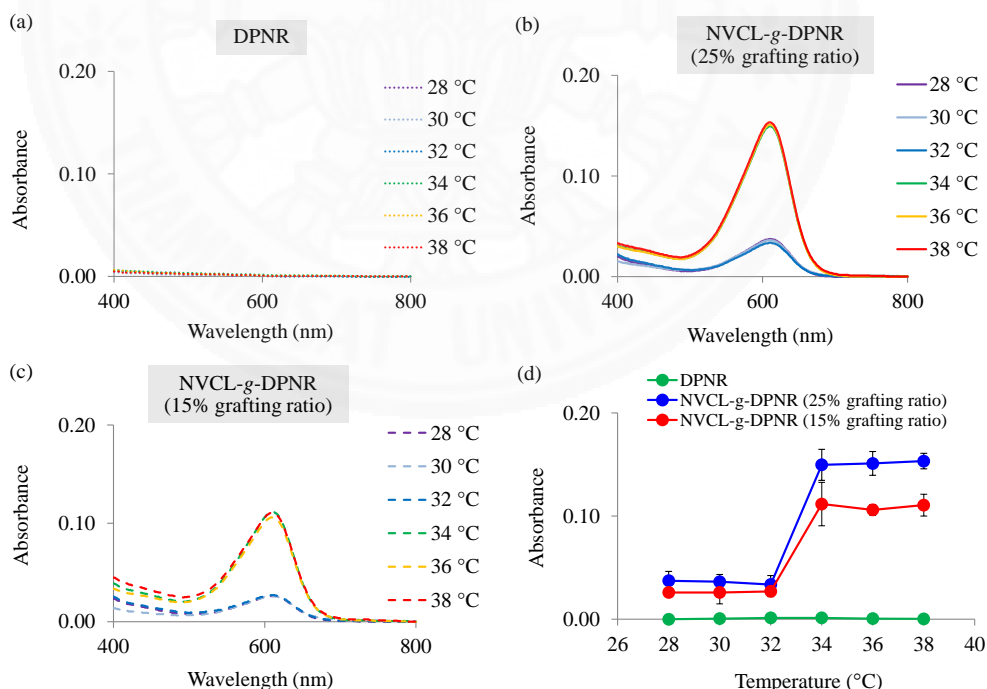


Figure 4.41 UV-visible spectra of solutions after desorption of indigo carmine from (a) DPNR, (b) NVCL-*g*-DPNR (25% grafting ratio), and (c) NVCL-*g*-DPNR (15% grafting ratio) at different temperatures, and (d) release profiles of indigo carmine from DPNR and NVCL-*g*-DPNR samples at $\lambda_{\text{max}} = 610$ nm.

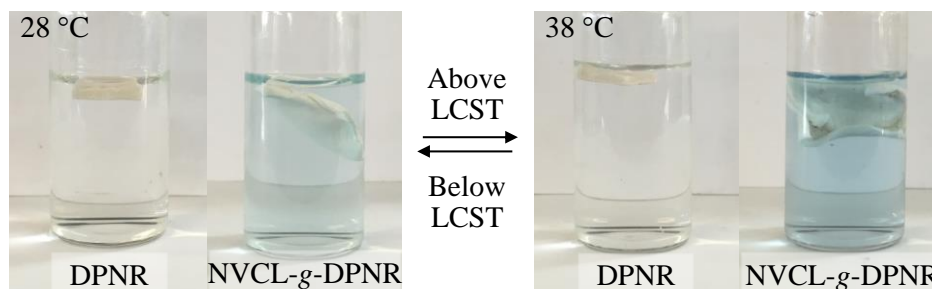


Figure 4.42 Photograph images of DPNR and NVCL-*g*-DPNR (25% grafting ratio) after desorption.

4.2.2.6 Adsorption studies of NVCL-*g*-DPNR

This study was used to make clear the specific interaction between adsorbate molecules (dyes) and the surface of adsorbent (NVCL-*g*-DPNR samples). For an appropriate understanding the adsorption mechanism, the grafted specimens were soaked with indigo carmine solution for 1 week at room temperature. Thereafter, the adsorption data would be calculated using mathematical equations of each isotherm model in order to achieve the R^2 values, regarded as the essential parameter which could explain the adsorption behavior of dyes-grafted material interaction by comparing this parameter with those of four renowned adsorption models including the Langmuir, Freundlich, Temkin, and Dubinin-Radushkevich isotherms. Besides, the other important constants of these isotherm models were subsequently computed as tabulated in Table 4.11.

The Langmuir adsorption isotherm was found to be a proper theoretical model to describe the nature of adsorption due to its expressed the R^2 close to the unity ($R^2 = 1$) with the maximum value about 0.92, among others as shown by the linear plot in Figure 4.43. This result confirmed that the indigo carmine was greatly covered with Q_0 or maximum monolayer coverage capacity of 1.70 mg/g on the homogeneous surface of NVCL-*g*-DPNR by monolayer adsorption process [107,117].

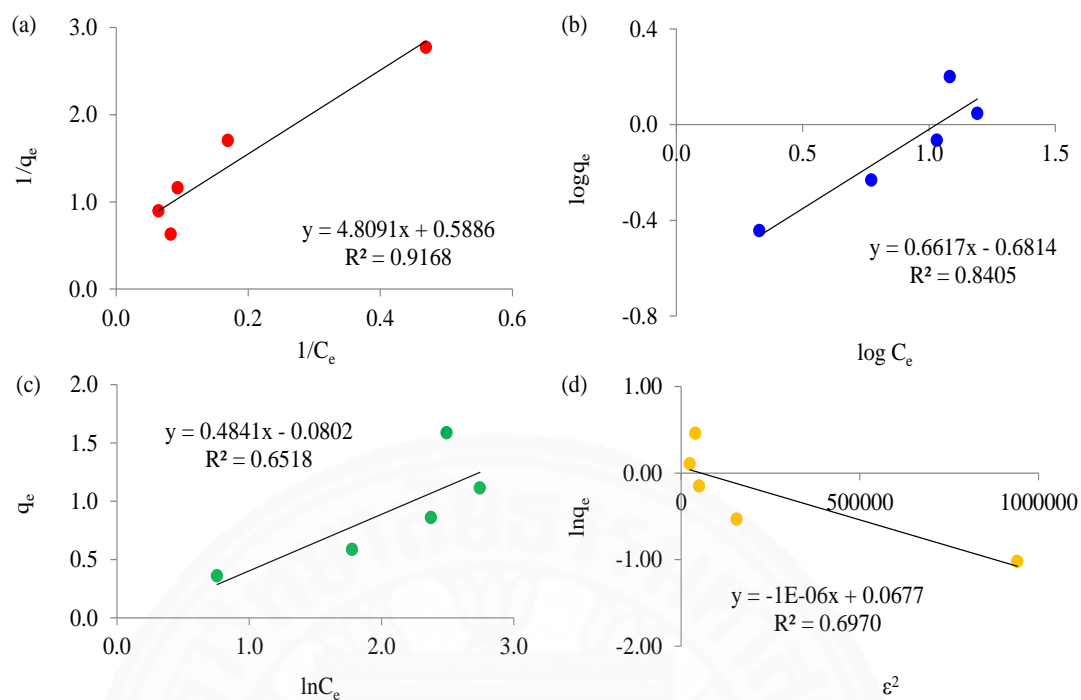


Figure 4.43 Linear plots of (a) Langmuir, (b) Freundlich, (c) Temkin, and (d) Dubinin-Radushkevich adsorption isotherms for the adsorption process of indigo carmine onto NVCL-*g*-DPNR (25% grafting ratio) surface.

The R_L value of the Langmuir adsorption isotherm was found between 0 and 1 ($R_L = 0.14$ - 0.45) with different dye concentrations from 10-50 ppm, suggesting that the absorbed indigo carmine onto the NVCL-*g*-DPNR surface was favorable (Figure 4.44) [108,110,111,146].

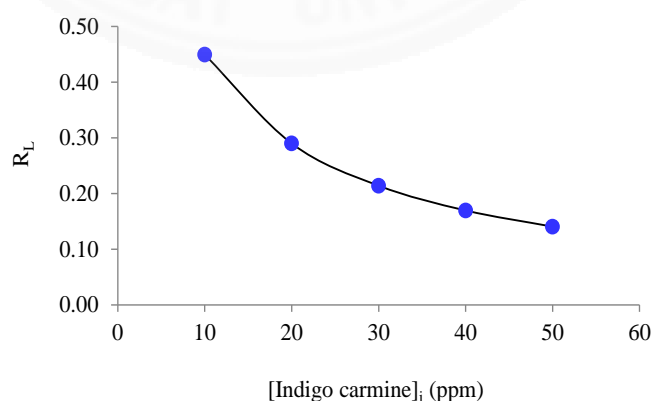


Figure 4.44 Plot between equilibrium parameter and initial dye concentration for the adsorption process of indigo carmine onto NVCL-*g*-DPNR (25% grafting ratio) surface.

The n parameter from the Freundlich isotherm was employed to affirm the favorability of sorption mechanism. In this current part, the n value was exhibited higher than 1 ($n = 1.51$), meaning that the favorable physisorption of dye molecules occurred on the surface of NVCL-*g*-DPNR [108,111,135,147].

The heat sorption of the process could be determined from the B parameter from the Temkin isotherm (chemical adsorption when $B > 20$ kJ/mol and physical adsorption when $B < 20$ kJ/mol). The B value was found to be 0.48 J/mol. Therefore, the adsorption process was indicated as physisorption [113-115,146].

Besides, the Dubinin-Radushkevich isotherm reported the E value around 0.71 kJ/mol which lower than 8 kJ/mol, representing that the type of adsorption of indigo carmine onto NVCL-*g*-DPNR surface was a physical process [113,136,137,148].

Table 4.11 Constants of each adsorption isotherm for the adsorption process of indigo carmine onto NVCL-*g*-DPNR surface.

Langmuir constants				Freundlich constants			
Q_0 (mg/g)	K_L (L/mg)	R_L	R^2	$1/n$	n	K_f (mg/g)	R^2
1.70	0.12	0.14-0.45	0.92	0.66	1.51	0.21	0.84
Temkin constants				Dubinin-Radushkevich constants			
b_T	A_T (L/mg)	B (J/mol)	R^2	q_s (mg/g)	K_{ad} (mol ² /kJ ²)	E (kJ/mol)	R^2
5206.34	0.85	0.48	0.65	1.07	1×10^{-6}	0.71	0.70

CHAPTER 5

CONCLUSIONS AND RECOMMENDATIONS

5.1 Conclusions

In our research work, the NVCL-functionalized NR materials with temperature responsiveness were prepared *via* crosslinking and grafting processes. From the results, the conclusions could be made as follows,

- 5.1.1 The as-synthesized polymer of PNVCL was prepared through free radical polymerization and obtained in the form of white powder. Based on their structure, it exhibited the amphiphilic character with an LCST around 32-34 °C, which is near the physiological human temperature. Moreover, the average molecular weights and dispersity of PNVCL were characterized using GPC technique, revealing the M_n , M_w , and M_z of 940, 1200, and 1500 g/mol, respectively, and dispersity of 1.3.
- 5.1.2 Both crosslinked and grafted materials were structurally characterized using FT-IR and $^1\text{H-NMR}$ techniques. The spectra of both materials showed both characteristic signals of pristine rubber and NVCL units.
- 5.1.3 According to the XPS results, it was found that only modified thermo-responsive materials showed a significant increase in N_{1s} signal at 399 eV because of the existence of caprolactam groups of NVCL units in the modified rubbers.
- 5.1.4 The thermal properties of crosslinked and grafted materials were investigated using DSC and TGA techniques. From the DSC thermograms, the T_g value of crosslinked material was found around 133 °C, which presented between those of intrinsic NR and PNVCL. By contrast, grafted material exhibited two endothermic transitions at -60.3 and 175.7 °C which were attributed to the T_g values of DPNR and NVCL units, respectively. Although, the TGA

thermograms of both modified rubbers resembled those to that of unmodified rubber, but it was found to slightly more stable.

- 5.1.5 Crosslink density of the crosslinked material was obtained using the solvent swelling experiment. It reported that the solvent swelling behavior was affected by the degree of gel content.
- 5.1.6 The temperature responsiveness of both crosslinked and grafted materials was investigated using water absorption and water contact angle determination. These results clearly confirmed that both of them displayed the LCST value in the range of 32-34 °C in an aqueous medium and also showed the reversible behaviors upon change the temperature at below and above its LCST.
- 5.1.7 In order to test the potentials in biomedical applications, crosslinked and grafted materials were studied through dye adsorption and desorption experiment. Indigo carmine was used as a drug model. After adsorption process for 1 week, both modified rubbers could absorb dyes, owing to the hydrogen bonding between caprolactam groups of NVCL units and amino groups of indigo carmine molecules. These dyes could be released upon raising the solution above the LCSTs.
- 5.1.8 The adsorption studies were carried out to evaluate the isotherm of the dye adsorption. According to the R^2 of both modified rubbers, Langmuir model showed the maximum value of R^2 , indicating that a monolayer adsorption of indigo carmine likely occurred on the surface of modified rubbers.

Based on these results, the temperature-responsive, hydrogel-like rubbers will be useful in a variety of biomedical applications. Potential consumer products include smart bandages and facial masks with the ability to efficiently release medicine or other healing ingredients, upon contact with human skin. Other applications include smart tires for automobiles that change their adhesion in response to a change in temperature. The strategy presented in this work allows the preparation of multi-

stimuli-responsive rubbers through reactions with multiple responsive materials, extending their properties of the rubbers.

5.2 Recommendations for future work

Although a number of studies had been performed in this thesis work, future work and recommendations are detailed as follows,

- 5.2.1 Determine the molecular weight of both unmodified and modified rubbers.
- 5.2.2 Explore the effects of initiator type, agitation speed, emulsifier concentration or other interesting parameters on the reaction efficiency of temperature-responsive NVCL-functionalized NRs.
- 5.2.3 Investigate the percentage of grafting ratio using the high ammonia NR latex compared to DPNR latex.
- 5.2.4 Observe the morphology of rubber particles compared to grafted rubber particles using transmission electron microscopy (TEM).
- 5.2.5 Calculate the percentage of a free homopolymer of PNVCL and free NR in graft copolymerization.

REFERENCES

- [1] Graves, D. F. (2007). Rubber : Kent and Riegel's handbook of industrial chemistry and biotechnology. *Springer US*, 689-718.
- [2] Petchseechoung, W. (2016). Thailand industry : Rubber industry. 18, 1-4.
- [3] Manufacture of natural rubber in Thailand. (11/05/2017). Available from http://www.rubberthai.com/statistic/stat_index.htm
- [4] Prize of concentrated latex and ribbed smoke sheet of Thailand (11/05/2017). Available from http://www.rubberthai.com/statistic/stat_index.htm
- [5] Thangavelu, K., Kyu, K. I., and Young, P. S. (2014). Poly(*N*-vinyl caprolactam) grown on nanographene oxide as an effective nanocargo for drug delivery. *Colloids and Surfaces B : Biointerfaces*, 115, 37-45.
- [6] Lau, A. C. W., and Wu, C. (1999). Thermally sensitive and biocompatible Poly(*N*-vinylcaprolactam) : Synthesis and characterization of high molar mass linear chains. *Macromolecules*, 32(3), 581-584.
- [7] Kozanoğlu, S., Özdemir, T., and Usanmaz, A. (2011). Polymerization of *N*-vinylcaprolactam and characterization of poly(*N*-vinylcaprolactam). *Journal of Macromolecular Science, Part A*, 48(6), 467-477.
- [8] Usanmaz, A., Özdemir, T., and Polat, Ö. (2009). Solid state polymerization of *N*-vinylcaprolactam via gamma irradiation and characterization. *Journal of Macromolecular Science, Part A*, 46(6), 597-606.
- [9] Prabakaran, M., Grailer, J. J., Steeber, D. A., et al. (2008). Stimuli-responsive chitosan-graft-poly(*N*-vinylcaprolactam) as a promising material for controlled hydrophobic drug delivery. *Macromolecular Bioscience*, 8(9), 843-851.
- [10] Rejinold, N. S., Chennazhi, K. P., Nair, S. V., et al. (2011). Biodegradable and thermo-sensitive chitosan-g-poly(*N*-vinylcaprolactam) nanoparticles as a 5-fluorouracil carrier. *Carbohydrate Polymers*, 83(2), 776-786.
- [11] Mundargi, R. C., Rangaswamy, V., and Aminabhavi, T. M. (2010). A novel method to prepare 5-fluorouracil, an anti-cancer drug, loaded microspheres from poly(*N*-vinyl caprolactam-co-acrylamide) and controlled release studies. *Designed Monomers and Polymers*, 13(4), 325-336.

- [12] Mundargi, R. C., Rangaswamy, V., and Aminabhavi, T. M. (2011). Poly(*N*-vinylcaprolactam-co-methacrylic acid) hydrogel microparticles for oral insulin delivery. *Journal of Microencapsulation*, 28(5), 384-394.
- [13] Bitar, A., Fessi, H., and Elaissari, A. (2012). Synthesis and characterization of thermally and glucose-sensitive poly *N*-vinylcaprolactam-based microgels. *Journal of Biomedical Nanotechnology*, 8(5), 709-719.
- [14] Nasimova, I. R., Makhaeva, E. E., and Khokhlov, A. R. (2001). Poly(*N*-vinylcaprolactam) gel/organic dye complexes as sensors for metal ions in aqueous salt solutions. *Journal of Applied Polymer Science*, 81(13), 3238-3243.
- [15] Shakya, A. K., Holmdahl, R., Nandakumar, K. S., et al. (2014). Polymeric cryogels are biocompatible, and their biodegradation is independent of oxidative radicals. *Journal of Biomedical Materials Research Part A*, 102(10), 3409-3418.
- [16] Lee, B., Jiao, A., Yu, S., et al. (2013). Initiated chemical vapor deposition of thermoresponsive poly(*N*-vinylcaprolactam) thin films for cell sheet engineering. *Acta Biomaterialia*, 9(8), 7691-7698.
- [17] Seena, J., Maya, J. J., Laly A., P., et al. (2010). Raw and renewable polymers : Polymers, opportunities, and risks II (sustainability, product design and processing). *Springer Berlin Heidelberg*, 55-80.
- [18] Resing, W. (2000). Natural rubber 1st quarter : Production, processing and properties. 17, 2-3.
- [19] Whitby, G. S. (1967). Rubber : Natural and synthetic. *Journal of Applied Polymer Science*, 11(9), 1823-1823.
- [20] Ong, E. L., and Eng, A. H. (2001). Natural rubber polymer handbook second edition.
- [21] Properties of natural rubber. (11/05/2017). Available from http://www.allsealsinc.com/Natural_Rubber-popup.html
- [22] Aguele, F. O., Idiaghe, J. A., and Nwosu, T. U. A. (2015). A study of quality improvement of natural rubber products by drying methods. *Journal of Materials Science and Chemical Engineering*, 3(11), 7-12.

- [23] Ibrahim, S., Daik, R., and Abdullah, I. (2014). Functionalization of liquid natural rubber via oxidative degradation of natural rubber. *Polymers*, 6(12), 2928-2941.
- [24] Zhong, J. P., Li, S. D., Wei, Y. C., et al. (1999). Study on preparation of chlorinated natural rubber from latex and its thermal stability. *Journal of Applied Polymer Science*, 73(14), 2863-2867.
- [25] Hinchiranan, N., Charmondusit, K., Prasassarakich, P., et al. (2006). Hydrogenation of synthetic *cis*-1,4-polyisoprene and natural rubber catalyzed by [Ir(COD)py(PCy₃)]PF₆. *Journal of Applied Polymer Science*, 100(5), 4219-4233.
- [26] Azhar, N. H. A., Jamaluddin, N., Rasid, H. M., et al. (2015). Studies on hydrogenation of liquid natural rubber using diimide. *International Journal of Polymer Science*, 2015, 1-6.
- [27] Choothong, N., Kosugi, K., Yamamoto, Y., et al. (2017). Characterization of brominated natural rubber by solution-state 2D NMR spectroscopy. *Reactive and Functional Polymers*, 113, 6-12.
- [28] Onchoy, N., and Phinyocheep, P. (2016). Preparation and characterization of brominated natural rubber applied in silica-filled natural rubber vulcanizates. *Rubber Chemistry and Technology*, 89(3), 406-418.
- [29] Riyajan, S. A., and Sakdapipanich, J. T. (2006). Cationic cyclization of deproteinized natural rubber latex using sulfuric acid. *KGK rubberpoint*, 59(3), 104-109.
- [30] Chuayjuljit, S., Nutchapong, T., Saravari, O., et al. (2015). Preparation and characterization of epoxidized natural rubber and epoxidized natural rubber/carboxylated styrene butadiene rubber blends. *Journal of Metals, Materials and Minerals*, 25(1), 27-36.
- [31] Kato, H., Nakatsubo, F., Abe, K., et al. (2015). Crosslinking via sulfur vulcanization of natural rubber and cellulose nanofibers incorporating unsaturated fatty acids. *RSC Advances*, 5(38), 29814-29819.

- [32] Mathew, A. P., Packirisamy, S., Radusch, H. J., et al. (2001). Effect of initiating system, blend ratio and crosslink density on the mechanical properties and failure topography of nano-structured full-interpenetrating polymer networks from natural rubber and polystyrene. *European Polymer Journal*, 37(9), 1921-1934.
- [33] Mathew, A. P., Packirisamy, S., Kumaran, M. G., et al. (1995). Transport of styrene monomer through natural rubber. *Polymer*, 36(26), 4935-4942.
- [34] Nakason, C., Kaesaman, A., and Supasanthitikul, P. (2004). The grafting of maleic anhydride onto natural rubber. *Polymer Testing*, 23(1), 35-41.
- [35] Kangwansupamonkon, W., Gilbert, R. G., and Kiatkamjornwong, S. (2005). Modification of natural rubber by grafting with hydrophilic vinyl monomers. *Macromolecular Chemistry and Physics*, 206(24), 2450-2460.
- [36] Kochthongrasamee, T., Prasassarakich, P., and Kiatkamjornwong, S. (2006). Effects of redox initiator on graft copolymerization of methyl methacrylate onto natural rubber. *Journal of Applied Polymer Science*, 101(4), 2587-2601.
- [37] Pisuttisap, A., Hinchiranan, N., Rempel, G. L., et al. (2013). ABS modified with hydrogenated polystyrene-grafted-natural rubber. *Journal of Applied Polymer Science*, 129(1), 94-104.
- [38] Schneider, M., Pith, T., and Lambla, M. (1996). Preparation and morphological characterization of two- and three-component natural rubber-based latex particles. *Journal of Applied Polymer Science*, 62(2), 273-290.
- [39] Nabil, H., Ismail, H., and Azura, A. R. (2013). Compounding, mechanical and morphological properties of carbon-black-filled natural rubber/recycled ethylene-propylene-diene-monomer (NR/R-EPDM) blends. *Polymer Testing*, 32(2), 385-393.
- [40] Kampouris, E. M., and Andreopoulos, A. G. (1987). Benzoyl peroxide as a crosslinking agent for polyethylene. *Journal of Applied Polymer Science*, 34(3), 1209-1216.
- [41] Loan, L. D. (1972). Peroxide crosslinking reactions of polymers. *Pure and Applied Chemistry*, 30(1-2), 173.

- [42] Poh, B. T., and Lim, C. H. (2014). Effect of cross-linking on adhesion property of benzoyl-peroxide-cured epoxidized natural rubber (ENR 50) adhesives. *Journal of Elastomers and Plastics*, 46(2), 187-198.
- [43] Bobear, W. J. (1964). Crosslink densities in peroxide-cured silicone gum vulcanizates. *Industrial and Engineering Chemistry Product Research and Development*, 3(4), 277-281.
- [44] Boon, A. J. (1988). Hock cleavage : The cause of main-chain scission in natural rubber autoxidation. *Journal of Natural Rubber Research*, 3(2), 90-106.
- [45] Bateman, L. (1954). Olefin oxidation. *Quarterly Reviews, Chemical Society*, 8(2), 147-167.
- [46] Kim, I. S., Lee, B. W., Sohn, K. S., et al. (2016). Characterization of the UV oxidation of raw natural rubber thin film using image and FT-IR analysis. *Elastomers and Composites*, 51(1), 1-9.
- [47] Wongthep, W., Srituileong, S., Martwiset, S., et al. (2013). Grafting of poly(vinyl alcohol) on natural rubber latex particles. *Journal of Applied Polymer Science*, 127(1), 104-110.
- [48] Nakason, C., Kaesaman, A., and Yimwan, N. (2003). Preparation of graft copolymers from deproteinized and high ammonia concentrated natural rubber latices with methyl methacrylate. *Journal of Applied Polymer Science*, 87(1), 68-75.
- [49] Oliveira, P. C., Oliveira, A. M., Garcia, A., et al. (2005). Modification of natural rubber : A study by ¹H-NMR to assess the degree of graftization of polyDMAEMA or polyMMA onto rubber particles under latex form in the presence of a redox couple initiator. *European Polymer Journal*, 41(8), 1883-1892.
- [50] Claramma, N. M., Mathew, N. M., and Thomas, E. V. (1989). Radiation induced graft copolymerization of acrylonitrile on natural rubber. *International Journal of Radiation Applications and Instrumentation. Part C. Radiation Physics and Chemistry*, 33(2), 87-89.
- [51] Turner, D. T. (1959). γ -Irradiation of rubber and styrene : Graft polymer formation. *Journal of Polymer Science*, 35(128), 17-29.

- [52] Hossain, K. M. Z., and Chowdhury, A. M. S. (2010). Grafting of n-butyl acrylate with natural rubber latex film by gamma radiation: a reaction mechanism., 5(1), 81-88.
- [53] George, K. M., Claramma, N. M., and Thomas, E. V. (1987). Studies on graft copolymerization of methyl methacrylate in natural rubber latex induced by gamma radiation. *International Journal of Radiation Applications and Instrumentation. Part C. Radiation Physics and Chemistry*, 30(3), 189-192.
- [54] Mazam, M. S., Makunchi, K., and Hagiwara, M. (1983). Modification of natural rubber latex in the presence of vinyl monomers by gamma radiation [hevea]. v. 31.
- [55] Anancharungsuk, W., Tanpantree, S., Sruanganurak, A., et al. (2007). Surface modification of natural rubber film by UV-induced graft copolymerization with methyl methacrylate. *Journal of Applied Polymer Science*, 104(4), 2270-2276.
- [56] Oster, G., and Shibata, O. (1957). Graft copolymer of polyacrylamide and natural rubber produced by means of ultraviolet light. *Journal of Polymer Science*, 26(113), 233-234.
- [57] Hoven, V. P., Chombanpaew, K., Iwasaki, Y., et al. (2009). Improving blood compatibility of natural rubber by UV-induced graft polymerization of hydrophilic monomers. *Journal of Applied Polymer Science*, 112(1), 208-217.
- [58] Rezaifard, A. H., Hodd, K. A., Tod, D. A., et al. (1994). Toughening epoxy resins with poly(methyl methacrylate)-grafted-natural rubber, and its use in adhesive formulations. *International Journal of Adhesion and Adhesives*, 14(2), 153-159.
- [59] Promdum, Y., Klinpituksa, P., and Ruamcharoen, J. (2009). Grafting copolymerization of natural rubber with 2-hydroxyethyl methacrylate for plywood adhesion improvement. *Songklanakarinn Journal of Science and Technology*, 31(4), 453-457.
- [60] Oliveira, P. C., Guimarães, A., Cavailé, J.-Y., et al. (2005). Poly(dimethylaminoethyl methacrylate) grafted natural rubber from seeded emulsion polymerization. *Polymer*, 46(4), 1105-1111.

- [61] Angnanon, S., Prasassarakich, P., and Hinchiranan, N. (2011). Styrene/Acrylonitrile graft natural rubber as compatibilizer in rubber blends. *Polymer-Plastics Technology and Engineering*, 50(11), 1170-1178.
- [62] Ragupathy, L., Ziener, U., Robert, G., et al. (2011). Grafting polyacrylates on natural rubber latex by miniemulsion polymerization. *Colloid and Polymer Science*, 289(3), 229-235.
- [63] Derouet, D., Intharapat, P., Tran, Q. N., et al. (2009). Graft copolymers of natural rubber and poly(dimethyl(acryloyloxymethyl)phosphonate) (NR-g-PDMAMP) or poly(dimethyl(methacryloyloxyethyl)phosphonate) (NR-g-PDMMEP) from photopolymerization in latex medium. *European Polymer Journal*, 45(3), 820-836.
- [64] Nawamawat, K., Sakdapipanich, J. T., Ho, C. C., et al. (2011). Surface nanostructure of *Hevea brasiliensis* natural rubber latex particles. *Colloids and Surfaces A : Physicochemical and Engineering Aspects*, 390(1-3), 157-166.
- [65] Tarachiwin, L., Tanaka, Y., and Sakdapipanich, J. (2005). Structure and origin of long-chain branching and gel in natural rubber. *KGK rubberpoint*, 58(3), 115-122.
- [66] Cornish, K., Wood, D. F., and Windle, J. J. (1999). Rubber particles from four different species, examined by transmission electron microscopy and electron-paramagnetic-resonance spin labeling, are found to consist of a homogeneous rubber core enclosed by a contiguous, monolayer biomembrane. *Planta*, 210(1), 85-96.
- [67] Tanaka, Y. (2001). Structural characterization of natural polyisoprenes : Solve the mystery of natural rubber based on structural study. *Rubber Chemistry and Technology*, 74(3), 355-375.
- [68] Ho, C. C., Kondo, T., Muramatsu, N., et al. (1996). Surface structure of natural rubber latex particles from electrophoretic mobility data. *Journal of Colloid and Interface Science*, 178(2), 442-445.
- [69] Berthelot, K., Lecomte, S., Estevez, Y., et al. (2014). Rubber particle proteins, HbREF and HbSRPP, show different interactions with model membranes. *Biochimica et Biophysica Acta (BBA) - Biomembranes*, 1838(1), 287-299.

- [70] Ferreira, M., Mendonça, R. J., Coutinho Netto, J., et al. (2009). Angiogenic properties of natural rubber latex biomembranes and the serum fraction of *Hevea brasiliensis*. *Brazilian Journal of Physics*, 39, 564-569.
- [71] Yeang, H. Y., Arif, S. A. M., Yusof, F., et al. (2002). Allergenic proteins of natural rubber latex. *Methods*, 27(1), 32-45.
- [72] Rogero, S. O., Lugão, A. B., Yoshii, F., et al. (2003). Extractable proteins from irradiated field natural rubber latex. *Radiation Physics and Chemistry*, 67(3-4), 501-503.
- [73] Perrella, F. W., and Gaspari, A. A. (2002). Natural rubber latex protein reduction with an emphasis on enzyme treatment. *Methods*, 27(1), 77-86.
- [74] Kawahara, S., Kawazura, T., Sawada, T., et al. (2003). Preparation and characterization of natural rubber dispersed in nano-matrix. *Polymer*, 44(16), 4527-4531.
- [75] Fukushima, Y., Kawahara, S., and Tanaka, Y. (1998). Synthesis of graft copolymers from highly deproteinised natural rubber. 1.
- [76] Wongthong, P., Nakason, C., Pan, Q., et al. (2013). Modification of deproteinized natural rubber via grafting polymerization with maleic anhydride. *European Polymer Journal*, 49(12), 4035-4046.
- [77] Wongthong, P., Nakason, C., Pan, Q., et al. (2014). Styrene-assisted grafting of maleic anhydride onto deproteinized natural rubber. *European Polymer Journal*, 59, 144-155.
- [78] Kosugi, K., Sutthangkul, R., Chaikumpollert, O., et al. (2012). Preparation and characterization of natural rubber with soft nanomatrix structure. *Colloid and Polymer Science*, 290(14), 1457-1462.
- [79] Nawamawat, K., Sakdapipanich, J. T., and Ho, C. C. (2010). Effect of deproteinized methods on the proteins and properties of natural rubber latex during storage. *Macromolecular Symposia*, 288(1), 95-103.
- [80] Chaikumpollert, O., Yamamoto, Y., Suchiva, K., et al. (2012). Protein-free natural rubber. *Colloid and Polymer Science*, 290(4), 331-338.
- [81] Yamamoto, Y., Nghia, P. T., Klinklai, W., et al. (2008). Removal of proteins from natural rubber with urea and its application to continuous processes. *Journal of Applied Polymer Science*, 107(4), 2329-2332.

- [82] Kawahara, S., Klinklai, W., Kuroda, H., et al. (2004). Removal of proteins from natural rubber with urea. *Polymers for Advanced Technologies*, 15(4), 181-184.
- [83] Hou, Y., Hansen, T. B., Staby, A., et al. (2010). Effects of urea induced protein conformational changes on ion exchange chromatographic behavior. *Journal of Chromatography A*, 1217(47), 7393-7400.
- [84] Junoi, S., Chisti, Y., and Hansupalak, N. (2015). Optimal conditions for deproteinizing natural rubber using immobilized alkaline protease. *Journal of Chemical Technology and Biotechnology*, 90(1), 185-193.
- [85] Chaikumpollert, O., Yamamoto, Y., Suchiva, K., et al. (2012). Preparation and characterization of protein-free natural rubber. *Polymers for Advanced Technologies*, 23(4), 825-828.
- [86] Ward, M. A., and Georgiou, T. K. (2011). Thermoresponsive polymers for biomedical applications. *Polymers*, 3, 1215-1242.
- [87] Yasarawan, N. (2014). Temperature-responsive polymers for biomedical applications. *KKU Science Journal*, 42(3), 499-513.
- [88] Medeiros, S. F., Barboza, J. C. S., Ré, M. I., et al. (2010). Solution polymerization of *N*-vinylcaprolactam in 1,4-dioxane : Kinetic dependence on temperature, monomer, and initiator concentrations. *Journal of Applied Polymer Science*, 118(1), 229-240.
- [89] Solomon, O. F., Corciovei, M., Ciută, I., et al. (1968). Properties of solutions of poly-*N*-vinylcaprolactam. *Journal of Applied Polymer Science*, 12(8), 1835-1842.
- [90] Kroker, J., Schneider, R., Schupp, E., et al. (1998). United States Patent, 5,739,195.
- [91] Stuart, B. H. (2002). Polymer Analysis (Chapter 3-4). *John Wiley and Sons*.
- [92] Meeussen, F., Nies, E., Berghmans, H., et al. (2000). Phase behaviour of poly(*N*-vinylcaprolactam) in water. *Polymer*, 41(24), 8597-8602.
- [93] Sun, S., and Wu, P. (2011). Infrared spectroscopic insight into hydration behavior of poly(*N*-vinylcaprolactam) in water. *The Journal of Physical Chemistry B*, 115(40), 11609-11618.

- [94] Tyrrell, Z. L., Shen, Y., and Radosz, M. (2010). Fabrication of micellar nanoparticles for drug delivery through the self-assembly of block copolymers. *Progress in Polymer Science*, 35(9), 1128-1143.
- [95] Kavitha, T., Kang, I. K., and Park, S. Y. (2014). Poly(*N*-vinylcaprolactam) grown on nanographene oxide as an effective nanocargo for drug delivery. *Colloids and Surfaces B: Biointerfaces*, 115, 37-45.
- [96] Imaz, A., and Forcada, J. (2010). *N*-vinylcaprolactam-based microgels for biomedical applications. *Journal of Polymer Science Part A : Polymer Chemistry*, 48(5), 1173-1181.
- [97] Thangavelu, K., Oh, K. J., Seungwook, J., et al. (2016). Multifaceted thermoresponsive poly(*N*-vinylcaprolactam) coupled with carbon dots for biomedical applications. *Materials Science and Engineering : C*, 61, 492-498.
- [98] Cortez Lemus, N. A., and Licea Claverie, A. (2016). Poly(*N*-vinylcaprolactam), a comprehensive review on a thermoresponsive polymer becoming popular. *Progress in Polymer Science*, 53, 1-51.
- [99] Patel, R., Ahn, S. H., Chi, W. S., et al. (2012). Poly(vinyl chloride)-graft-poly(*N*-vinyl caprolactam) graft copolymer: synthesis and use as template for porous TiO₂ thin films in dye-sensitized solar cells. *Ionics*, 18(4), 395-402.
- [100] Lequieu, W., Shtanko, N. I., and Du Prez, F. E. (2005). Track etched membranes with thermo-adjustable porosity and separation properties by surface immobilization of poly(*N*-vinylcaprolactam). *Journal of Membrane Science*, 256(1-2), 64-71.
- [101] Liang, X., Kozlovskaya, V., Cox, C. P., et al. (2014). Synthesis and self-assembly of thermosensitive double-hydrophilic poly(*N*-vinylcaprolactam)-*b*-poly(*N*-vinyl-2-pyrrolidone) diblock copolymers. *Journal of Polymer Science Part A : Polymer Chemistry*, 52(19), 2725-2737.
- [102] Negru, I., Teodorescu, M., Stanescu, P. O., et al. (2010). Poly(*N*-vinylcaprolactam-*b*-poly(ethylene glycol)-*b*-poly(*N*-vinylcaprolactam) triblock copolymers: synthesis by ATRP and thermal gelation properties of the aqueous solutions. *Materiale Plastice*, 47(1), 35-41.

- [103] Jiang, X., Lu, G., Feng, C., et al. (2013). Poly(acrylic acid)-graft-poly(*N*-vinylcaprolactam) : A novel pH and thermo dual-stimuli responsive system. *Polymer Chemistry*, 4(13), 3876-3884.
- [104] Obando Mora, Á., Acevedo Gutiérrez, A. C., Pérez Cinencio, G. J., et al. (2015). Synthesis of a pH- and thermo- responsive binary copolymer poly(*N*-vinylimidazole-co-*N*-vinylcaprolactam) grafted onto silicone films. *Coatings*, 5(4).
- [105] Melendez Ortiz, H. I., Alvarez Lorenzo, C., Concheiro, A., et al. (2015). Grafting of *N*-vinyl caprolactam and methacrylic acid onto silicone rubber films for drug-eluting products. *Journal of Applied Polymer Science*, 132(17), 1-11.
- [106] González, L., Rodríguez, A., Valente, J. L., et al. (2005). Conventional and efficient crosslinking of natural rubber. *KGK rubberpoint*, 58, 638-643.
- [107] Dada, A. O., Olalekan, A. P., Olatunya, A. M., et al. (2012). Langmuir, Freundlich, Temkin and Dubinin–Radushkevich isotherms studies of equilibrium sorption of Zn²⁺ unto phosphoric acid modified rice husk. *IOSR Journal of Applied Chemistry*, 3(1), 38-45.
- [108] Meroufel, B., Benali, O., Benyahia, M., et al. (2013). Adsorptive removal of anionic dye from aqueous solutions by algerian kaolin : Characteristics, isotherm, kinetic and thermodynamic studies. *Journal of Materials and Environmental Science*, 4(3), 482-491.
- [109] Saleh, M. I., and Adam, F. (1994). Adsorption isotherms of fatty acids on rice hull ash in a model system. *Journal of the American Oil Chemists' Society*, 71(12), 1363-1366.
- [110] Samarghandi, M. R., Hadi, M., Moayedi, S., et al. (2009). Two-parameter isotherms of methyl orange sorption by pinecone derived activated carbon. *Iranian Journal of Environmental Health Science and Engineering*, 6(4), 285-294.
- [111] Hameed, B. H. (2009). Evaluation of papaya seeds as a novel non-conventional low-cost adsorbent for removal of methylene blue. *Journal of Hazardous Materials*, 162(2–3), 939-944.

- [112] Kannan, N., and Sundaram, M. M. (2001). Kinetics and mechanism of removal of methylene blue by adsorption on various carbons—a comparative study. *Dyes and Pigments*, 51(1), 25-40.
- [113] Itodo, A. U., and Itodo, H. U. (2010). Sorption energies estimation using dubinin-radushkevich and temkin adsorption isotherms. *Life Science Journal*, 7(4), 31-39.
- [114] Sawasdee, S., and Watcharabundit, P. (2015). Equilibrium, kinetics and thermodynamic of dye adsorption by low-cost adsorbents. *International Journal of Chemical Engineering and Applications*, 6(6), 444.
- [115] Boldizsár, N., Manzatu, C., Toeroek, A., et al. (2015). Isotherm and thermodynamic studies of Cd (II) removal process using chemically modified lignocellulosic adsorbent. *Rev. Roum. Chim*, 60(2-3), 257-264.
- [116] Dawodu, F. A., Akpomie, G. K., and Ogbu, I. C. (2012). Isotherm modeling on the equilibrium sorption of cadmium (II) from solution by Agbani clay. *International Journal of Multidisciplinary Sciences and Engineering*, 3(9), 9-14.
- [117] Elmorsi, T. (2011). Equilibrium isotherms and kinetic studies of removal of methylene blue dye by adsorption onto miswak leaves as a natural adsorbent. *Journal of Environmental Protection*, 2(6), 817-827.
- [118] Tamboli, S. M., Mhaske, S. T., and Kale, D. D. (2004). Crosslinked polyethylene. *Indian Journal of Chemical Technology*, 11, 853-864.
- [119] Maitra, J., and Shukla, V. K. (2014). Cross-linking in hydrogels - A review. *American Journal of Polymer Science*, 4(2), 25-31.
- [120] Chuayjuljit, S., Moolsin, S., and Potiyaraj, P. (2005). Use of natural rubber-g-polystyrene as a compatibilizer in casting natural rubber/polystyrene blend films. *Journal of Applied Polymer Science*, 95(4), 826-831.
- [121] Oommen, Z., Groeninckx, G., and Thomas, S. (2000). Dynamic mechanical and thermal properties of physically compatibilized natural rubber/poly(methyl methacrylate) blends by the addition of natural rubber-graft-poly(methyl methacrylate). *Journal of Polymer Science Part B : Polymer Physics*, 38(4), 525-536.

- [122] Hamdan, S., Hashim, D. M., Muhamad, M., et al. (2000). Thermal analysis of natural rubber hevea brasiliensis latex. *Journal of Rubber Research*, 3(1), 25-33.
- [123] Liu, J., Debuigne, A., Detrembleur, C., et al. (2014). Poly(*N*-vinylcaprolactam) : A thermoresponsive macromolecule with promising future in biomedical field. *Advanced Healthcare Materials*, 3(12), 1941-1968.
- [124] Lebedev, V. T., Török, G., Cser, L., et al. (2002). Molecular dynamics of poly(*N*-vinylcaprolactam) hydrate. *Applied Physics A*, 74(1), s478-s480.
- [125] Yamashita, K., Ito, K., Tsuboi, H., et al. (1990). Graft copolymerization by iniferter method ; structural analyses of graft copolymer by glass transition temperature. *Journal of Applied Polymer Science*, 40(9-10), 1445-1452.
- [126] Hagen, R., Salmén, L., and Stenberg, B. (1996). Effects of the type of crosslink on viscoelastic properties of natural rubber. *Journal of Polymer Science Part B : Polymer Physics*, 34(12), 1997-2006.
- [127] Zhao, F., Bi, W., and Zhao, S. (2011). Influence of crosslink density on mechanical properties of natural rubber vulcanizates. *Journal of Macromolecular Science, Part B*, 50(7), 1460-1469.
- [128] Mane, S., Ponrathnam, S., and Chavan, N. (2015). Effect of chemical cross-linking on properties of polymer microbeads : A review. *Canadian Chemical Transactions*, 3(4), 473-485.
- [129] Yi, G., Huang, Y., Xiong, F., et al. (2011). Preparation and swelling behaviors of rapid responsive semi-IPN NaCMC/PNIPAm hydrogels. *Journal of Wuhan University of Technology-Mater. Sci. Ed.*, 26(6), 1073-1078.
- [130] Hebeish, A., Farag, S., Sharaf, S., et al. (2014). Thermal responsive hydrogels based on semi interpenetrating network of poly(NIPAm) and cellulose nanowhiskers. *Carbohydrate Polymers*, 102, 159-166.
- [131] Cai, Y., Shen, W., Loo, S. L., et al. (2013). Towards temperature driven forward osmosis desalination using Semi-IPN hydrogels as reversible draw agents. *Water Research*, 47(11), 3773-3781.
- [132] Samart, C., and Sookman, C. (2009). Effect of silica sources in nanoporous silica synthesis on releasing behavior of indigo carmine. *Songklanakarin Journal of Science and Technology*, 31(5), 511-515.

- [133] Shi, J., Alves, N. M., and Mano, J. F. (2006). Drug release of pH/temperature-responsive calcium alginate/poly(*N*-isopropylacrylamide) semi-IPN beads. *Macromolecular Bioscience*, 6(5), 358-363.
- [134] Oliveira, A. M. d., Oliveira, P. C. d., Santos, A. M. d., et al. (2009). Synthesis and characterization of thermo-responsive particles of poly(hydroxybutyrate-co-hydroxyvalerate)-*b*-poly(*N*-isopropylacrylamide). *Brazilian Journal of Physics*, 39, 217-222.
- [135] Vimonses, V., Lei, S., Jin, B., et al. (2009). Adsorption of congo red by three Australian kaolins. *Applied Clay Science*, 43(3-4), 465-472.
- [136] Jain, M., Garg, V. K., and Kadirvelu, K. (2009). Chromium(VI) removal from aqueous system using *Helianthus annuus* (sunflower) stem waste. *Journal of Hazardous Materials*, 162(1), 365-372.
- [137] Ibrahim, M. B., and Sani, S. (2014). Comparative isotherms studies on adsorptive removal of congo red from wastewater by watermelon rinds and neem-tree leaves. *Open Journal of Physical Chemistry*, 4(4), 139-146.
- [138] Canchi, D. R., Paschek, D., and García, A. E. (2010). Equilibrium study of protein denaturation by urea. *Journal of the American Chemical Society*, 132(7), 2338-2344.
- [139] Pichayakorn, W., Suksaeree, J., Boonme, P., et al. (2012). Preparation of deproteinized natural rubber latex and properties of films formed by itself and several adhesive polymer blends. *Industrial and Engineering Chemistry Research*, 51(41), 13393-13404.
- [140] Ghosh, P., and Sengupta, P. K. (1967). Graft copolymerization of methyl methacrylate and natural rubber. *Journal of Applied Polymer Science*, 11(8), 1603-1611.
- [141] Oliveira, P. C., Guimarães, A., Cavallé, J. Y., et al. (2005). Poly(dimethylaminoethyl methacrylate) grafted natural rubber from seeded emulsion polymerization. *Polymer*, 46(4), 1105-1111.
- [142] Prasoesopha, N., Chumsamrong, P., and Suppakarn, N. (2011). Effects of type and concentration of initiator on grafting of acrylic monomer onto depolymerized natural rubber. *Advanced Materials Research*, 264-265, 565-570.

- [143] Arayapranee, W., Prasassarakich, P., and Rempel, G. L. (2002). Synthesis of graft copolymers from natural rubber using cumene hydroperoxide redox initiator. *Journal of Applied Polymer Science*, 83(14), 2993-3001.
- [144] Brandrup, J., Immergut, E. H., and Grulke, E. A. (1999). Polymer handbook (4th edition). *John Wiley*, 2-69.
- [145] Gooch, J. W. (2010). Encyclopedic Dictionary of Polymers. *Springer Berlin Heidelberg*, 1.
- [146] Erhayem, M., Tohami, F. A., Mohamed, R., et al. (2015). Isotherm, kinetic and thermodynamic studies for the sorption of mercury (II) onto activated carbon from *Rosmarinus officinalis* leaves. *American Journal of Analytical Chemistry*, 6(1), 6-10.
- [147] Jiang, J. Q., Cooper, C., and Ouki, S. (2002). Comparison of modified montmorillonite adsorbents : Part I : preparation, characterization and phenol adsorption. *Chemosphere*, 47(7), 711-716.
- [148] Thirumalisamy, S., and Subbian, M. (2010). Removal of methylene blue from aqueous solution by activated carbon prepared from the peel of cucumis sativa fruit by adsorption. *BioResources*, 5(1), 419-437.



APPENDIX A
EFFECT OF REACTION PARAMETERS
ON REACTION EFFICIENCY

Table A.1 The amount of each variable parameter for the crosslinking reaction.

No.	DNR (g)	PNVCL (phr)	BPO (phr)	Reaction temperature (°C)	Reaction time (h)	Gel content (%)
1	1	50	10	75	24	36.05
2	1	100	10	75	24	55.62
3	1	150	10	75	24	84.90
4	1	100	5	75	24	51.28
5	1	100	50	75	24	66.69
6	1	100	10	85	24	36.64
7	1	100	10	95	24	26.05
8	1	100	10	75	12	21.09
9	1	100	10	75	36	99.80

*No.2 was chosen as a standard condition.

Table A.2 The amount of each variable parameter for the graft copolymerization.

No.	DPNR (g)	NVCL (phr)	AIBN (phr)	Reaction temperature (°C)	Reaction time (h)	Grafting ratio (%)
1	5	50	10	90	6	11.21
2	5	100	10	90	6	18.21
3	5	150	10	90	6	37.59
4	5	100	5	90	6	21.37
5	5	100	15	90	6	10.32
6	5	100	10	80	6	51.02
7	5	100	10	100	6	10.94
8	5	100	10	90	4	28.80
9	5	100	10	90	8	5.88

*No.2 was chosen as a standard condition.

APPENDIX B
THE WATER ABSORPTION MEASUREMENT

Table B.1 Degree of water swelling of NR.

Temperature (°C)	No.									Average	SD
	1			2			3				
	W ₁ (g)	W ₂ (g)	Swelling (%)	W ₁ (g)	W ₂ (g)	Swelling (%)	W ₁ (g)	W ₂ (g)	Swelling (%)		
28	0.1518	0.1536	1.1858	0.1755	0.1805	2.8490	0.1679	0.1713	2.0250	2.0199	0.8316
30	0.1742	0.1797	3.1573	0.1780	0.1802	1.2360	0.1796	0.1818	1.2249	1.8727	1.1125
32	0.1784	0.1817	1.8498	0.1856	0.1886	1.6164	0.1852	0.1903	2.7538	2.0733	0.6007
34	0.1543	0.1581	2.4627	0.1513	0.1565	3.4369	0.1614	0.1635	1.3011	2.4002	1.0693
36	0.1536	0.1587	3.3203	0.1522	0.1546	1.5769	0.1327	0.1342	1.1304	2.0092	1.1572
38	0.1628	0.1679	3.1327	0.1539	0.1560	1.3645	0.1562	0.1578	1.0243	1.8405	1.1319

Table B.2 Degree of water swelling of PNVCL-NR (31% gel content).

Temperature (°C)	No.									Average	SD
	1			2			3				
	W ₁ (g)	W ₂ (g)	Swelling (%)	W ₁ (g)	W ₂ (g)	Swelling (%)	W ₁ (g)	W ₂ (g)	Swelling (%)		
28	0.1750	0.2017	15.2571	0.1734	0.2021	16.5513	0.1747	0.2056	17.6875	16.4986	1.2160
30	0.1794	0.2049	14.2140	0.1821	0.2148	17.9572	0.1835	0.2179	18.7466	16.9726	2.4214
32	0.1761	0.2021	14.7643	0.1756	0.2059	17.2551	0.1857	0.2173	17.0167	16.3454	1.3744
34	0.1505	0.1670	10.9635	0.1635	0.1780	8.8685	0.1511	0.1657	9.6625	9.8315	1.0577
36	0.1714	0.1854	8.1680	0.1698	0.1893	11.4841	0.1715	0.1887	10.0292	9.8938	1.6622
38	0.1839	0.2026	10.1686	0.1794	0.2003	11.6499	0.1799	0.1993	10.7838	10.8674	0.7442

Table B.3 Degree of water swelling of PNVCL-NR (19% gel content).

Temperature (°C)	No.									Average	SD
	1			2			3				
	W ₁ (g)	W ₂ (g)	Swelling (%)	W ₁ (g)	W ₂ (g)	Swelling (%)	W ₁ (g)	W ₂ (g)	Swelling (%)		
28	0.1942	0.2159	11.1740	0.1923	0.2123	10.4004	0.1876	0.2045	9.0085	10.1943	1.0974
30	0.1843	0.2022	9.7124	0.1812	0.1995	10.0993	0.1743	0.1945	11.5892	10.4670	0.9909
32	0.1978	0.2162	9.3023	0.1899	0.2132	12.2696	0.1785	0.1978	10.8123	10.7948	1.4837
34	0.1894	0.1987	4.9102	0.1843	0.1927	4.5578	0.1729	0.1852	7.1139	5.5273	1.3853
36	0.1936	0.2018	4.2355	0.1969	0.2074	5.3327	0.1885	0.1991	5.6233	5.0638	0.7319
38	0.1948	0.2031	4.2608	0.1889	0.2015	6.6702	0.1846	0.1954	5.8505	5.5938	1.2250

Table B.4 Degree of water swelling of DPNR.

Temperature (°C)	No.									Average	SD
	1			2			3				
	W ₁ (g)	W ₂ (g)	Swelling (%)	W ₁ (g)	W ₂ (g)	Swelling (%)	W ₁ (g)	W ₂ (g)	Swelling (%)		
28	0.1731	0.1742	0.6355	0.1735	0.1779	2.5360	0.1645	0.1698	3.2219	2.1311	1.3399
30	0.1714	0.1749	2.0420	0.1734	0.1778	2.5375	0.1684	0.1748	3.8005	2.7933	0.9067
32	0.1831	0.1866	1.9155	0.1850	0.1918	3.6757	0.1854	0.1898	2.3732	2.6535	0.9149
34	0.1542	0.1559	1.1025	0.1511	0.1559	3.1767	0.1501	0.1557	3.7575	2.6789	1.3958
36	0.1628	0.1642	0.8600	0.1621	0.1658	2.2825	0.1589	0.1642	3.3354	2.1593	1.2423
38	0.1783	0.1830	2.6360	0.1693	0.1721	1.6539	0.1585	0.1649	4.0379	2.7759	1.1981

Table B.5 Degree of water swelling of NVCL-*g*-DPNR (25% grafting ratio).

Temperature (°C)	No.									Average	SD
	1			2			3				
	W ₁ (g)	W ₂ (g)	Swelling (%)	W ₁ (g)	W ₂ (g)	Swelling (%)	W ₁ (g)	W ₂ (g)	Swelling (%)		
28	0.1560	0.1935	24.0385	0.1543	0.1950	26.3772	0.1442	0.1842	27.7393	26.0516	1.8718
30	0.1516	0.1876	23.7467	0.1497	0.1886	25.9853	0.1395	0.1779	27.5296	25.7530	1.9008
32	0.1302	0.1621	24.5008	0.1439	0.1821	26.5462	0.1018	0.1263	24.0668	25.0379	1.3241
34	0.1214	0.1437	18.3690	0.1194	0.1398	17.0854	0.1024	0.1232	20.3125	18.5890	1.6247
36	0.1237	0.1461	18.1083	0.1107	0.1332	20.3252	0.1312	0.1548	17.9878	18.8071	1.3161
38	0.1174	0.1406	19.7615	0.1018	0.1224	20.2358	0.1881	0.2187	16.2679	18.7551	2.1669

Table B.6 Degree of water swelling of NVCL-*g*-DPNR (15% grafting ratio).

Temperature (°C)	No.									Average	SD
	1			2			3				
	W ₁ (g)	W ₂ (g)	Swelling (%)	W ₁ (g)	W ₂ (g)	Swelling (%)	W ₁ (g)	W ₂ (g)	Swelling (%)		
28	0.1744	0.2016	15.5963	0.1695	0.2041	20.4130	0.1642	0.1958	19.2448	18.4180	2.5125
30	0.1532	0.1769	15.4700	0.1529	0.1804	17.9856	0.1423	0.1689	18.6929	17.3828	1.6939
32	0.1854	0.2187	17.9612	0.1795	0.2153	19.9443	0.1675	0.1947	16.2388	18.0481	1.8543
34	0.1936	0.2138	10.4339	0.1921	0.2164	12.6497	0.1874	0.2129	13.6073	12.2303	1.6277
36	0.1767	0.1936	9.5642	0.1585	0.1779	12.2397	0.1728	0.1933	11.8634	11.2225	1.4483
38	0.1613	0.1814	12.4613	0.1534	0.1731	12.8422	0.1669	0.1854	11.0845	12.1293	0.9247

APPENDIX C
THE CONTACT ANGLE DETERMINATION

Table C.1 Contact angle of NR.



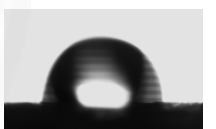
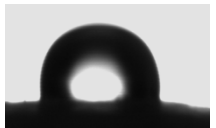


Temperature (°C)	Contact angle value (°)			Average	SD	Figure
	No.					
	1	2	3			
28	106.39	108.28	96.59	103.75	6.28	
30	119.26	114.86	91.55	108.56	14.89	
32	111.80	108.93	95.16	105.30	8.90	
34	109.29	115.67	99.82	108.26	7.98	
36	97.04	105.58	120.96	107.86	12.12	
38	96.79	118.19	101.85	105.61	11.18	

Table C.2 Contact angle of PNVCL-NR (31% gel content).

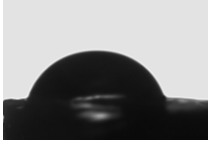
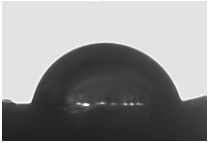


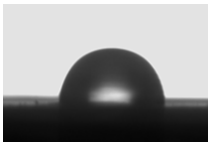

Temperature (°C)	Contact angle value (°)			Average	SD	Figure
	No.					
	1	2	3			
28	62.98	77.12	81.17	73.76	9.55	
30	71.25	88.78	73.11	77.71	9.63	
32	68.77	75.90	87.01	77.23	9.19	
34	99.82	89.90	100.29	96.67	5.87	
36	90.48	104.39	97.36	97.41	6.96	
38	88.21	95.12	99.40	94.24	5.65	

Table C.3 Contact angle of DPNR.


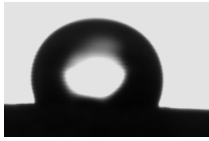

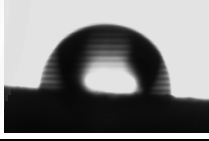

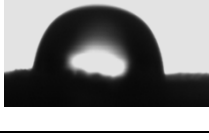

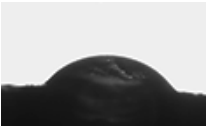
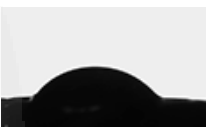
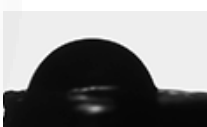


Temperature (°C)	Contact angle value (°)			Average	SD	Figure
	No.					
	1	2	3			
28	106.25	118.67	98.10	107.67	10.36	
30	114.14	112.84	99.76	108.91	7.95	
32	96.51	115.54	108.88	106.98	9.66	
34	95.73	112.82	110.78	106.44	9.33	
36	108.18	99.08	112.17	106.48	6.71	
38	96.77	114.27	101.82	104.29	9.01	

Table C.4 Contact angle of NVCL-*g*-DPNR (25% grafting ratio).

Temperature (°C)	Contact angle value (°)			Average	SD	Figure
	No.					
	1	2	3			
28	58.84	48.54	68.43	58.60	9.95	
30	48.90	65.44	58.17	57.50	8.29	
32	68.74	50.28	58.28	59.10	9.26	
34	69.23	75.59	89.69	78.17	10.47	
36	83.11	79.49	72.94	78.51	5.15	
38	89.32	78.54	70.12	79.33	9.62	

APPENDIX D

ADSORPTION STUDIES

Table D.1 Parameters for linear plotting in adsorption isotherms of indigo carmine onto PNVCL-NR (31% gel content) surface.

			Langmuir		Freundlich		Temkin		Dubinin-Radushkevich	
No.	C_i (mg/L)	C_e (mg/L)	$1/C_e$	$1/q_e$	$\log C_e$	$\log q_e$	$\ln C_e$	q_e	ε^2	$\ln q_e$
1	10	0.5261	1.9009	2.9344	-0.2790	-0.4675	-0.6424	0.3408	7205493.9139	-1.0765
2	20	4.5856	0.2181	1.8924	0.6614	-0.2770	1.5229	0.5284	247206.4891	-0.6378
3	30	5.5707	0.1795	0.9456	0.7459	0.0243	1.7175	1.0575	173150.8732	0.0559
4	40	10.1687	0.0983	0.8377	1.0073	0.0769	2.3193	1.1937	55891.5179	0.1771
5	50	30.2531	0.0331	1.2549	1.4808	-0.0986	3.4096	0.7969	6717.9053	-0.2270

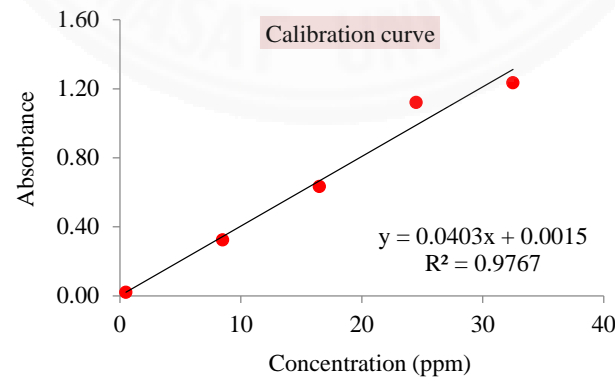
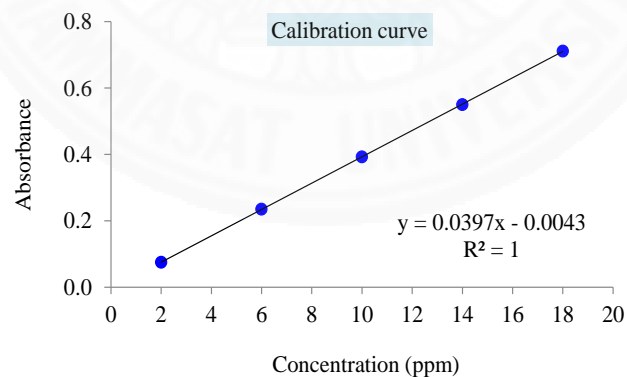


Table D.2 Parameters for linear plotting in adsorption isotherms of indigo carmine onto NVCL-g-DPNR (25% grafting ratio) surface.

No.	C_i (mg/L)	C_e (mg/L)	Langmuir		Freundlich		Temkin		Dubinin-Radushkevich	
			$1/C_e$	$1/q_e$	$\log C_e$	$\log q_e$	$\ln C_e$	q_e	ε^2	$\ln q_e$
1	10	2.1310	0.4693	2.7742	0.3286	-0.4431	0.7566	0.3605	940423.4333	-1.0204
2	20	5.9093	0.1692	1.7054	0.7715	-0.2318	1.7765	0.5864	155266.5725	-0.5338
3	30	10.7305	0.0932	1.1614	1.0306	-0.0650	2.3731	0.8610	50432.7966	-0.1496
4	40	15.5416	0.0643	0.8978	1.1915	0.0468	2.7435	1.1138	24701.4980	0.1078
5	50	12.0806	0.0828	0.6303	1.0821	0.2005	2.4916	1.5866	40178.1382	0.4616



APPENDIX E

DYE RELEASE STUDIES

Figure E.1 UV-visible spectra and release profiles (at $\lambda_{\text{max}} = 610 \text{ nm}$) of solution after desorption of indigo carmine from NR as a function of temperature and time.

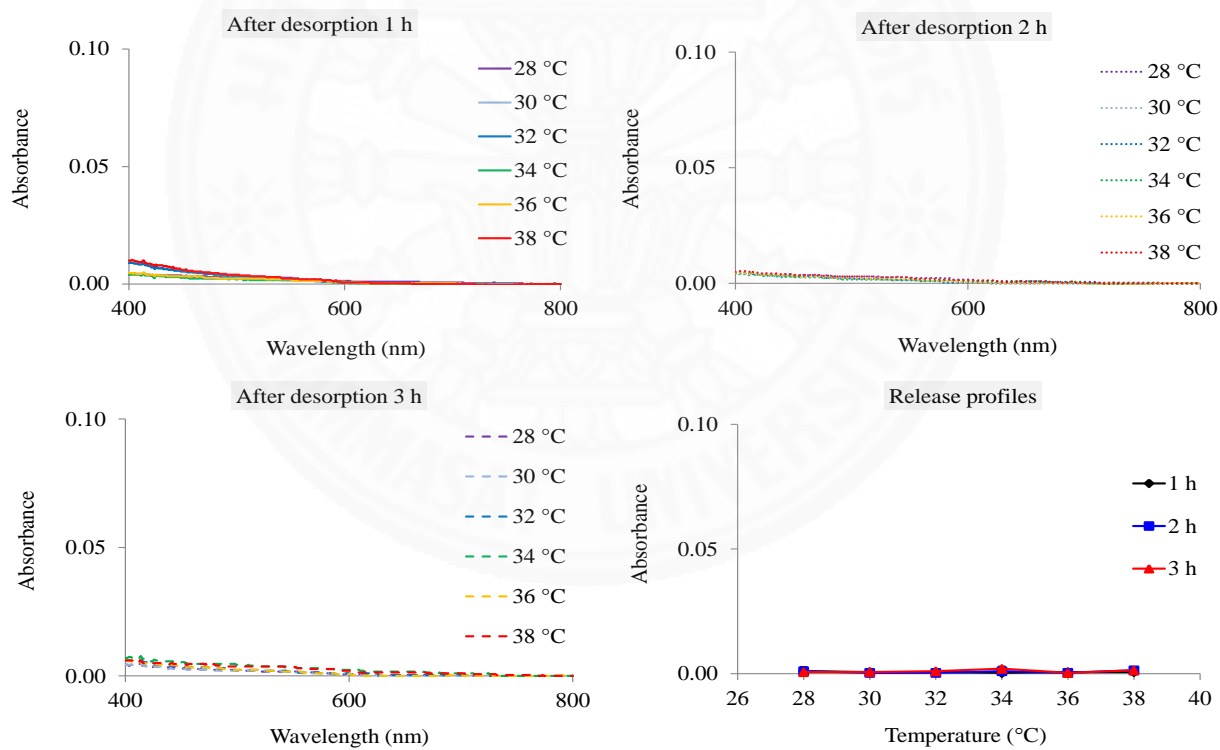


Figure E.2 UV-visible spectra and release profiles (at $\lambda_{\max} = 610$ nm) of solution after desorption of indigo carmine from PNVCL-NR (31% gel content) as a function of temperature and time.

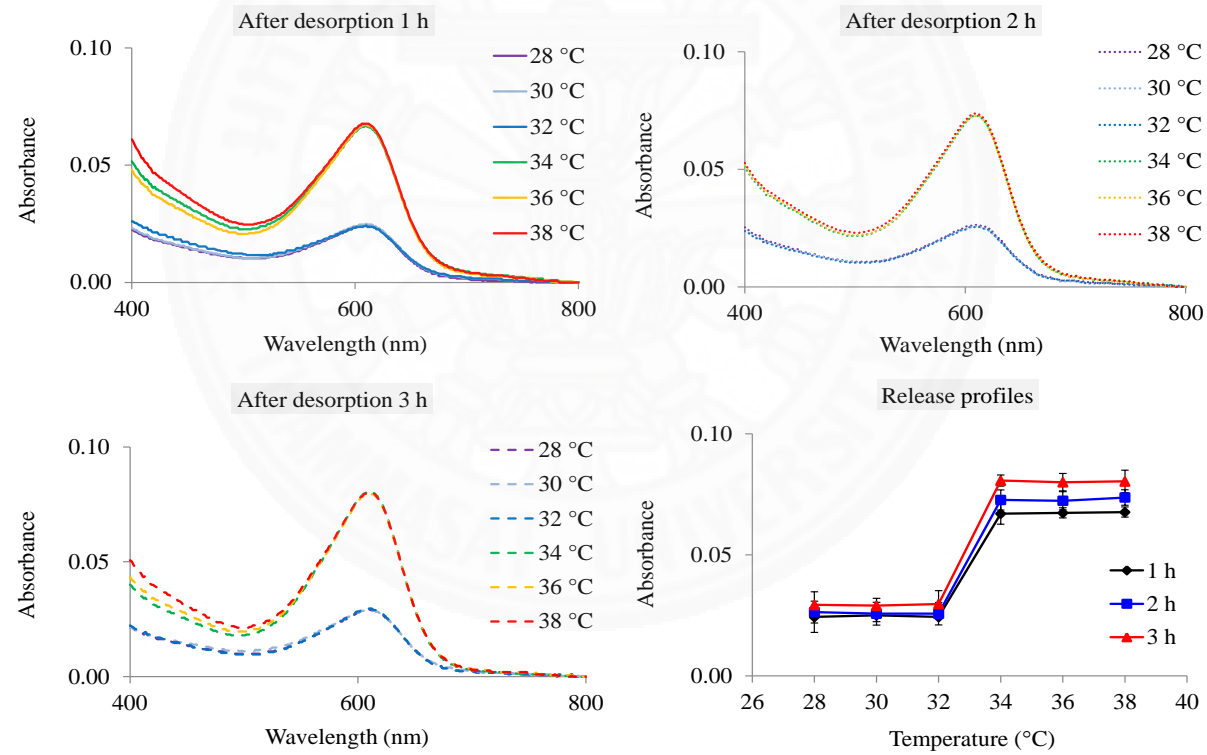


Figure E.3 UV-visible spectra and release profiles (at $\lambda_{\max} = 610$ nm) of solution after desorption of indigo carmine from PNVCL-NR (19% gel content) as a function of temperature and time.

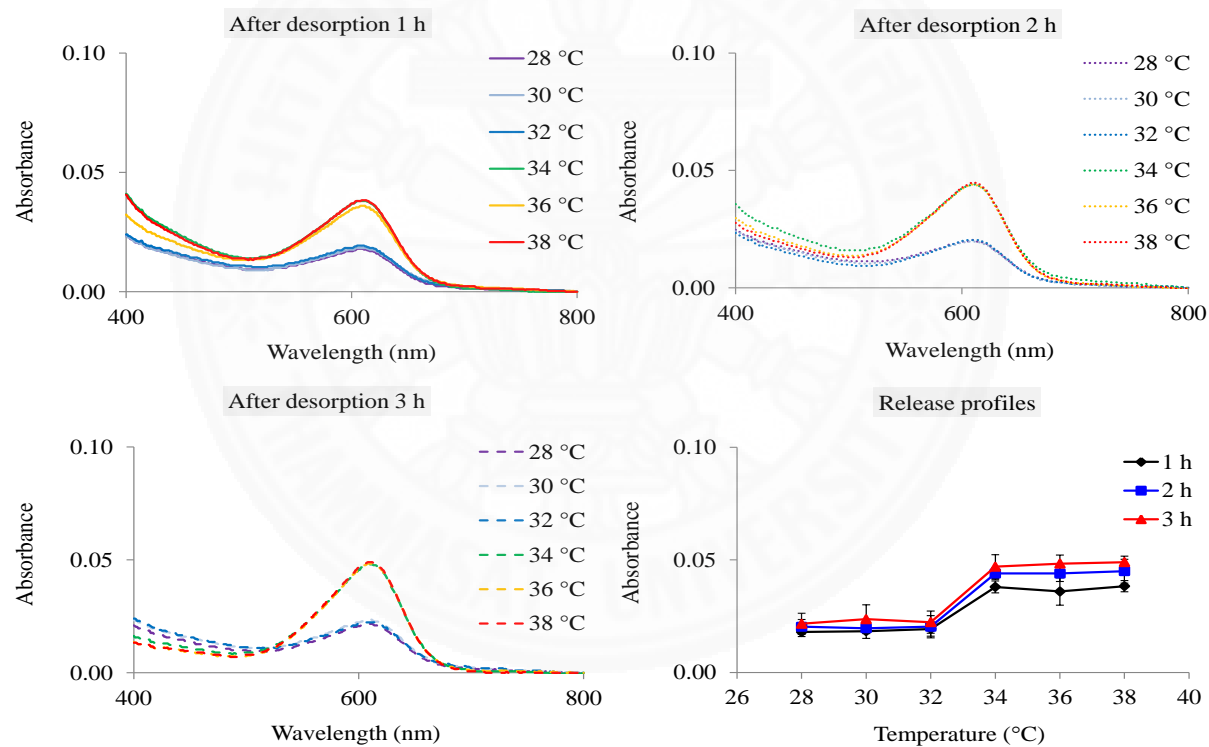


Figure E.4 UV-visible spectra and release profiles (at $\lambda_{\text{max}} = 610 \text{ nm}$) of solution after desorption of indigo carmine from DPNR as a function of temperature and time.

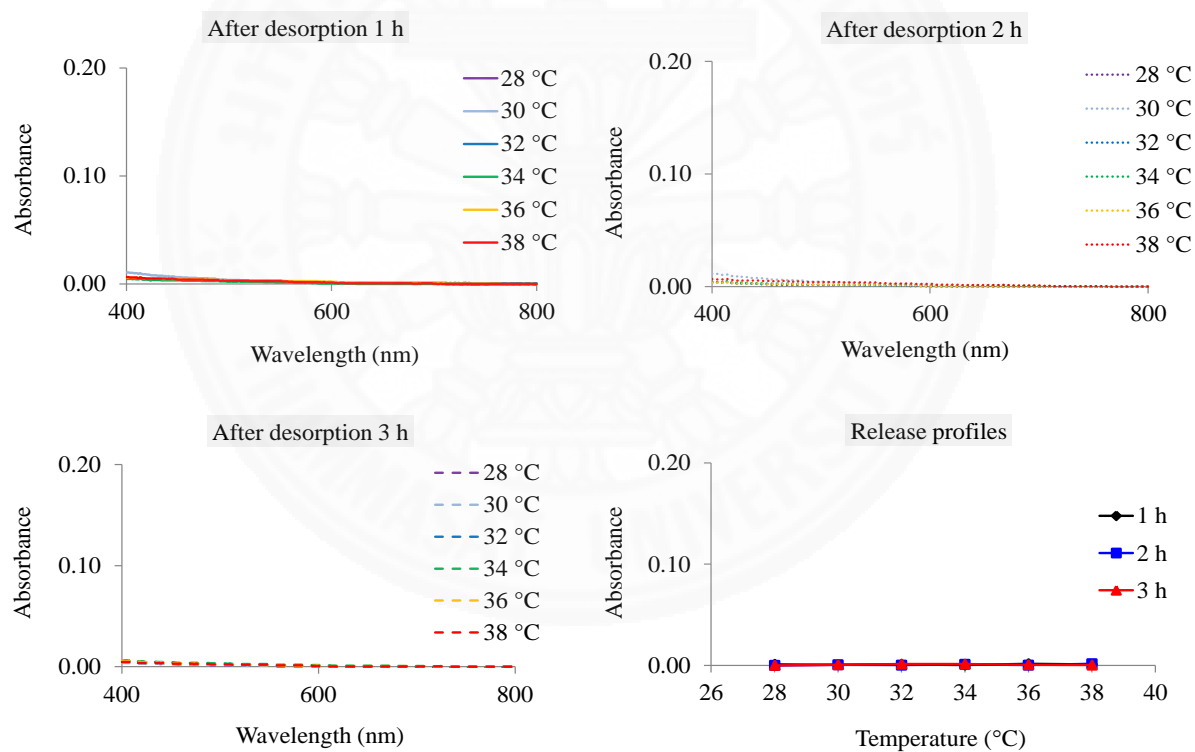


Figure E.5 UV-visible spectra and release profiles (at $\lambda_{\max} = 610$ nm) of solution after desorption of indigo carmine from NVCL-*g*-DPNR (25% grafting ratio) as a function of temperature and time.

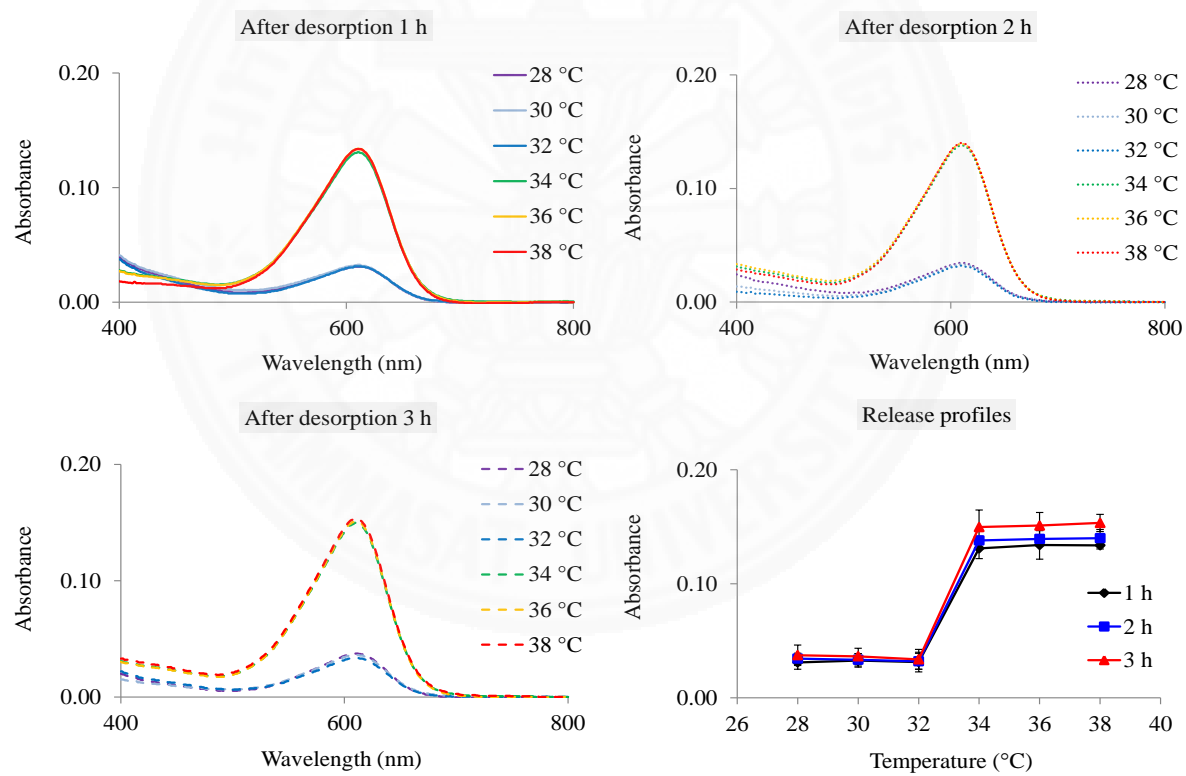
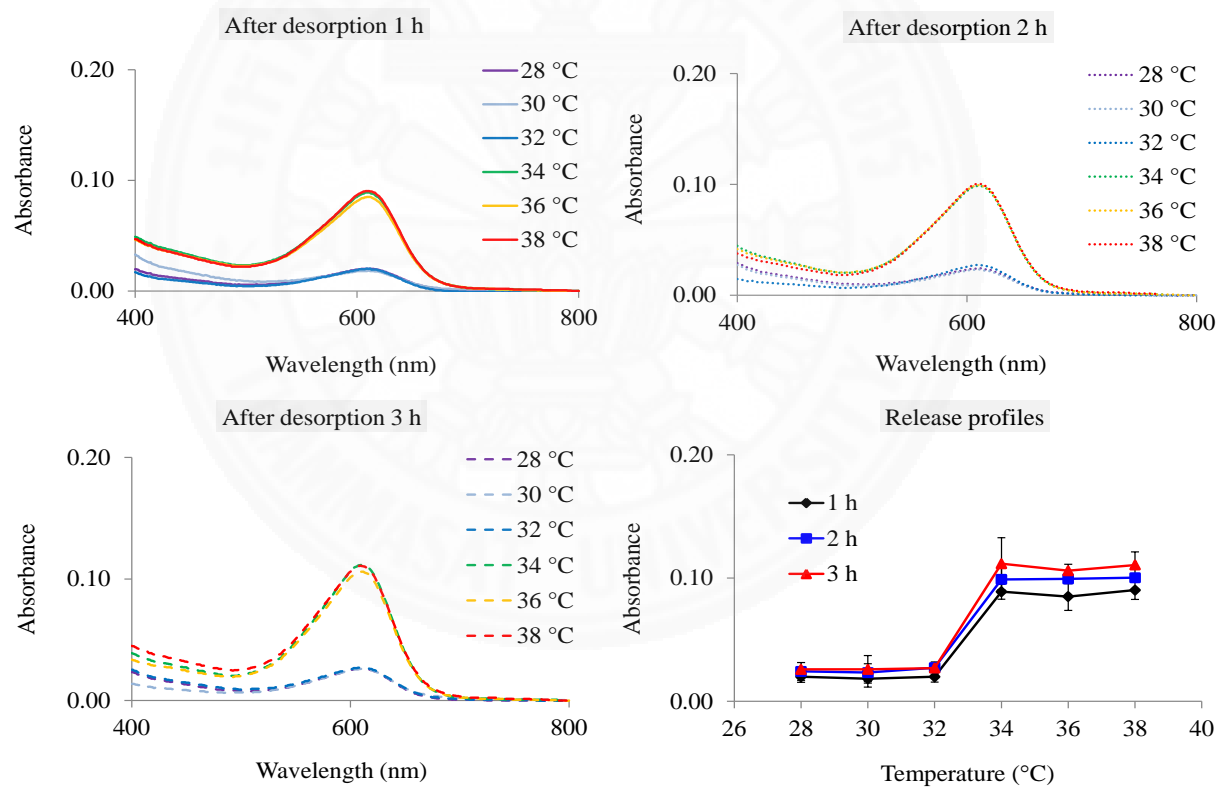


Figure E.6 UV-visible spectra and release profiles (at $\lambda_{\max} = 610$ nm) of solution after desorption of indigo carmine from NVCL-*g*-DPNR (15% grafting ratio) as a function of temperature and time.



APPENDIX F

PUBLICATIONS

Temperature-Responsive Crosslinked Materials Prepared from Natural Rubber and Poly(*N*-vinylcaprolactam)

Sopitcha Phetrong¹
Chanon Sansuk¹

Pramuan Tangboriboonrat²
Peerasak Paoprasert*¹

¹ Department of Chemistry, Faculty of Science and Technology, Thammasat University, Pathumthani, 12120, Thailand

² Department of Chemistry, Faculty of Science, Mahidol University, Bangkok, 10400, Thailand

Received December 28, 2016 / Revised February 27, 2017 / Accepted March 10, 2017

Abstract: A straightforward method for functionalizing natural rubber (NR) with poly(*N*-vinylcaprolactam) (PNVCL), a temperature-responsive polymer having lower critical solution temperature (LCST) near human body temperature, has been successfully developed using free radical crosslinking reaction. Effects of polymer and initiator concentrations, reaction temperature, and reaction time on immobilization percentage of the synthesized polymer were investigated. Results showed 100% immobilization percentage when using 100 phr of PNVCL, 10 phr of benzoyl peroxide at 75 °C within 36 h. For the temperature responsiveness, the water swelling, water contact angle, and dye release of the crosslinked NR were measured. Its LCST ca. 32–34 °C was close to that of the pristine PNVCL. The dye adsorption studies revealed the Langmuir isotherm indicating monolayer coverage. Dye release could be triggered by increasing the temperature above the LCST, suggesting its potential uses in drug release technology. In addition, this temperature-responsive NR would potentially be used as a novel responsive rubber-based material in various applications, such as sensors and biomedical materials.

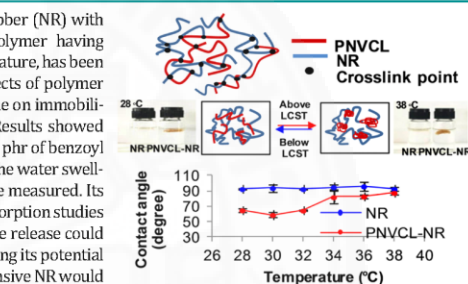
Keywords: temperature-responsive polymer, poly(*N*-vinylcaprolactam), natural rubber.

1. Introduction

Stimuli-responsive materials can sense and respond to changes in environmental conditions such as pH, temperature, light, ionic strength, electric field, and magnetic field^{1–3} leading to the alteration of their physical and chemical properties such as size, shape, hydrophobicity/hydrophilicity, and degradation rate. Due to the relative ease of control, temperature is one of the most widely used external stimuli. Temperature-responsive materials undergo a volume transition or soluble-to-insoluble change or vice versa in solution around the lower critical solution temperature (LCST).¹ Among the temperature-responsive polymers, poly(*N*-vinylcaprolactam) (PNVCL) is of interest because its LCST at ca. 32 °C in water is near human body temperature.^{2–4} In addition, this water-soluble and biocompatible PNVCL is relatively stable against hydrolysis and does not produce toxic low molecular-weight amines due to the presence of cyclic amide instead of aliphatic amides in other polymers.⁵ Since its LCST can be tuned via polymer concentration, molecular weight, or the composition of the solution,⁶ NVCL-based polymers have

Acknowledgments: This work is financially supported by the Thailand Research Fund (TRF) and the Faculty of Science and Technology, Thammasat University (TRG5880199). The authors acknowledge the Central Scientific Instrument Center (CSIC), Department of Chemistry, Faculty of Science and Technology, and Thammasat University.

*Corresponding Author: Peerasak Paoprasert (peerasak@tu.ac.th)



many potential uses in sensing and biomedical applications.

Natural rubber (NR) is a renewable biomaterial obtained from *Hevea brasiliensis* tree,⁷ used for a variety of applications due to high elasticity and fatigue resistance. However, NR is not resistant to oxidation, ozone, weathering, various chemicals, and solvents because it consists of *cis*-polyisoprene. Their physical and chemical properties can be improved *via* chemical reactions, *eg.*, hydrogenation,^{8,9} chlorination,^{10,11} epoxidation,^{12,13} bromination,¹⁴ sulfonation,^{15,16} grafting,^{17–22} and crosslinking.^{23,24} Among the new rubber-based materials, NR with temperature-responsive functions is rare and our group was the first to develop temperature-responsive NR using a one-step crosslinking reaction between poly(*N*-isopropylacrylamide) (PNIPAM) and NR.²⁵ The crosslinked material possessing an LCST of ca. 30–34 °C and temperature-controlled release properties can potentially be utilized in sensing and biomedical applications. However, hydrolysis of PNIPAM produces toxic isopropylamine. Hence, a non-toxic, temperature-responsive NR material is desirable.

In this work, we reported a straightforward method for the preparation of temperature-responsive NR via free radical crosslinking reaction with PNVCL using benzoyl peroxide (BPO) as an initiator. The crosslinked NR was characterized using Fourier transform infrared spectroscopy, differential scanning calorimetry, thermogravimetric analysis, and X-ray photoelectron spectroscopy. The immobilization percentage as a function of initiator concentration, polymer concentration, reaction temperature, and reaction time was studied. The LCST of the mate-

Macromolecular Research

rials was measured *via* water swelling, water contact angle, and dye release measurements. Dye adsorption experiments were carried out and four adsorption isotherms including the Langmuir, Freundlich, Temkin, and Dubinin-Radushkevich isotherm models were used to investigate the adsorption characteristics of the dye onto the modified NR.

2. Experimental

2.1. Materials

High ammonia preserved NR latex with 60% dry rubber content was obtained from the Department of Agriculture, Thailand. The latex was coagulated in formic acid solution (5% v/v) before being washed several times with deionized water and then dried in an oven at 60 °C for 24 h. The dried yellowish rubber was purified by soxhlet extraction using acetone for 24 h and dried again at 60 °C for 24 h. Initiators, i.e., 2,2'-azobisisobutyronitrile (AIBN), benzoyl peroxide (BPO) (Sigma-Aldrich, USA), and *N*-vinylcaprolactam (NVCL) monomer (Sigma-Aldrich, USA) were recrystallized in methanol and hexane, respectively, before use. Formic acid, acetone, hexane, diethyl ether, and chloroform (Labscon, AR) were used as received. Deionized (DI) water was used throughout the experiments.

2.2. Synthesis of PNVC

NVCL (3 g), AIBN (0.15 g), and hexane (15 mL) were mixed in a 100 mL round bottom flask and stirred in an oil bath at 60 °C for 6 h. The solution mixture was then precipitated in diethyl ether, and the polymer was filtered and dried under vacuum at 60 °C overnight to yield white powder (2.8 g).

2.3. Preparation of temperature-responsive crosslinked material

PNVCL (50-150 parts per hundred of rubber (phr)) in chloroform (10 mL) and BPO (5-50 phr with respect to dried NR) in chloroform (5 mL) were then slowly added into NR (1 g) dissolved in chloroform (30 mL). The mixture was heated to a predetermined temperature (75-95 °C), while stirring for a specified amount of time (12-36 h). After being cooled to room temperature, the solid polymer product was filtered, washed with chloroform, and dried under vacuum at 60 °C for 24 h. The resulting polymer was purified by soxhlet extraction in acetone for 24 h and dried overnight at 60 °C.

The immobilization percentage was calculated from the following equation:

$$\text{Immobilization percentage} = \frac{W_2 - W_1}{W_1} \times 100$$

where W_1 and W_2 are the weights of the rubbers before and after crosslinking reaction, respectively.

2.4. Determination of crosslink density

Thin PNVCL-NR samples (0.75×0.75 cm²) were immersed in

toluene at room temperature for one week. The crosslink density was calculated using the Flory-Rehner Equation:^{26,27}

$$p_c = -\frac{1}{2V_s} \frac{\ln(1 - V_r^0) + V_r^0 + \chi(V_r^0)^2}{(V_r^0)^{1/3} - \frac{V_r^0}{2}}$$

where p_c is the crosslink density (mol m⁻³), V_s is the molar volume of toluene (1.069×10⁻⁴ m³ mol⁻¹) at 25 °C, χ is the interaction parameter (0.44+0.18 V_r^0), and V_r^0 is the fraction of crosslinked rubber in the swollen gel, which can be calculated as follows:

$$V_r^0 = \frac{1}{1 + \frac{\rho_1}{\rho_2} \left(\frac{W_s - W_d}{W_d} \right)}$$

where ρ_2 and ρ_1 are the densities of toluene (0.87 g mL⁻¹) and rubber (0.92 g mL⁻¹), respectively, and W_s and W_d are the weights of swollen and dried crosslinked rubbers, respectively.

2.5. Determination of LCST by water swelling experiment

Thin PNVCL-NR samples (0.75×0.75 cm²) were immersed in DI water at a predetermined temperature (28-38 °C) for 2 h. After removing the surface liquid gently with tissue paper, the weight of the materials was obtained and the degree of swelling in percentage was calculated from the following equation:

$$\text{Degree of swelling (\%)} = \frac{W_2 - W_1}{W_1} \times 100$$

where W_1 and W_2 are the weights of the materials before and after immersion in DI water, respectively. LCST was determined from the abrupt change of degree of swelling.

2.6. Release of dyes

Thin PNVCL-NR samples (0.75×0.75 cm²) were immersed in an aqueous solution of indigo carmine (10 ppm) at 30 °C for one week. The solution was then placed in a temperature-controlled water bath at a predetermined temperature ranging from 28 to 38 °C for 24 h. Aliquots were withdrawn for absorbance measurement using UV-visible spectrophotometer (UV-1700 PharmaSpec Shimadzu).

2.7. Adsorption studies

Five indigo carmine solutions (10, 20, 30, 40, and 50 ppm) were prepared using DI water. The absorbance of these solutions was measured using UV-visible spectrophotometer. The PNVCL-NR samples (0.2 g) were immersed in the indigo carmine solutions (10 mL), which were then placed on a shaker for one week. The rubber samples were removed and the absorbance of solutions was measured. Concentration of indigo carmine remaining in the solution was then calculated from the absorbance using the calibration curve.

The amount of adsorbed indigo carmine on PNVCL-NR sample was calculated using the following equation:

$$q_e = \frac{(C_0 - C_e)V}{W}$$

where q_e (mg g^{-1}) is the adsorption capacity of the rubber, C_0 (mg L^{-1}) is the initial concentration of indigo carmine in the solution, C_e (mg L^{-1}) is the concentration of indigo carmine remaining in the solution, V (L) is the volume of the solution, and W (g) is the dry weight of rubber sample.

2.8. Characterization

^1H (400 MHz) nuclear magnetic resonance (NMR) spectra were obtained using an AVANCE Bruker NMR spectrometer using chloroform- d as a solvent. The Fourier transform infrared (FT-IR) spectra were obtained using a Perkin Elmer FT-IR spectrometer (Spectrum GX model) and NaCl salt windows. Thermogravimetric analysis (TGA) of the polymers was carried out using an SDTA851e Mettler Toledo analyzer. The samples were heated at a rate of $10\text{ }^\circ\text{C min}^{-1}$ under a nitrogen atmosphere. The glass transition temperatures of the polymers were obtained using a DSC822e Mettler Toledo differential scanning calorimeter. The samples were heated at a rate of $10\text{ }^\circ\text{C min}^{-1}$ under a nitrogen atmosphere. The surface elements of the sample were investigated using an X-ray photoelectron spectrometer (XPS; AXIS ULTRA^{DD}, Kratos analytical, Manchester UK). The samples were excited using X-ray hybrid mode at a $700\times 300\text{ }\mu\text{m}$ spot area with monochromatic Al $K_{1,2}$ radiation at 1.4 keV. The molecular weights of the polymer were measured using Waters gel permeation chromatography (e2695 model) and tetrahydrofuran as a solvent at 1 mL min^{-1} . Polystyrene was used as a standard. The water contact angle was measured using a TL100 Theta Lite tensiometer. The size of water droplet was $8\text{ }\mu\text{L}$.

3. Results and discussion

3.1. Analysis of PNVCN-NR

In the preparation of crosslinked material, PNVCN was first prepared by free radical polymerization of NVCL using AIBN as an initiator. The NMR spectrum of PNVCN showed signals at 4.36, 3.1, 2.4 and 1.65 ppm corresponding to $-\text{CH}-\text{N}$, $-\text{CH}_2-\text{N}$, $-\text{CH}_2-\text{CO}$, and $-\text{CH}_2-$, respectively (Figure 1). The FT-IR signals at 2900–3000, 1631, and 1479 cm^{-1} corresponded to C-H stretches, C=O stretches, and C-N stretches, respectively (Figure 2). Both NMR and FT-IR results of PNVCN agreed well with those reported in the previous work.²⁶

Then, the solid NR, coagulated from NR latex in an acidic

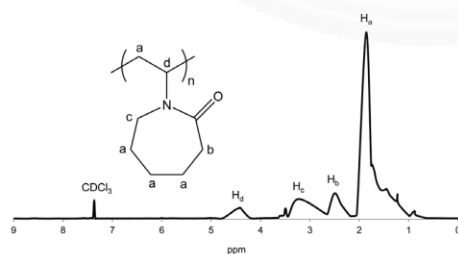


Figure 1. NMR spectrum of PNVCN.

Macromol. Res.

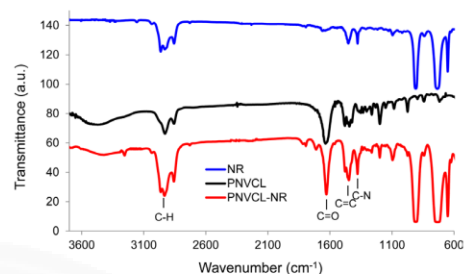


Figure 2. FT-IR spectra of NR, PNVCN, and PNVCN-NR.

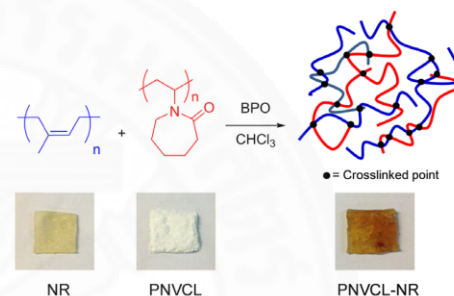


Figure 3. Schematic representation of the crosslinking reaction and photographs of NR, PNVCN, and PNVCN-NR. Sample size was approximately $1\times 1\text{ cm}^2$.

solution, was mixed with PNVCN in chloroform before being crosslinked using BPO as initiator. The crosslinked material was indicated by an insoluble polymer or the gel formation, which was possibly occurred through free radical active centers produced by BPO via hydrogen abstraction process and created on the PNVCN and NR chains.^{29–32} After purification, photographs of the NR, PNVCN, and PNVCN-NR in Figure 3 were yellow, white, and brown, respectively. The PNVCN-NR sample was less elastic compared to the NR. The decrease of elasticity and change of color of PNVCN-NR sample is due to the formation of network structure and thermal treatment, respectively.

The FT-IR spectrum of PNVCN-NR confirmed the presence of both PNVCN and NR. The peaks at 1631 and 1479 cm^{-1} corresponded to C=O and C-N stretching of the caprolactam, whereas those at 1461 , 918 , and 745 cm^{-1} related to C=C stretching and CH_2 bending modes of the *cis*-polyisoprene, respectively. XPS spectra of both NR and PNVCN-NR samples showed signals of O_{1s} , C_{1s} , Si_{2p} , and Si_{2p} at 531 , 284 , 152 , and 101 eV , respectively (Figure 4). Silicon signals belonged to the substrate used for the sample preparation. Unlike NR, PNVCN-NR sample showed a nitrogen signal at 400 eV , which arises from a caprolactam ring. To further confirm the formation of crosslinked material, a blend sample between NR and PNVCN was prepared and subjected to soxhlet extraction in acetone. The NMR spectrum (not shown) showed no signals from PNVCN indicating that a physical mixing between PNVCN and NR did not retain the PNVCN after ace-

© The Polymer Society of Korea and Springer 2017

Macromolecular Research

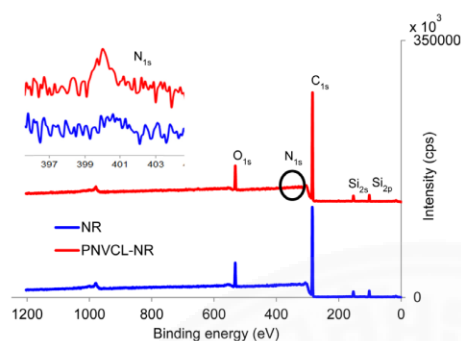


Figure 4. XPS spectra of NR and PNVCN-NR (immobilization percentage=56%). The inset shows the multiplex-scan spectra in the N_{1s} region.

tone extraction. Hence, the presence of both PNVCN and NR in the PNVCN-NR sample after acetone extraction shown by the FT-IR and XPS results was attributed to the formation of a crosslinked structure that was inseparable by solvent extraction. The formation of insoluble gel and the results from FT-IR, NMR, and XPS thus confirmed the formation of crosslinked material from PNVCN and NR.

The thermal properties of NR and PNVCN-NR were investigated using DSC and TGA techniques. The DSC thermograms show that the glass transition temperatures (T_g) of NR and PNVCN-NR were similar in values at -58.9 and -54.9 °C, respectively (Figure 5). This result suggests that the crosslinked rubber still comprised an amorphous region within the NR sample. However, the T_g of PNVCN at ca. 1.8 °C was not observed possibly because that the formation of crosslinked structure led to a loss of amorphous domains of the PNVCN.²⁸ The slightly higher T_g of PNVCN-NR than that of NR was due to the crosslinked structure restricting chain motions. From the TGA thermograms, the NR and PNVCN-NR started to lose weight at ca. 300 and 200 °C, respectively. The PNVCN showed a thermal decomposition at ca. 400 °C (Figure 6).

Effects of PNVCN content, BPO concentration, reaction temperature and time on the immobilization percentage were investigated. The immobilization percentages as a function of PNVCN concentration using BPO of 10 phr, a reaction time of 24 h at 75 °C

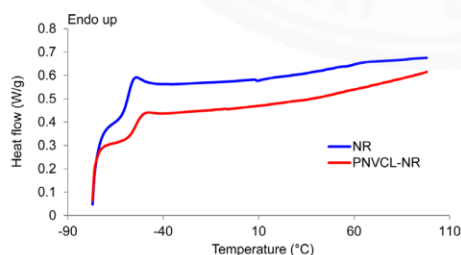


Figure 5. DSC thermograms of NR and PNVCN-NR (immobilization percentage=56%).

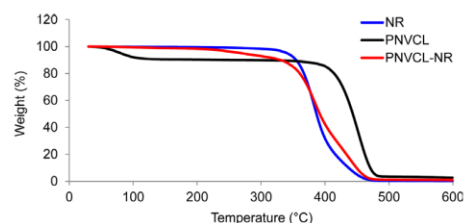


Figure 6. TGA thermograms of NR and PNVCN-NR (immobilization percentage=56%).

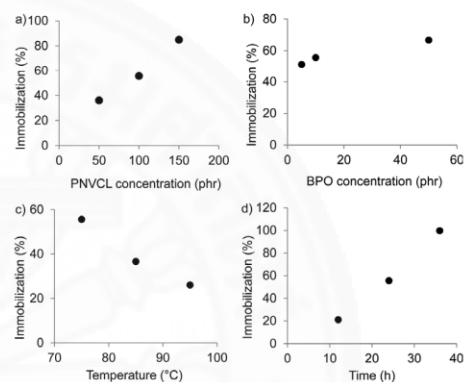


Figure 7. Immobilization percentages as a function of (a) PNVCN concentration, (b) BPO concentration, (c) reaction temperature, and (d) reaction time.

increased from 36% to 85% when the amount of PNVCN increased from 50 to 150 phr (Figure 7(a)). Then, the effect of BPO concentration on immobilization percentage using a PNVCN concentration of 100 phr, a reaction time of 24 h, at 75 °C was studied. When the initiator concentration was increased from 5 to 15 phr, the immobilization percentage increased from 51 to 67% (Figure 7(b)) due to the increase in free radicals. By using PNVCN concentration of 100 phr, BPO concentration of 10 phr within 24 h, and changing the reaction temperature from 75 to 95 °C, the immobilization percentage linearly decreased from 56 to 26% (Figure 7(c)). It was explained that the high temperature may lead to high termination rates of free radicals.³³ Lastly, the effect of reaction time on immobilization percentage at 75 °C using a PNVCN concentration of 100 phr, a BPO concentration of 10 phr was studied. It was found that the immobilization percentage increased from 21 to 100% when increasing the reaction time from 12 to 36 h (Figure 7(d)).

3.2. Crosslink density

The crosslink density of the modified rubber was measured using the Flory-Rehner method and toluene as solvent.^{26,34} It was found that when the immobilization percentages increased, the degree of swelling decreased (Figure 8(a)). The crosslink

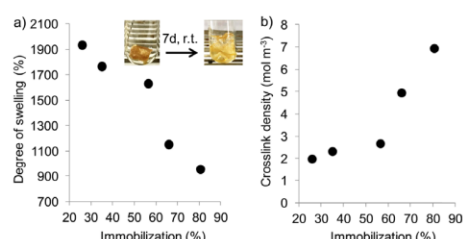


Figure 8. (a) Degree of swelling and (b) crosslink density of PNVCN-NR as a function of immobilization percentage.

density increased with the immobilization percentage (Figure 8(b)). At 26% immobilization percentage, the crosslink density was 2 mol m^{-3} and increased to 7 mol m^{-3} at 80% immobilization percentage (Figure 8), comparable to previous studies.^{26,27}

3.3. Temperature-responsive behaviors

Temperature-responsive behaviors of PNVCN-NR in water were investigated by using the water-swelling experiment at a temperature range of 28–38 °C (Figure 9). The PNVCN-NR showed hydrogel-like characteristics. At 28 °C, its degree of swelling was higher than that of NR due to the presence of hydrophilic NVCL units. The higher immobilization percentage led to the higher degree of swelling. As increasing the temperature, the degree of swelling of the NR did not change, whereas that of the PNVCN-NR significantly decreased at >32 °C. The LCST of the PNVCN-NR was therefore ca. 32–34 °C, which is similar to the coil-to-globule transition temperature of PNVCN.^{6,28} These results suggest that the presence of NR and crosslinked structure in the PNVCN-NR did not significantly affect the LCST of the PNVCN. This finding is consistent with other reports on temperature-responsive crosslinked materials.^{35–39}

The LCST of PNVCN-NR was also determined using a temperature-controlled tensiometry. Results showed that the contact angles of the NR samples remained of 93–95°, agreed with previous report.⁴⁰ The contact angles of PNVCN-NR increased significantly from 60° to 82° when the temperature was increased

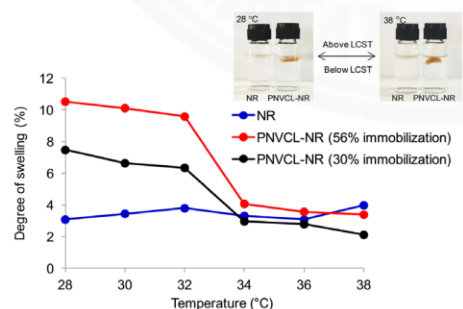


Figure 9. Degree of swelling of NR and PNVCN-NR in water at different temperatures.

Macromol. Res.

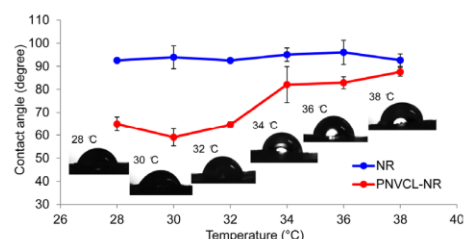


Figure 10. Contact angles of NR and PNVCN-NR at different temperatures.

from 32 to 34 °C, indicating an increase in hydrophobicity (Figure 10). This was due to the breakage of hydrogen bonds between the water molecules and caprolactam units. The LCSTs determined from the abrupt change in contact angles were ca. 32–34 °C, which are similar to those determined by the water swelling method described above.

The controlled release properties of PNVCN-NR were demonstrated via dye absorption and desorption experiments. Indigo carmine, an anionic dye, was chosen as it is soluble in water and possesses strong absorbance in the visible region. After being immersed in indigo carmine solution for one week at room temperature, the PNVCN-NR absorbed dye more than the NR as shown by a greater reduction of dye absorbance for the PNVCN-NR sample (Figure 11). At > 34 °C, the PNVCN-NR released the dye into the solution as indicated by the increase in absorbance, whereas the absorbance of the NR did not change across the temperature range. The dye desorbed from the PNVCN-NR sample due to the increase in hydrophobicity of the NVCL units as the temperature was above the LCST. Photographs of indigo carmine solution upon absorption and desorption from the rubber samples are presented (Figure 12). The PNVCN-NR absorbed and then released the dye when the temperature was raised above the LCST as confirmed by the change of color, which agrees well with the UV-visible results. The solution color of the NR sample was almost unchanged because NR is not temperature-responsive. From the temperature-controlled release properties, PNVCN-NR would be potentially used in biomedical appli-

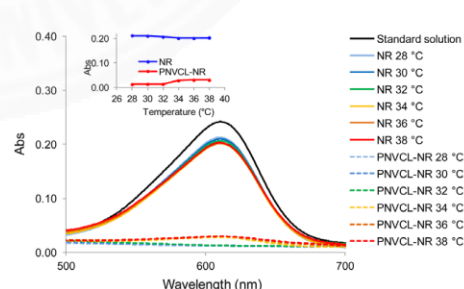


Figure 11. UV-visible spectra of indigo carmine solutions after immersion of NR and PNVCN-NR at different temperatures. The inset is the plot of absorbance values as a function of temperature.

© The Polymer Society of Korea and Springer 2017

Macromolecular Research

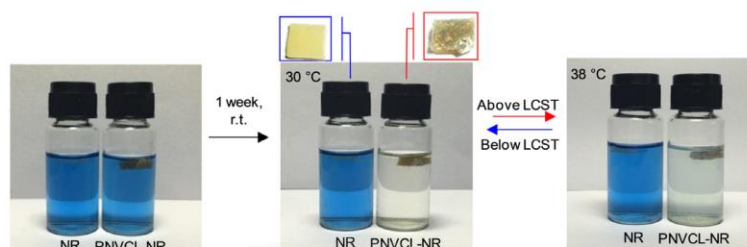


Figure 12. Photographs of indigo carmine solutions with NR and PNVCL-NR samples.

cations, separation membranes, and activator for enzymes.⁴¹⁻⁴³

3.4. Adsorption isotherm studies

Four well-known adsorption isotherms including the Langmuir, Freundlich, Temkin, and Dubinin-Radushkevich isotherm models were used to investigate the interaction between indigo carmine and PNVCL-NR. The Langmuir adsorption isotherm is based on the assumption that monolayer coverage is formed on the

surface of the adsorbent. The Freundlich adsorption isotherm describes the adsorption characteristics of the multilayer adsorption. The Temkin adsorption isotherm takes account the indirect effects, such as heat, on adsorbate/adsorbent interaction. Lastly, the Dubinin-Radushkevich describes the adsorption model on both homogeneous and heterogeneous surfaces based on pore filling mechanism. The mathematical equations of these four models were summarized (Table 1).⁴⁴⁻⁴⁶ On the basis of the R-squared (R^2) of these models (Figure 13), Langmuir model

Table 1. Mathematical equations of Langmuir, Freundlich, Temkin, and Dubinin-Radushkevich isotherms^a

Isotherm	Nonlinear form	Linear form	Plot
Langmuir	$q_e = \frac{Q_0 K_L C_e}{1 + K_L C_e}$	$\frac{1}{q_e} = \frac{1}{Q_0} + \frac{1}{Q_0 K_L C_e}$	$\frac{1}{q_e}$ vs. $\frac{1}{C_e}$
Freundlich	$q_e = K_f C_e^{1/n}$	$\log(q_e) = \log(K_f) + \frac{1}{n} \log(C_e)$	$\log(q_e)$ vs. $\log(C_e)$
Temkin	$q_e = \frac{RT}{b_T} \ln(A_T C_e)$	$q_e = B \ln(A_T) + B \ln C_e$	q_e vs. $\ln C_e$
Dubinin-Radushkevich	$q_e = (q_s) \exp(-K_{ad} \epsilon^2)$	$\ln(q_e) = \ln(q_s) - (K_{ad} \epsilon^2)$	$\ln(q_e)$ vs. ϵ^2

^a C_e is the equilibrium concentration of adsorbate (mg L^{-1}), q_e is the amount of metal adsorbed per gram of the adsorbent at equilibrium (mg g^{-1}), Q_0 is the maximum monolayer coverage capacity (mg g^{-1}), K_L is the Langmuir isotherm constant (L mg^{-1}), K_f is the Freundlich isotherm constant (mg g^{-1}), n is the adsorption intensity, A_T is the Temkin isotherm equilibrium binding constant (L mg^{-1}), b_T is the Temkin isotherm constant, R is the universal gas constant ($8.314 \text{ J mol}^{-1} \text{ K}^{-1}$), T is the temperature at 303.15 K, B is constant related to heat of sorption (J mol^{-1}), q_s is the theoretical isotherm saturation capacity (mg g^{-1}), K_{ad} is the Dubinin-Radushkevich isotherm constant ($\text{mol}^2 \text{ g}^{-2}$), and ϵ is the Dubinin-Radushkevich isotherm constant.

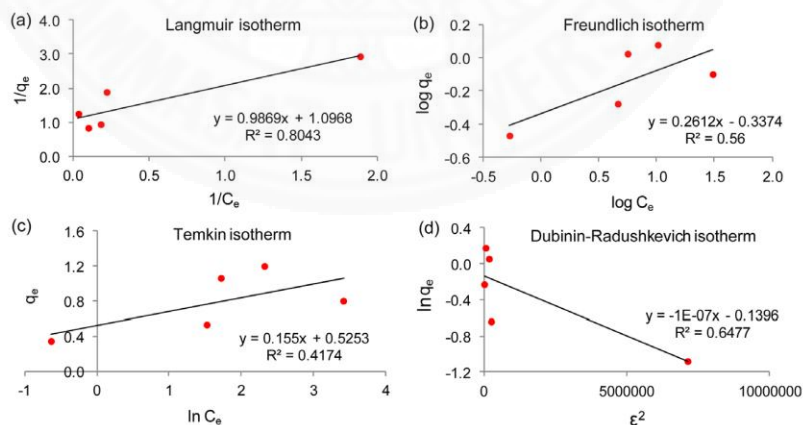


Figure 13. Plots of (a) Langmuir, (b) Freundlich, (c) Temkin, and (d) Dubinin-Radushkevich adsorption isotherms.

shows the highest value of R^2 . Therefore, this analysis suggests that indigo carmine absorbed onto the surface of PNVCN-NR as monolayer coverage. The maximum monolayer coverage capacity (Q_0) and Langmuir isotherm constant (K_L) determined from the slope and intercept were 0.91 mg g^{-1} and 1.11 L mg^{-1} , respectively.

4. Conclusions

Crosslinked materials from PNVCN and NR were successfully prepared via free radical crosslinking reaction using BPO as an initiator. The crosslinked materials were rubber-like hydrogels with thermal properties close to those of NR. Immobilization percentage as a function of reaction conditions was found to depend on the reaction conditions. The temperature responsiveness of PNVCN-NR in water showed an LCST of 32–34 °C close to the human body temperature. The dye absorption and desorption experiments also confirmed the monolayer coverage and temperature responsiveness, respectively. The elastic and temperature-responsive properties make these crosslinked rubbers potentially useful in a variety of biomedical and sensing applications and for consumer products. Potential consumer products include smart bandages and facial masks with the ability to efficiently release medicines or healing ingredients upon contact with human skin, and smart tires for automobiles that change their adhesion in response to changing temperatures. In addition, the preparation of multi-stimuli-responsive rubbers through reactions of multiple responsive materials will extend the properties of the rubbers and expand the range of applications.

References

- J.-K. Chen and C.-J. Chang, *Materials* **7**, 805 (2014).
- T. Yoshida, T. C. Lai, G. S. Kwon, and K. Sakoi, *Expert Opin. Drug Deliv.* **10**, 1497 (2013).
- H. Almeida, M. H. Amaral, and P. Lobão, *J. Appl. Pharma. Sci.* **2**, 01 (2012).
- M. R. Aguilar, C. Elvira, A. Gallardo, B. Vázquez, and J. S. Román, *Topics in Tissue Engineering* (2013).
- T. Kavitha, I.-K. Kang, and S.-Y. Park, *Colloids and Surfaces B: Biointerfaces* **115**, 37 (2014).
- K. M. Rao, B. Mallikarjuna, K. S. V. K. Rao, S. Siraj, K. C. Rao, and M. C. S. Subha, *Colloids and Surfaces B: Biointerfaces* **102**, 891 (2013).
- D. F. Graves, Rubber. In *Handbook of Industrial Chemistry and Biotechnology*, Kent, J. A., Ed. Springer US: 2007; pp 689.
- N. Hinchiranan, K. Charmondusit, P. Prasassarakich, and G. L. Rempel, *J. Appl. Polym. Sci.* **100**, 4219 (2006).
- C. Kookarirrat and P. Paoprasert, *Iran. Polym. J.* **24**, 123 (2015).
- J.-P. Zhong, S.-D. Li, Y.-C. Wei, Z. Peng, and H.-P. Yu, *J. Appl. Polym. Sci.* **73**, 2863 (1999).
- T. Chanroj and P. Paoprasert, *Rubber. Chem. Technol.* **89**, 251 (2016).
- P. Phinyocheep, C. W. Phetphaisit, D. Derouet, I. Campistron, and J. C. Brosse, *J. Appl. Polym. Sci.* **95**, 6 (2005).
- S. Chuayjuljit, C. Yaowsang, N. Na-Ranong, and P. Potiyaraj, *J. Appl. Polym. Sci.* **100**, 3948 (2006).
- X. Xue, Y. Wu, F. Wang, J. Ling, and X. Fu, *J. Appl. Polym. Sci.* **118**, 25 (2010).
- T. Xavier, J. Samuel, K. B. Manjoran, and T. Kurian, *J. Elastom. Plast.* **34**, 91 (2002).
- Y. Y. Patjaree Suksawad, and Seichi Kawahara, *European Polymer Journal* **47**, 330 (2011).
- C. Nakason, A. Kaesaman, and P. Supasanthitkul, *Polym. Test.* **23**, 35 (2004).
- W. Kangwansupamonkon, R. G. Gilbert, and S. Kiatkamjornwong, *Macromol. Chem. Phys.* **206**, 2450 (2005).
- T. Kochthongrasamee, P. Prasassarakich, and S. Kiatkamjornwong, *J. Appl. Polym. Sci.* **101**, 2587 (2006).
- S. Amnuaypanich and P. Ratpolsan, *J. Appl. Polym. Sci.* **113**, 3313 (2009).
- P. Juntuek, C. Ruksakulpiwat, P. Chumsamrong, and Y. Ruksakulpiwat, *J. Appl. Polym. Sci.* **122**, 3152 (2011).
- A. Pisuttisap, N. Hinchiranan, G. L. Rempel, and P. Prasassarakich, *J. Appl. Polym. Sci.* **129**, 94 (2013).
- D. T. Turner, *Polymer* **1**, 27 (1960).
- P. M. Lewis, *NR technology* **17**, 57 (1986).
- Nuntahirun, O. Yamamoto, P. Paoprasert, *Macr. Res. DOI 10.1007/s13233-016-4114-5* (2016).
- D. Saijun, C. Nakason, A. Kaesaman, and P. Klinpituksa, *Songklanakaraj. J. Sci. Technol.* **31**, 561 (2009).
- C. Vudjung, U. Chaisuwan, U. Pangan, N. Chaipugdee, S. Boonyod, O. Santawitee, and S. Saengsuwan, *Energy Procedia* **56**, 255 (2014).
- K. Selin, T. Özdemir, and A. Usanmaz, *Macr. Sci. A* **48**, 467 (2011).
- Halimatuddahlia, H. Ismaila, and H. M. Akil, *Int. J. Polym. Mater.* **54**, 1169 (2005).
- H. Liu, C. Chuai, M. Iqbal, H. Wang, B. B. Kalsoom, M. Khattak, and M. Q. Khattak, *J. Appl. Polym. Sci.* **122**, 973 (2011).
- S. M. Tamboli, S. T. Mhaske, and D. D. Kale, *J. Appl. Polym. Sci.* **122**, 973 (2011).
- E. Manaila, M. D. Stelescu, G. Craciun, and L. Surdu, *Polym. Bull.* **71**, 2001 (2014).
- P. Paoprasert, S. Moonrinta, and S. Kanokul, *Polym. Int.* **63**, 1041 (2014).
- U. C. Chaiwute Vudjung, Uraivan Pangan, Nattiya Chaipugdee, and O. S. A. S. Saowaluk Boonyod, *Energy Procedia* **56**, 255 (2014).
- G. Yi, Y. Huang, F. Xiong, B. Liao, J. Yang, and X. Chen, *Journal of Wuhan University of Technology-Mater. Sci. Ed.* **26**, 1073 (2011).
- X. Xia and Z. Hu, *Langmuir* **20**, 2094 (2004).
- Y. Cai, W. Shen, S. L. Loo, W. B. Krantz, R. Wang, A. G. Fane, and X. Hua, *Water Res.* **47**, 3773 (2013).
- A. Hebeish, S. Farag, S. Sharaf, and T. I. Shaheen, *Carbo. Polym.* **102**, 159 (2014).
- A. Zadrazil and F. Stepánek, *Colloids and Surfaces A* **372**, 115 (2010).
- H. Liu, Q. Wang, L. Wei, and H. Yu, *Polym. Sci. Ser. B* **57**, 623 (2015).
- J. Tobis, L. Boch, Y. Thomann, and J. C. Tiller, *J. Memb. Sci.* **372**, 219 (2011).
- M. Hanko, N. Bruns, J. C. Tiller, and J. Heinze, *Analytical and Bioanalytical Chem.* **386**, 1273 (2006).
- N. Bruns, W. Bannwarth, and J. C. Tiller, *Biotechnol. Bioengineering* **101**, 19 (2008).
- X. Chen, *Information* **4**, 14 (2015).
- A. O. Dada, A. P. Olalekan, A. M. Olatunya, and O. Dada, *IOSR J. Appl. Chem.* **3**, 38 (2012).
- H. Zheng, D. Liu, Y. Zheng, S. Liang, and Z. Liu, *J. Hazard Mater.* **167**, 141 (2009).

Synthesis and Temperature-Responsive Behavior of *N*-vinylcaprolactam-grafted Natural Rubber

Sopitcha Phetrong¹, Chanon Sansuk¹, and Peerasak Paoprasert^{1,a}

¹ Department of Chemistry, Faculty of Science and Technology, Thammasat University, Pathumthani, Thailand

^a Corresponding author : peerasak@tu.ac.th

Abstract: Temperature-responsive polymers are smart materials because they can respond to change in surrounding temperature and are applicable for various applications. In this work, we reported a synthesis and temperature-responsive behavior of *N*-vinylcaprolactam-grafted deproteinized natural rubber (NVCL-g-DPNR). The grafting reaction was carried out using deproteinized natural rubber (DPNR) latex, *N*-vinylcaprolactam (NVCL) as monomer, and 2,2'-azoisobutyronitrile (AIBN) as free radical initiator. The temperature responsiveness of the grafted copolymers was investigated using water swelling and compared with that of pure DPNR. The lower critical solution temperature (LCST) of the grafted copolymer was found to be in the range 32-34 °C whereas the DPNR was not responsive to temperature. The temperature-responsiveness of grafted copolymer near human body temperature can be utilized to be fabricated as biomedical materials. Based on this study, the temperature-responsive natural rubber would potentially be used as a novel responsive rubber-based material in various applications.

Keywords: Temperature-responsive material, *N*-vinylcaprolactam, Deproteinization, Natural rubber, Grafting

1. Introduction

Stimuli-responsive materials are smart materials because they can sense and respond to changes in environmental conditions, such as pH, temperature, light, ionic strength, electric field, and magnetic field [1]. Changes in surrounding conditions trigger a change in the physical and chemical properties of stimuli-responsive materials, such as size, shape, hydrophobicity/hydrophilicity, and degradation rate [2]. These responsive materials can therefore be used to fabricate responsive and active devices that can regulate and introduce new functionalities for various applications. Temperature is considered as one of the most widely used external stimuli in stimuli-responsive materials because it can be simply modulated by temperature-programmed equipment or ambient conditions. Temperature-responsive materials are those that generally undergo a volume transition or soluble-to-insoluble change or vice versa in solvents around the lower critical solution temperature (LCST). One of the most widely studied temperature-responsive polymers is based on poly(*N*-vinylcaprolactam) (PNVCL) because it possesses LCSTs of around 32 °C in water, which is near the human body temperature [3, 4]. The non-toxicity, high water solubility, and biocompatibility of PNVCL make it applicable in various biomedical applications. In addition, PNVCL is water-soluble, biocompatible, and relatively stable against hydrolysis and does not produce toxic low molecular-weight amines due to the presence of cyclic amide instead of aliphatic amides in other polymers [5]. A range of temperature-responsive copolymers have also been prepared to increase strength and impart new properties to hybrid materials. *N*-vinylcaprolactam (NVCL) has been copolymerized and grafted copolymerized with several polymers, for example, chitosan [6], methacrylic

acid (MAA) [7], poly(acrylic acid) (PAA) [8], and polypropylene (PP) [9]. NVCL-based copolymers thus have the potentials to be used for a wider range of applications.

Natural rubber (NR) is a well-known renewable elastomeric material obtained from the *Hevea brasiliensis* tree in the form of a milky white fluid called latex [10]. NR is a versatile material widely used in various applications. Although the presence of double bonds makes *cis*-polyisoprene susceptible to degradation, double bonds are places to which new functionalities can be added. Several chemical reactions have been used to modify NR which produces hybrid structures with high strength and stability. Various monomers have been grafted with NR, including glycidyl methacrylate (GMA) [11], methyl methacrylate (MMA) [12-14], styrene (ST) [15, 16], 2-hydroxyethyl methacrylate (HEMA) [17], vinyl alcohol (VA) [18], and maleic anhydride (MA) [19, 20].

Grafting of hydrophilic monomers on NR backbone remains a challenge because of the presence of surface proteins as rubber particle shells. Monomers are not well incorporated in the hydrophobic NR cores in latex and therefore often homopolymerize [21-23]. However, several monomers and polymers have been grafted with NR, the main goal has been to improve the thermal, chemical, and mechanical properties of NR. The addition of responsive functions to NR via grafting reaction has never been reported. Thus, the objective of this study was to develop a method for grafting NVCL onto NR for preparing rubber-based, temperature-responsive materials. Furthermore, in this work grafting reaction was carried out using deproteinized natural rubber (DPNR) latex and 2,2'-azoisobutyronitrile (AIBN) as an initiator. The LCST of the grafted copolymers was measured and compared with pristine NR. Based on these results, this work shows that temperature responsiveness can be introduced to NR, which will expand the range of applications.

2. Materials and Methods

2.1. Materials

High-ammonia NR latex (60% dry rubber content (DRC)) was purchased from the Department of Agriculture, Thailand. All other chemicals were purchased from Sigma-Aldrich and used as received unless otherwise noted. NVCL was purified by recrystallization in methanol. Organic solvents (Labscan, AR) were used as received. Deionized (DI) water was used throughout the experiments. PNVCL was synthesized from NVCL via free radical polymerization using AIBN and used as a reference.

2.2. Deproteinization of NR latex

NR latex (100 g) used in this study was commercial high ammonia latex (60% DRC). The incubation of the latex was performed with 0.1 wt% urea (0.2 g) in the presence of 1 wt% sodium dodecyl sulfate (SDS, 2 g) dissolved in DI water (100 g). This mixture was then incubated for 30 min with continuous stirring at room temperature. After that, the resulting latex was purified by centrifugation at 10,000 rpm for 1 h at 25 °C. The cream fraction was re-dispersed in 1 wt% SDS and washed twice by centrifugation to prepare DPNR latex (32% DRC).

2.3. Grafting of NVCL on DPNR backbone

The DPNR latex (5 g) was placed in 100 ml, round-bottom flask. Then, SDS (0.15 g) as an emulsifier and potassium hydroxide (KOH, 0.15 g) diluted in DI water was added while vigorous stirring. Subsequently, NVCL monomer (50-150 phr with respect to dry rubber content) was added continuously and the reaction mixture was heated at 80 °C for at least 30 min with continuous stirring. Next, AIBN (5-15 phr with respect to dry rubber content) as an initiator was dissolved with a slight amount of toluene and slowly charged into the reactor. The polymerization reaction was performed at the desired polymerization temperature (80-100 °C). The reaction mixture was allowed to react for a specified length of time (4-8 h). After that, the reaction mixture was cooled down to room temperature and coagulated by using 5 wt% acetic acid solution. The modified product was purified by soxhlet extraction in acetone for 24 h to remove contaminants, unreacted monomer and homopolymer. The grafted product was dried under vacuum at 60 °C overnight. After drying, the grafted product was dissolved with chloroform-d for investigating grafting efficiency. The ¹H-NMR intensity of the product was

used to determine grafting efficiency percentage. Grafting efficiency (%) was determined from $^1\text{H-NMR}$ spectra using the following equation:

$$\text{Grafting efficiency (\%)} = \frac{I_{4.4}}{I_{5.2}} \times 100, \quad (1)$$

where $I_{4.4}$ was the integrated signal area of the proton in $-\text{NCH}-$ of the α position of PNVCL unit and $I_{5.2}$ was the integrated signal area of the unsaturated methyne proton of polyisoprene backbone chain.

2.4. Determination of LCST

The grafted material and dry DPNR were cut into small pieces ($0.75 \times 0.75 \text{ cm}^2$) and compressed to remove air bubbles and reduce porosity by sandwiching them between two glass slides and heating at $60 \text{ }^\circ\text{C}$ for 24 h. The samples were immersed in deionized water for 2 h at a range of temperatures from 28 to $38 \text{ }^\circ\text{C}$. After removing the surface liquid gently with tissue paper, the weight of the materials was measured and the swelling percentage was calculated to determine the LCST from the following equation:

$$\text{Swelling (\%)} = \frac{W_2 - W_1}{W_1} \times 100, \quad (2)$$

where W_1 and W_2 was the weight of the material before and after immersion, respectively.

2.5. Characterization

CHN data was obtained using CHN-2000 LECO analyzer. ^1H (400 MHz) nuclear magnetic resonance (NMR) spectra were obtained using an AVANCE Bruker NMR spectrometer with chloroform- d as a solvent. The Fourier transform infrared (FT-IR) spectra were obtained using a Perkin Elmer FT-IR (Spectrum GX model) and NaCl salt windows. The surface elements of the sample were investigated using an X-ray photoelectron spectrometer (XPS; AXIS ULTRA^{DL}, Kratos analytical, Manchester UK.) The base pressure in the XPS analysis chamber was about 5×10^{-9} torr. The samples were excited using X-ray hybrid mode at a $700 \times 300 \text{ }\mu\text{m}$ spot area with a monochromatic Al $K_{\alpha 1,2}$ radiation at 1.4 keV. The X-ray anode was run at 15kV 10mA 150 W. The photoelectrons were detected with a hemispherical analyzer positioned at an angle of 45° with respect to the sample surface.

3. Results and Discussion

3.1. Synthesis and characterizations of grafted copolymer

NVCL-grafted DPNR (NVCL- g -DPNR) was prepared via free radical grafting in aqueous system using AIBN as an initiator. NR latex was deproteinized prior to grafting reaction because deproteinization removed surface protein, leading to higher grafting efficiency. Deproteinization was carried out using urea as a deproteinizing agent [24]. The DPNR was characterized using CHN analysis. It was found that the nitrogen content in DPNR was less than that of NR by 43% while carbon and hydrogen remained almost unchanged (Table 1). This result indicates that deproteinization of NR removed approximately 50% of protein from NR latex, comparable with previous study [25].

TABLE I: Elemental analysis of NR and DPNR

Sample name	Chemical composition		
	Carbon (%)	Hydrogen (%)	Nitrogen (%)
DPNR	84.19	12.88	0.43
NR	84.79	12.68	0.76

Grafting of NVCL onto DPNR was carried out in an aqueous system using AIBN as free radical initiator (Figure 1). The formation of grafting copolymer is believed to proceed by two possible pathways: a reaction between the free radicals and double bonds of the isoprene units and a hydrogen abstraction mechanism [26, 27].

The NVCL-*g*-DPNR was purified by soxhlet extraction in acetone in order to remove impurities, unreacted NVCL, and PNVCL homopolymer.

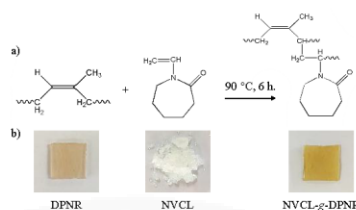


Fig. 1: a) schematic representation for the synthesis of NVCL-*g*-DPNR from DPNR and NVCL and b) their respective images.

The NVCL-*g*-DPNR was characterized using FT-IR and $^1\text{H-NMR}$ techniques and compared with the DPNR and PNVCL. The FT-IR spectrum of NVCL-*g*-DPNR showed signature signals of both DPNR and PNVCL (Figure 2). The FT-IR signals at 3440, 3255, 1631, and 1379 cm^{-1} corresponded to O-H stretching, N-H stretching, C=O stretching and C-N stretching of caprolactam ring of PNVCL, respectively. The signal at 1442 cm^{-1} corresponded to C=C stretching of the polyisoprene. The FT-IR results are consistent with those in previous work [28].

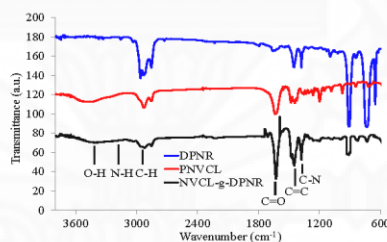


Fig. 2: FT-IR spectra of DPNR, PNVCL, and NVCL-*g*-DPNR.

$^1\text{H-NMR}$ spectrum of DPNR showed signals at 5.2, 2.1 and 1.7 ppm, corresponding to C-H, CH_2 , and CH_3 respectively (Figure 3), consistent with previous report [29]. The $^1\text{H-NMR}$ spectrum of the PNVCL showed signals at 4.4, 3.3, 2.5, and 1.8 ppm, corresponding to CH-NH, CH_2 -NH, CH_2 -CO, and CH_2 respectively. The $^1\text{H-NMR}$ spectrum of NVCL-*g*-DPNR showed signals corresponding to both DPNR and PNVCL. The signal at 4.4 ppm corresponded to CH-NH of the PNVCL, whereas the signal at 5.2 ppm corresponded to C-H of the isoprene units. These signals were used to calculate grafting efficiency, which was found to be 25%.

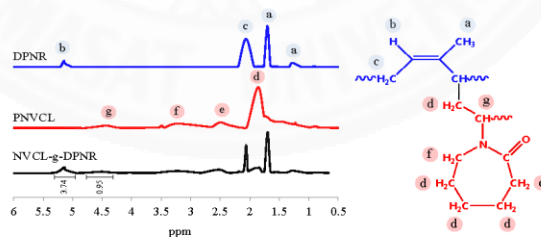


Fig. 3: $^1\text{H-NMR}$ spectra of DPNR, PNVCL, and NVCL-*g*-DPNR.

In addition, only the XPS spectrum of NVCL-*g*-DPNR showed strong N_{1s} signal at 400 eV, which was not observed in the DPNR sample due to the presence of amide group of NVCL units in grafted-rubber (Figure 4).

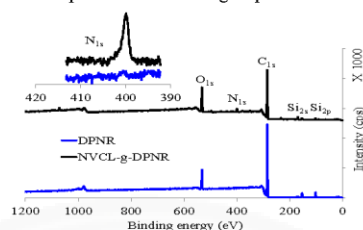


Fig. 4: XPS spectra of DPNR and NVCL-*g*-DPNR. The inset is the high-resolution spectra in the N_{1s} region.

To further confirm the formation of grafted copolymer, a blend sample between DPNR latex and PNVCL was prepared in water solution and dried by placing on glass plate as a thin film. After that, the film was peeled off and purified via stirring in acetone twice and dried in an oven at 60 °C overnight. It was found that PNVCL was not detected in 1H -NMR spectrum as it was soluble in acetone. Therefore, the presence of both PNVCL and DPNR in the NVCL-*g*-DPNR sample must be due to the formation of a grafted structure inseparable by stirring in acetone. This result also confirmed that stirring in acetone twice effectively removed unbound PNVCL homopolymer.

3.2. Temperature-responsive studies

The temperature responsiveness of DPNR and NVCL-*g*-DPNR in water were characterized at a temperature range of 28-38 °C. At 28 °C, NVCL-*g*-DPNR swelled by 15% of its original weight and about 8 times more than the DPNR, due to the presence of hydrophilic NVCL units. The NVCL-*g*-DPNR can be thus considered as a hydrogel-like material. As the temperature was increased, the percentage of swelling of the DPNR did not change, whereas that of the NVCL-*g*-DPNR started to decrease when the temperature of water exceeded 30 °C and became constant above 34 °C (Figure 5).

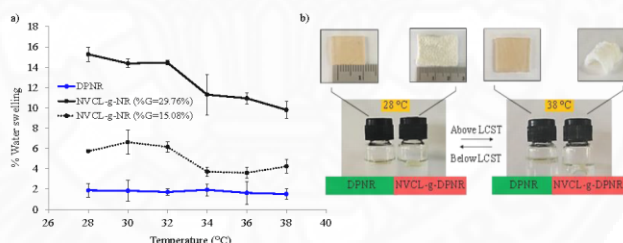


Fig. 5: a) water swelling percentage of DPNR and NVCL-*g*-DPNR in aqueous solutions at different temperatures and b) schematic illustration of water swelling studies of DPNR and NVCL-*g*-DPNR in aqueous solutions at below and above LCST.

The LCST of NVCL-*g*-DPNR was therefore determined to fall in the range of 32-34 °C, which is similar to the coil-to-globule transition temperature of PNVCL. These results suggest that the presence of DPNR and grafted structure in the NVCL-*g*-DPNR did not significantly affect the LCST of the PNVCL. This finding is consistent with other reports on temperature-responsive crosslinked materials [30, 31].

4. Conclusions

In this work, the grafted copolymers between NVCL and DPNR were successfully prepared via grafting reaction in emulsion using AIBN as an initiator. The characterizations were performed by FT-IR, 1H -NMR and

XPS techniques. The FT-IR and $^1\text{H-NMR}$ spectra were showed both DPNR and PNVCL signals which were strongly confirmed that the NVCL units were introduced onto DPNR backbone. Furthermore, the XPS spectra of the grafted materials showed a significant increase in N_{1s} signal at 400 eV, that confirm the amide group of NVCL units in grafted materials whereas this signal was not observed in DPNR. The temperature responsiveness of NVCL-*g*-DPNR was studied by water swelling experiment that showed an LCST around 32-34 °C, which was close to the phase transition of PNVCL. These temperature-responsive rubbers will be useful for a variety of biomedical applications. Potential consumer products include, smart bandages and facial masks with the ability to efficiently release medicine or healing ingredients upon contact with human skins.

5. Acknowledgement

This work is financially supported by the Thailand Research Fund (TRF) and the Faculty of Science and Technology, Thammasat University (TRG5880199). The authors acknowledge the Central Scientific Instrument Center (CSIC), Department of Chemistry, Faculty of Science and Technology, and Thammasat University.

6. References

- [1] H. Almeida, M. H. Amaral, and P. Lobão, "Temperature and pH stimuli-responsive polymers and their applications in controlled and self-regulated drug delivery," *J. Appl. Pharma. Sci.*, vol. 02, no. 06, pp. 01-10, 2012.
- [2] R. Liu, M. Fraylich, and B. R. Saunders, "Thermoresponsive copolymers: from fundamental studies to applications," *Colloid Polym. Sci.*, vol. 287, pp. 627-643, 2009.
- [3] M.R. Aguilar, C. Elvira, A. Gallardo *et al.*, "Smart Polymers and Their Applications as Biomaterials," *Topics in Tissue Engineering*, 2013.
- [4] T. Yoshida, T. C. Lai, G. S. Kwon *et al.*, "pH- and ion-sensitive polymers for drug delivery," *Expert Opin. Drug Deliv.*, vol. 10, no. 11, pp. 1497-1513, 2013.
- [5] K. Thangavelu, K. Inn-Kyu, and P. Soo-Young, "Poly(N-vinyl caprolactam) grown on nanographene oxides as an effective nanocargo for drug delivery," *Colloids and Surfaces B: Biointerfaces*, vol. 115, pp. 37-45, 2014.
- [6] M. Prabakaran, J. J. Grailler, D. A. Steeber *et al.*, "Stimuli-Responsive Chitosan-graft-Poly(N-vinylcaprolactam) as a Promising Material for Controlled Hydrophobic Drug Delivery," *Macromolecular Bioscience*, vol. 8, no. 9, pp. 843-851, 2008.
- [7] D. Crespy, A. Golosova, E. Makhaeva *et al.*, "Synthesis and characterization of temperature-responsive copolymers based on N-vinylcaprolactam and their grafting on fibres," *Polymer International*, vol. 58, no. 11, pp. 1326-1334, 2009.
- [8] X. Jiang, G. Lu, C. Feng *et al.*, "Poly(acrylic acid)-graft-poly(N-vinylcaprolactam): a novel pH and thermo dual-stimuli responsive system," *Polymer Chemistry*, vol. 4, no. 13, pp. 3876-3884, 2013.
- [9] V. N. Kudryavtsev, V. Y. Kabanov, N. A. Yanul' *et al.*, "Polypropylene Modification by the Radiation Graft Polymerization of N-Vinylcaprolactam," *High Energy Chemistry*, vol. 37, no. 6, pp. 382-388, 2003.
- [10] D. F. Graves, "Rubber," *Handbook of Industrial Chemistry and Biotechnology*, J. A. Kent, ed., pp. 689-718: Springer US, 2007.
- [11] P. Juntuck, C. Ruksakulpiwat, P. Chumsamrong *et al.*, "Glycidyl methacrylate grafted natural rubber: synthesis, characterization, and mechanical property," *J. Appl. Polym. Sci.*, vol. 122, pp. 3152-3159, 2011.
- [12] P. Satraphan, A. Intasiri, V. Tangprasuthadol *et al.*, "Effects of methyl methacrylate grafting and in situ silica particle formation on the morphology and mechanical properties of natural rubber composite films," *Polymers for Advanced Technologies*, vol. 20, no. 5, pp. 473-486, 2009.
- [13] T. Kochthongrasamee, P. Prasassarakich, and S. Kiatkamjornwong, "Effects of redox initiator on graft copolymerization of methyl methacrylate onto natural rubber," *Journal of Applied Polymer Science*, vol. 101, no. 4, pp. 2587-2601, 2006.

- [14] S. Zhang, L. Cao, F. Shao *et al.*, "Grafting of methyl methacrylate onto natural rubber in supercritical carbon dioxide," *Polymers for Advanced Technologies*, vol. 19, no. 1, pp. 54-59, 2008.
- [15] P. Suksawad, Y. Yamamoto, and S. Kawahara, "Preparation of thermoplastic elastomer from natural rubber grafted with polystyrene," *European Polymer Journal*, vol. 47, no. 3, pp. 330-337, 2011.
- [16] W. Arayaprance, and G. L. Rempel, "Morphology and mechanical properties of natural rubber and styrene-grafted natural rubber latex compounds," *Journal of Applied Polymer Science*, vol. 109, no. 3, pp. 1395-1402, 2008.
- [17] Y. Premdum, P. Klinpituksa, and J. Ruamcharoen, "Grafting copolymerization of natural rubber with 2-hydroxyethyl methacrylate for plywood adhesion improvement," *Songklanakarin Journal of Science and Technology*, vol. 31, no. 4, pp. 453-457, 2009.
- [18] W. Wongthep, S. Srituileong, S. Martwiset *et al.*, "Grafting of poly(vinyl alcohol) on natural rubber latex particles," *J. Appl. Polym. Sci.*, vol. 127, no. 1, pp. 104-110, 2013.
- [19] P. Wongthong, C. Nakason, Q. Pan *et al.*, "Grafting of maleic anhydride onto deproteinized natural rubber via differential microemulsion polymerization," pp. 183-190.
- [20] C. Nakason, A. Kaesaman, and P. Supasanthitkul, "The grafting of maleic anhydride onto natural rubber," *Polymer Testing*, vol. 23, no. 1, pp. 35-41, 2004.
- [21] C. Nakason, A. Kaesaman, and N. Yinwan, "Preparation of graft copolymers from deproteinized and high ammonia concentrated natural rubber latices with methyl methacrylate," *Journal of Applied Polymer Science*, vol. 87, no. 1 SPECC., pp. 68-75, 2003.
- [22] N. Pukkate, Y. Yamamoto, and S. Kawahara, "Mechanism of graft copolymerization of styrene onto deproteinized natural rubber," *Colloid and Polymer Science*, vol. 286, no. 4, pp. 411-416, 2008.
- [23] P. Wongthong, C. Nakason, Q. Pan *et al.*, "Modification of deproteinized natural rubber via grafting polymerization with maleic anhydride," *European Polymer Journal*, vol. 49, no. 12, pp. 4035-4046, 2013.
- [24] I. Fukuhara, K. Miyano, Y. Yamamoto *et al.*, "Preparation of purified natural rubber by removal of proteins," *Kobunshi Ronbunshu*, vol. 72, no. 1, pp. 1-6, 2015.
- [25] S. Kawahara, W. Klinklai, H. Kuroda *et al.*, "Removal of proteins from natural rubber with urea," *Polymers for Advanced Technologies*, vol. 15, no. 4, pp. 181-184, 2004.
- [26] H. Liu, C. Chuai, M. Iqbal *et al.*, "Improving foam ability of polypropylene by crosslinking," *J. Appl. Polym. Sci.*, vol. 122, pp. 973-980, 2011.
- [27] S. M. Tamboli, S. T. Mhaske, and D. D. Kale, "Improving Foam Ability of Polypropylene by Crosslinking," *J. Appl. Polym. Sci.*, vol. 122, no. 2, pp. 973-980, 2011.
- [28] K. Selin, T. Özdemir, and A. Usaramaz, "Polymerization of N-vinylcaprolactam and characterization of poly (N-vinylcaprolactam)," *Macr. Sci. A*, vol. 48, no. 6, pp. 467-477, 2011.
- [29] C. Jem-Kun, and C. Chi-Jung, "Fabrications and Applications of Stimulus-Responsive Polymer Films and Patterns on Surfaces: A Review," *Materials*, vol. 7, pp. 805-875, 2014.
- [30] G. Yi, Y. Huang, F. Xiong *et al.*, "Preparation and swelling behaviors of rapid responsive semi-IPN NaCMC/PNIPAm hydrogels," *Journal of Wuhan University of Technology-Mater. Sci. Ed.*, vol. 26, no. 6, pp. 1073-1078, 2011.
- [31] X. Xia, and Z. Hu, "Synthesis and Light Scattering Study of Microgels with Interpenetrating Polymer Networks," *Langmuir*, vol. 20, pp. 2094-2098, 2004.

BIOGRAPHY

Name	Miss Sopitcha Phetrong
Date of Birth	June 14, 1991
Educational Attainment	2014 : Bachelor degree of Science in Chemistry, Thammasat University
Position	Graduate student
Scholarships	2015-2016 : Scholarship for Talent Student to study graduate program in Faculty of Science and Technology, Thammasat University 2017 : TU Research Scholar of Thammasat University
Publications	<ol style="list-style-type: none">1. Sopitcha Phetrong, Chanon Sansuk, Pramuan Tangboriboonrat, and Peerasak Paoprasert. Temperature-Responsive Crosslinked Materials Prepared from Natural Rubber and Poly(<i>N</i>-vinylcaprolactam), <i>Macromolecular Research</i>, 2017, 1-7.2. Sopitcha Phetrong, Chanon Sansuk, and Peerasak Paoprasert. Synthesis and Temperature-Responsive Behavior of <i>N</i>-vinylcaprolactam-grafted Natural Rubber. 5th International Conference on Advances in Chemical, Biological, and Environmental Engineering (ACBEE-17), March 27-30, 2017, Ibis Singapore on Bencoolen, Singapore. (oral presentation)
Work Experience	Teaching assistant in chemical laboratory at Department of Chemistry, Faculty of Science and Technology, Thammasat University